Small scale/Large scale MFC Stacks for Improved Power Generation and Implementation in Robotic Applications

GEORGIOS PAPACHARALAMPOS

Faculty of Environment and Technology, University of the West of England, Bristol

October 2015

Abstract

Microbial Fuel Cells (MFCs) are biological electrical generators or batteries that have shown to be able to energise electronic devices solely from the breakdown of organic matter found in wastewater. The generated power from a single unit is currently insufficient to run standard electronics hence alternative strategies are needed for stepping-up their performance to functional levels. This thesis deals with MFC miniaturisation; their proliferation into large stacks; power improvement by using new electrode components and finally a novel method of energy harvesting that will enhance the operation of a self-sustainable robotic platform. A new small-MFC design was developed using 3D printing technology that outperformed a pre-existing MFC of the same volume (6.25 mL) highlighting the importance of reactor configuration and material selection. Furthermore, improvements were made by the use of a cathode electrode that facilitates a higher rate of oxygen reduction reaction (ORR) due to the high surface area carbon nanoparticles coated on the outer layer. Consequently, a 24-MFC stack was built to simulate a small-scale wastewater treatment system. The MFC units were connected in various arrangements, both fluidically as a series of cascades and electrically in-parallel or in-series, for identifying the best possible configuration for organic content reduction and power output. Results suggest that in-parallel connections allow for higher waste removal and the addition of extra units in a cascade is a possible way to ensure that the organic content of the feedstock is always reduced to below the set or permitted levels for environmental discharge. Finally, a new method of fault-proof energy harvesting in stacks was devised and developed to produce a unique energy-autonomous energy harvester without any voltage boosting and efficiencies above 90%. This thesis concludes with the transferability of the above findings to a robotic

test platform which demonstrates energy autonomous behaviour and highlights the synergy between the bacterial engine and the mechatronics.

Declaration

This dissertation is the result of my own work and includes nothing which is the outcome of work done in collaboration except where specifically indicated in the text and bibliography. All material previously published in scientific journals, has been granted with permission from the publishers to be reprinted for the requirements of this thesis and for internal use from the university's repository.

Glossary of Terms

ABS	Acrylonitrile Butadiene Styrene
AC	Activated Carbon
BES	Bioelectrochemical Systems
BiBC	Bristol BioEnergy Center
BOD	Biological Oxygen Demand
BRL	Bristol Robotics Laboratory
CCV	Closed circuit Voltage
CD	Current Density
COD	Chemical Oxygen Demand
DET	Direct Electron Transfer
D20	20-day period
D40	40-day period
EAB	Electro-active Biofilm
ESR	Equivalent in -Series Resistance
GDL	Gas Diffusion Layer
HRT	Hydraulic Retention Time
IEM	Ion Exchange Membrane
LED	Light Emitting Diode
MET	Mediated Electron Transfer
MFC	Microbial Fuel Cell
MOSFET	metal–oxide–semiconductor field-effect transistor
MPL	Micro porous layer
MPP	Maximum Power Point
MPPT	Maximum Power Point Tracking

OCV	Open Circuit Voltage
ORR	Oxygen Reduction Reaction
PC-ISO	medical-grade biocompatible Polycarbonate
PD	Power Density
PMS	Power Management Sytems
PTFE	Polytetrafluoroethylene
RC25 Nanocure	ceramic-filled photo curable resin
Re	Reynolds number
Rext	External Resistance
Rint	Internal Resistance
s.a	surface area
SEM	Scanning Electron Microscope
TI	Texas Instruments
TYE	Trypton Yeast Extract
UWE	University of the West of England

Contents

Chapter 1

Introduction and Background

1.1. Overview

Microbial Fuel Cells are an eco-friendly technology where anaerobic bacterial species harvest energy from organic compounds and convert it to electrical energy via their respiratory metabolism. Even though the MFC principle is over a hundred years old, the ability of MFCs to extract energy stored in wastewater has lately received the attention of the research community due to its advantages to aerobic treatment processes and the generation of useful amounts of electricity. A MFC resembles a galvanic cell hence it can be considered as a bio-battery with a maximum theoretical open-circuit voltage (OCV), dictated by the redox potential which can reach up to 1.14 V, whilst the operating voltage at maximum power transfer (MPP), should be approximately half this value. The majority of electrical circuits operate in the area of 1.5 V to 3 V, which is far from matching the output of an MFC unit. Developments in electrode material and the concomitant miniaturisation of MFCs have been the first step towards power optimisation. The main strategy for increasing the performance of individual MFC units is by connecting multiple MFCs in stack configuration or with the use of a plethora of DC-DC converting techniques for stepping-up the voltage from a single unit. To date, findings from various research groups have advanced the knowledge in miniaturisation and scaling-up of MFCs to the stage that can allow for the technology to become of practical value, providing benefit of wastewater treatment, carbon-neutral power, water and elemental re-cycling and other environmental advantages.

Even though there is still the room for progress in increasing power density, the technology is rapidly approaching real-world implementation and commercialisation. Thus, the philosophy behind this thesis is under the contention that:

It is feasible to develop reliable MFC systems capable of dynamic homeostasis, self-adjusting their performance to meet changes in the quality of their fuel feedstock and regulating their energy output to match that required for various functions.

1.2. Thesis outline

In an effort to provide a better understanding in the development of intelligent MFC systems, the experimental work is divided in seven distinct but yet interconnected chapters. The line of work involves miniaturisation of a single MFC unit, followed by power improvement of units and their multiplication into stacks of units.

Chapter 1 reports succinctly on the history of MFCs and the *modus operandi* followed by the fundamental principles that render MFC stacks feasible. Building on these foundations, the main objectives of this work are presented that move towards the realisation of energy autonomous systems.

Chapter 2 investigates different 3D printed structural materials as well as the reactor architecture of a novel MFC design (*Twist n' Play*) in an effort to provide a better understanding in reactor miniaturisation. Due to a limited number of studies reporting the effects that various thermo-polymer plastics have in MFC operation, this chapter reveals further aspects about the materials' properties which are likely to affect a MFC's performance and emphasises the importance of criteria such as

overall biocompatibility, selective electrical insulation and oxygen diffusion (low for anode; high for cathode) for high power output. **Results suggest that a better MFC reactor design built with the right material can improve the performance**.

Chapter 3 explores the theory that a higher surface area electrode can significantly increase the rate of cathodic reactions and result in improved power output. It is shown that the tested *substratum* used as an electrode in the cathode greatly enhanced the performance **allowing the demonstration (for the first time) of the powering of a digital wristwatch on-the-fly by just two small-scale MFCs connected in-series**.

Chapter 4 reports on the electrical and hydraulic repositioning of a 24 small-scale MFC stack set in a cascade-like waste stream. This system is simulating in a small scale, a series of possible continuous wastewater efflux scenarios with a simultaneous electrical reconfiguration and how that affects the COD treatment to power ratio. Results provide further insight on the system's internal resistance variance when MFC units are repositioned in the cascade and also **reveal for the first time the biofilm's dynamic homeostatic ability to rebound from a high internal resistance to a lower state** based on the organic substrate supply that reaches each cell in the cascade.

Chapter 5 highlights the significance of power management in MFC stacks and elaborates on the efficient energy harvesting from MFCs. The undertaken works reveals **a novel and revolutionary analogue way of passive harvesting whereby the progressive switching of parallel connections to series within a stack has an almost 2-fold improvement in power output and halves the time required for charging capacitors for storing this energy**.

In **Chapter 6**, the findings from the previous chapter are used to develop an automated system which allows for precise configuration switching with negligible efficiency losses. Results reveal that the system extracts energy at high rates **also allows for smooth and robust operation by preventing cell reversals under low external impedance conditions.** This discovery further leads to the construction of an energy autonomous circuitry, powered exclusively by MFCs, with the ability to harvest energy and auto-configure the electrical connections within the stack for optimal performance.

Chapter 7 examines the possible applicability of all the acquired knowledge onto the latest generation of a self-sustainable robotic platform, EcoBot-IV. The experimental plan concludes with an alternative approach in power control from MFC stacks for resilient energy harvesting.

1.3. The Microbial Fuel Cell technology

1.3.1. History of MFCs

A microbial fuel cell is a bio-electrochemical device that is capable of generating bioelectricity. The first to examine the bioelectric phenomenon and the term bioelectricity was Luigi Galvani in 1790, who noticed twitching of isolated frog leg when a brief electrical discharge was passed through it [1]. But the first MFC concept was demonstrated by Michael Cresse Potter in 1910 [2]. He produced electrical energy from living cultures of *Escherichia coli* and *Saccharomyces sp* by using platinum electrodes. In 1931, Barnet Cohen revived Potter's idea by creating the first stack of microbial fuel cells that were connected in-series, capable of producing over 35 V, though only under a current of 2 mA [3]. During the 1950's, Rohrback *et al*., [4] designed a biological fuel cell in which *Clostridium butyricum* was used as a biological catalyst for generating hydrogen from glucose fermentation but without generating any electrical energy. Microbial fuel cells became popular in the late 1950s, when NASA showed interest in converting organic waste into electricity on its long-distance space flights. However, these fuel cells did not produce sufficient power, were not appealing to the market and soon disappeared. Later, during the oil crisis of the 70s and 80s, the interest in the development of chemical fuel cells was revived. In 1966, Williams [5] showed that chemical fuel cells powered by rice husk produced 40 mA at 6 V. Rice husk is rich in lignocellulose, which under fermentative conditions yields many useful enzymes and biofuels like ethanol that could be used in conventional fuel cells. In 1969, Yao *et al*.[6] showed that glucose could be chemically oxidised in the presence of platinum and therefore used as a fuel. Karube *et al*.,[7] in 1986, reported the generation of about 300 mA from a microbial fuel cell

using *Anabaena spp*. as a biocatalyst, in which phosphoric acid was used as the electrolyte. The years that followed during the 1980s and the 1990s revealed significant results that are discussed below as part of the small MFC operation in this study.

1.3.2. Main principles that render MFC operation used in this study

1.3.2.1. Single chamber open-to-air cathode MFCs with mediator-less anodophillic biofilms.

1.3.2.1.1. Mediator-less MFCs

For many years, MFC studies were unable to provide sufficient answers to why the performance could not be sustained and improve any further. It was not until 1962 and 20 years later that work from various groups [8–11] noticed that the addition of synthetic electron mediators could benefit substantially the power output and current density of MFCs. Bennetto's group were the first to use this knowledge to power a DC motor for a short period of time [12]. Unless the bacteria were anodophillic, then their outer membrane layer acted as an insulator because it consists of lipids, peptididoglycans and lipopolysaccharides that prevent electrons to flow through [13–16]. Electron shuttles are capable of being reduced (by NADH, NADPH or reduced cytochromes) within the membrane and oxidised at the anode, which speeds the transfer of electrons from the bacteria membrane to the surface of the electrode.

However, a real breakthrough was made when some microbes were found to transfer electrons directly to the anode [17,18], operate in a stable manner and yield a high Coulombic efficiency [17,19]. In 2003, Chaudhuri and Lovely [17] reported that

Rhodoferax ferrireducens can recover up to 83 % of electrons from glucose oxidation in the presence of Fe^{3+} without a mediator.

This discovery, along with a study in 2005 [20], suggested that the use of artificial mediators in MFCs was less efficient than the already bacterial produced mediators or the direct electron transfer (DET) from the membrane to the electrode. Since that point, the use of added mediators in MFC studies was gradually avoided and the majority of studies focused to mediator-less MFC operation.

1.3.2.1.2. Anodophillic bacteria and electroactive biofilms

The first bacteria to show bio-electrochemical activity of transferring electrons directly by conductance through the membrane were *Shewanella putrefaciens* [19,21], *Geobacter sulfurreducens* [22], *Geobacter metallireducens* [23] and *Rhodoferax ferrireducens* [17]. In general, when a MFC is inoculated with a naturally occurring mixed culture, electrochemically active bacteria and other symbiotically related to these bacteria are expected to establish an electroactive biofilm when they are operated at R_{ext} values matching the R_{int}, and decreases the number of methanogenic species [24,25]. However, 16S rDNA sequencing analysis revealed an abundant phylogenetic diversity in the anode consortia with no single emergent bacterial species. This randomness suggested the presence of other bacterial strains, apart from the iron reducing species that contribute to electricity generation, and correlates to the inoculum and substrate type used [26–32].

When conditions are favourable these electrogenic strains form a structural matrix on the anode by attachment, called biofilm. This structure provides protection from toxic agents. An additional layer of proteins, polysaccharides and ions called a conditioning film creates a high affinity adhesion platform between the biofilm and

the substratum that allows it to firmly attach onto living organisms or solid surface areas [33]. In the latter case, the solid surface areas were shown to be carbon based or metal based electrodes that later revealed the direct electron transfer approach [22,23,34]. Hence electroactive biofilms (EAB) attached onto conductive surfaces are the bacterial engine that is favoured throughout this experimental process.

1.3.2.1.3. O_2-based cathodes

Diatomic oxygen gas (O_2) constitutes 20.8% of the volume of atmospheric air and is the third-most abundant element on Earth, after hydrogen. It has the second highest electronegative number which makes it a higly reactive chemical reaction reagent. Because of its availability and high electronegativity, oxygen greatly favours oxidation-reduction reactions (ORR). These are the most important reactions in fuel cells' cathode electrode and facilitate the 4-electron reaction from O_2 to H_2O and the 2-electron reduction from O_2 to H_2O_2 (hydrogen peroxide) [35]. A large bottleneck in ORR is the low rate of reaction on the cathode. Various metals have typically been used to catalyse the cathodic reaction [36] but reduction of oxygen at the cathode is currently an important limiting factor in a MFC. Hence, many studies suggested the use of other chemicals such as ferricyanide as a terminal electron acceptor on the cathode [37] that greatly improves the performance but at the expense of sustainability. When ferricyanide is reduced, then it is converted to ferrocyanide in a non-reversible reaction. That involves the frequent replacement of ferricyanide in the cathode and the safe disposal of ferrocyanide which renders this strategy as unsustainable and costly [38,39].

Scaling up is a fundamental problem for practical applications of MFCs for wastewater treatment and bioenergy production. The main challenges for commercialising scalable MFCs are the development of materials that are cost-effective, environmentally friendly, efficient in power generation but also identifying architectures that can be used at a larger scale. Maximum power densities in most high power MFCs are largely inhibited by cathode surface area and performance [40,41], which together with the cost of cathode materials and proton exchange membranes (PEM), can account for the greatest percentage (47%) of the MFC capital costs [42]. As such, this study has used of catalyst-free air cathodes and supports the notion for longevity and low cost cathode electrodes.

1.3.2.2. Batch mode and continuous flow MFCs

When substrate is provided in a batch fed MFC, then the biofilm bacteria go through three phases. The first stage involves a halt in growth until the nutrients reach the biofilm; the second phase describes an exponential growth followed by a stationary phase where no further growth occurs and soon after that the decay phase begins as the substrate concentration has been depleted [43]. For MFC operation, it is the exponential and the stationary phase where stable operation is achieved. Many researchers try to sustain this steady-state by maintaining optimal conditions using buffering agents, controlled temperature and highly concentrated carbon substrates. However, large substrate concentrations tend to inhibit enzyme activity [33] and along with the high maintenance required it is suggested that batch mode is far from feasible for wastewater situations [44]. On the contrary, continuous flow systems can maintain steady-states in MFCs and this study will endeavour in recreating semi- or continuous flow wastewater treatment scenarios wherever this is feasible.

1.3.2.3. Energy from wastewater

The use of an anode as a final electron acceptor and the mediator-less MFCs have led to the possibility of a wide range of applications in terms of viable alternative energy sources with numerous concomitant benefits, such as waste food and wastewater treatment, pure water generation (from the cathode), the potential to sense and measure the environmental Biological Oxygen Demand (BOD) and the levels of water contaminants [20]. One of the most active areas of MFC research is the production of power from wastewaters combined with the oxidation of organic or inorganic compounds. The first reported use of real industrial wastewater was in 1978 [45] whereby immobilized cells of *Clostridium butyricum* were used for hydrogen production. Studies that followed have demonstrated that any compound degradable by bacteria can be converted into electricity. The range of compounds included, but not limited to, acetate [46], glucose [47], starch [48], cellulose [49], wheat straw [50], pyridine [51], phenol [52], p-nitrophenol [53] and complex solutions such as domestic waste water [54], brewery waste [55], landfill leachate [56], chocolate industry waste [57], mixed fatty acids [58] and petroleum contaminates [59]. For the purposes of this study, activated sewage sludge (mixed with TYE) or real human urine were employed during the following experiments without the use of buffering agents.

1.3.3. MFC operation parameters

In its most basic form, a MFC is a device that uses microorganisms to generate an electrical current through the oxidation of organic matter. Figure 1.1 shows a generic schematic of how a MFC works. Anaerobic microorganisms oxidize organic substrates in the anode chamber and they liberate both electrons and protons to an electrode. Electrons are transferred to the anode and then to the cathode through an

electrical network. Protons travel from an anode compartment to a cathode compartment through an electrolyte membrane (i.e. electronically insulated proton-exchange membrane) or a salt bridge [60], and combine with the electron and a catholyte, containing a chemical such as oxygen, which is reduced at the cathode surface. As such, an electrical current is generated in a fashion similar to a chemical fuel cell, but with microbes acting as a biocatalyst on the anode surface. Catalysts generally increase the rate of a reaction without being changed by or receiving energy from the reaction they catalyse. The microbes in a MFC are not true catalysts since they obtain energy from the oxidation of the substrate to support their own growth and result in an energy loss. Microbes in a MFC may gain all the energy and carbon required for cellular growth, from the oxidation of the complex organic material and as such MFC technology has been considered self-sustaining [61]. As long as the microbes continue to be fed, a MFC has the potential to produce electricity indefinitely.

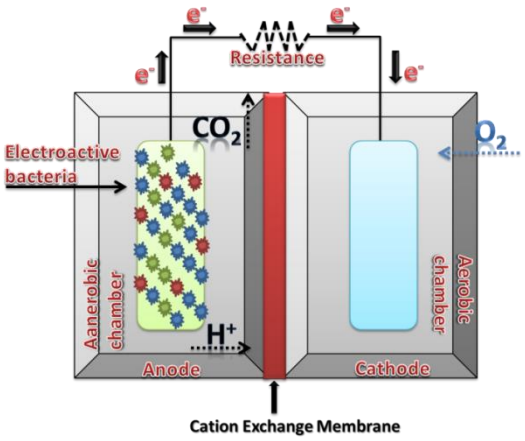

Fig. 1.1 Schematic of a dual chamber MFC. Anaerobic microorganisms oxidise organic matter in the anode chamber. Some microorganisms attach to the electrode as a biofilm and the electrons are transferred directly to the electrode and then through a wire to the oxygen diffused cathode, where the electrons reduce oxygen

to water. Protons are transferred in the same direction through a proton-exchange membrane [62].

1.4. Stacking of MFCs for powering real-word applications

1.4.1. Principles of stacking

Many research groups have attempted to improve power output from MFCs by isolating specific microbial species [60], by selecting strains that produce mediators [13,63], or by electrochemical optimisation of the electrode surface [64]. MFC voltages will inevitably never exceed redox limits; even neglecting the internal losses, open circuit voltage (OCV) will never transcend a theoretical of 1.14 V as determined by the NADH (0.32 V) and pure oxygen (0.82 V) redox potentials [65]. Moreover, 1.14 volts can never be achieved if the MFC is operating at MPP where voltage will be at 50% of this value (~ 0.57 V). The maximum current on the other hand is determined by (i) the MFC structure which determines the electrochemical losses (i.e., internal resistance) and electron transfer limitations [63,66], (ii) the fuel concentration which represents the total amount of electrons delivered by the substrate for current production, and finally, (iii) the Coulombic efficiency.

An effective way to increase the performance of individual MFC units is through the connection of multiple MFCs in stack configurations [3,67–73]. When connected in stacks, voltage, current or both can be stepped up depending on the stack size and configuration. A study from Ieropoulos *et al*., (2010) [42] suggests that smaller MFCs are more efficient in power generation compared to larger MFCs [73]. However, electricity production in a MFC is a bioelectrochemical process that adheres to external conditions [42,66]. Therefore, the external circuit may also affect electricity generation.

Connecting stacks of MFCs in series or parallel is the principal towards increasing the produced voltage and current. When a number of MFCs are connected in series the voltages add up, and the same current flows through all MFCs [74]. Conversely, if a stack of MFCs is connected in parallel, the voltage averages and the currents are added. Provided that an appropriate number of MFCs are connected in series and parallel, then any possible current or voltage can be achieved. A study in 2003 [71] operated a small robot, the first of the EcoBot series, by connecting 8 batch-fed MFCs with ferricyanide catholytes in a series/parallel configuration.

Parallel connection maximises current output but the operational voltage will be unamplified making it necessary for booster circuits to be developed. A practical electrical power source should have a nominal output voltage (V_{out}) that is higher than the threshold of the semiconductor components used in the circuit. For example for a Si based diode, a minimum of 0.7 V is required to switch on the diode. If the MFC needs to power a digital circuit, and if Low-Voltage Complementary Oxide Semiconductor (LVCMOS) components are used, then a voltage range of 3-3.5 V is needed. Voltage booster circuits have been used for MFC applications to achieve this level of V_{out} [75].

1.4.2. Implementation of MFC stacks in robotic applications

The epitome of MFCs utilising unrefined organic matter was a partially energetically autonomous robot (EcoBot-II) in 2006, developed by the Bristol Robotics team [67]. This was the first robotic application in the world which was powered with crude organic matter. EcoBot-II integrated 8 MFCs containing sludge in the anode as a bacterial source and consumed insects (flies), crustacean

organisms (prawn shells,) and fruits (peaches, pears, apples, plums). The predecessor of EcoBot-II, was EcoBot-I. It had 8 MFCs with *E.coli* inoculum and generated electricity by oxidising sugar [68].

The same team developed in 2010, a robot by the name EcoBot-III. It is so far the first self-sustainable robotic application which features an artificial stomach. EcoBot-III is capable of collecting food, digesting it with an on-board artificial stomach, distributing it to a stack of 48 MFCs and uses this power to perform tasks (i.e. temperature logging, moving and pump actuation) [69].

Prior to the EcoBots, two more robotic applications powered by MFCs were built to demonstrate the potentials of MFC technology. In 2000, Stuart Wilkinson developed a mobile robot platform (Gastronome) which derived its power using *E.Coli* K12 with sugar forms like sucrose, dextrose, or fructose [70].

Objectives

The main purpose of this study is to develop large-scale MFC stacks that consist of small-scale units with enhanced performance and sophisticated energy harvesting capabilities for powering robotic platforms that can remediate wastewater. For that reason a series of objectives were set:

a) Design a new small-MFC reactor with easier assembly and less manufacturing resources compared to an existing one of the same internal volume.
b) Testing of different 3D printing materials for building MFC reactors and the effect that their properties have on the overall performance.
c) Improve power generation using lower resistivity and high surface area carbon materials in the cathode compared to standard carbon veil.
d) Investigate the effect on COD to Power ratio by re-configuring fluidically and electrically a 24-MFC stack that utilises real human urine.
e) Develop a new and more efficient way for harvesting energy from MFC stacks whilst exploring the feasibility of an energy autonomous power management system.
f) Examine whether the implementation of the above findings could efficiently run a robotic test-platform and showcase self-sustainable behaviour.

Chapter 2

Parts of the following results presented in this chapter have been published in:
Papaharalabos, G., Greenman, J., Melhuish, C., & Ieropoulos, I. (2015)**. *A novel small scale Microbial Fuel Cell design for increased electricity generation and waste water treatment*.** International Journal of Hydrogen Energy, **40**(11), 4263–4268.

2. Design and optimisation of MFCs

The first experimental chapter focuses on the architecture and rapid prototyping materials used for building MFCs and how their structural properties can affect the overall performance.

2.1. Miniaturising MFC reactors

2.1.1. Current prediction for small MFCs

Miniaturisation of MFCs has been reported in the literature as a more efficient way of generating electricity [42] and powering small devices [76]. Small MFCs can generate higher power densities from a single MFC and the consequent assemblage in stacks results in operational voltages that can drive standard electronics[77]. To date, the highest volumetric power density of miniaturised MFCs reported, is 2,300 W/m^3 [78]. Although this is still 1000-fold lower than that of small lithium-ion batteries (7.2×10^7- 2.16×10^8 W/m^3, with a theoretical density of 3,000 kg/m^3) [79,80] which are widely used for running the majority of electrical devices; **MFCs can generate electricity from waste and last for as long as they are supplied with sufficient feedstock with non-existent carbon footprint and zero cost**. As such, this has led to a rapid development in terms of current density by over a 1000-fold [79] from

MFCs during the last decade and foresees promise that small MFCs can become a part of the energy harvesting community.

2.1.2. Physical & biochemical advantages of small-sized MFCs

Whilst reducing the dimensions of MFCs, some physical phenomena have shown to affect the performance and have shed light into the downsizing process. For instance, according to the diffusion law, when characteristic length goes down by one order of magnitude, the time for diffusion reduces by two orders of magnitudes. Also, as characteristic length decreases, forces such as surface tension and electrostatic force become dominant over inertial force [81]. The availability of substrate on the established biofilm of the small-sized electrodes is greatly increased in small-size MFCs. Hence, the mass transfer flux of substrate from the suspended solution to an anode becomes higher, and the anodophilic biofilm is exposed to higher substrate concentration. Assuming that the anodophiles establish a dense biofilm on the anode, the current density improves as the size of MFCs decreases. When the substrate flux is less than the consumption rate of anodophiles, the voltage drops significantly, resulting in lowering the power density [82]. This is often observed in macro scale MFCs, thus agitation is essential to increase the mass transfer of substrate at the large, but not at the small scale.

The limitation of proton transport inside the biofilm creates a proton redundancy and a concomitant acidic environment in the biofilm. High concentration of protons inside the biofilm impedes the metabolic activity of anodophiles [83]. This results in an increase of the internal resistance and a consequent loss in power [84]. In macro scale MFCs running under continuous flow, the pH gradient in the anode, is maintained close to neutral levels, as the flow of fresh anolyte neutralises the acidic environment

of the anode. As MFCs become smaller, neutralisation of the pH is greatly enhanced. This effect, along with the improved mass transfer capabilities of small-scale MFCs, enhances the reaction kinetics of the anodophiles and leads to higher power densities.

Overall, small scale MFCs benefit from (i) lower activation losses, and (ii) higher substrate utilisation (mass transfer), due to decreased diffusion resistance, which lowers the overall internal resistance [74,85]. As the surface to volume ratio is inversely proportional to the length scale, this ratio increases in small scale MFCs, gives more surface area at a given volume, and favours surface-based anodophilic reactions. On a small scale, the Reynolds numbers (Re) are relatively low thus, laminar flow occurs. Therefore, the fluidic fusion in the anode is due to diffusion, while convectional flux is minimized [84,86]. Moreover, two studies in 2008, suggested that large volume reactors suffer from higher ohmic and mass transfer losses because of the inactive reactor volume and diffusion limitation in high surface area (s.a). electrodes[87,88].

2.1.3. Reactor configuration of small-scale MFCs

When miniaturising MFCs, the dimensions and the electrical properties of materials change, and as a result this contributes significantly in minimising energy losses [89]. The electrode surface area decreases, therefore the distance that electrons need to travel from the source to the external circuit is decreased. This distance is negligible in small sized MFCs and it may not affect the total internal resistance, but in large scale MFCs, where the total internal resistance is 10-times larger; electrode resistance is the main attribute of the total potential loss [90]. Likewise, the internal resistance is affected by the electrolyte, and decreases as the

distance separating the anode and the cathode is shortened [90]. It has also been suggested by a study in 2008 that the positioning of the anode perpendicularly to the cathode showed a 36% increase compared to the parallel orientation of the electrodes [90].

Various types of MFC reactors have been developed from MFC research groups, including miniature, cylindrical, up flow, and stacked reactors either dual chambered (Fig. 2.1) or single chambered (Fig. 2.2) [62]. The BBiC team achieved high power densities using small, single-chamber MFC reactors (6.25 mL) which bear catalyst-free carbon fibre veil electrodes and generating 0.44 W/m^3 [88]. A scale up strategy was evaluated by constructing medium (29.63 mL) and large (500 mL) MFCs and comparing their performance with that of a 6.25 mL in continuous flow mode. The small MFC showed a 1.2-fold and 1.9-fold increase in power density, compared to the medium and the large MFC respectively. This suggests that power output can be significantly increased during MFC scale-up by utilising a greater number of smaller MFC units into stacks using appropriate material and design strategies [42].

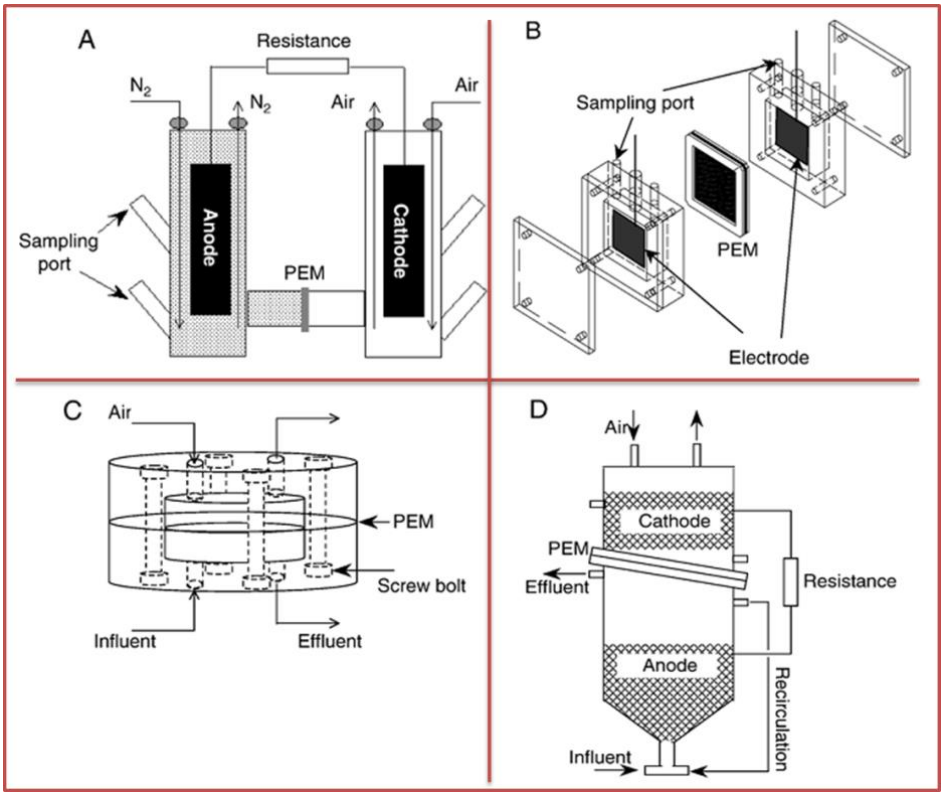

Figure 2.1. (A) Dual-chamber cylindrical MFC, (B) rectangular, (C) mini-MFC, (D) cylindrical with up flow configuration. Source: Du *et al*., 2007.

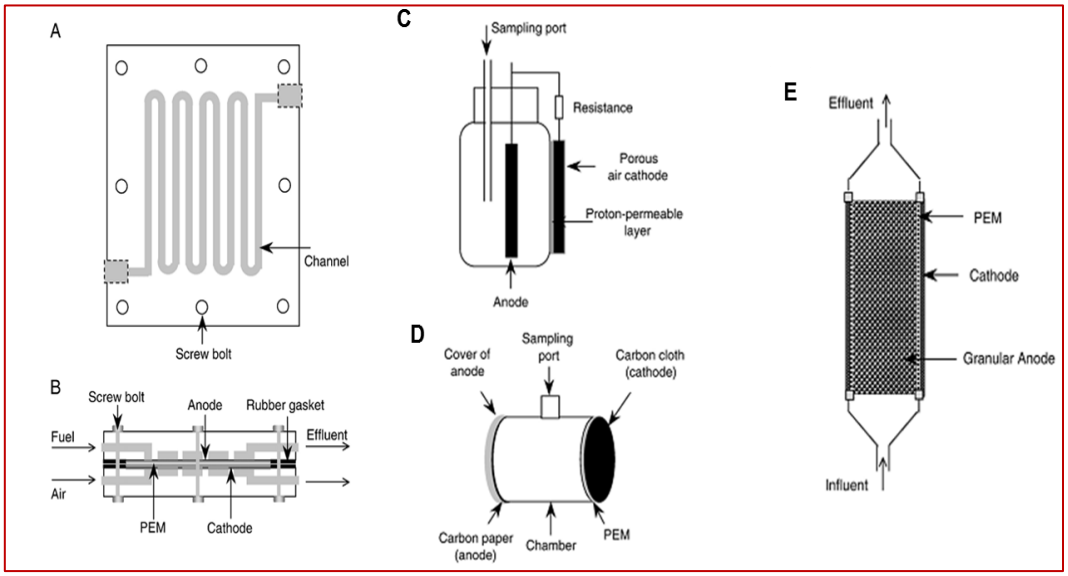

Figure 2.2. Single-chamber MFCs, (A) top view of a flat plate MFC and (B) side view, (C) IEM layer coating on the window-mounted cathode, (D) cylindrical MFC with anode and cathode separated by a IEM, (E) tubular MFC with anode and cathode consisting of graphite granules. Source: Du *et al*., 2007.

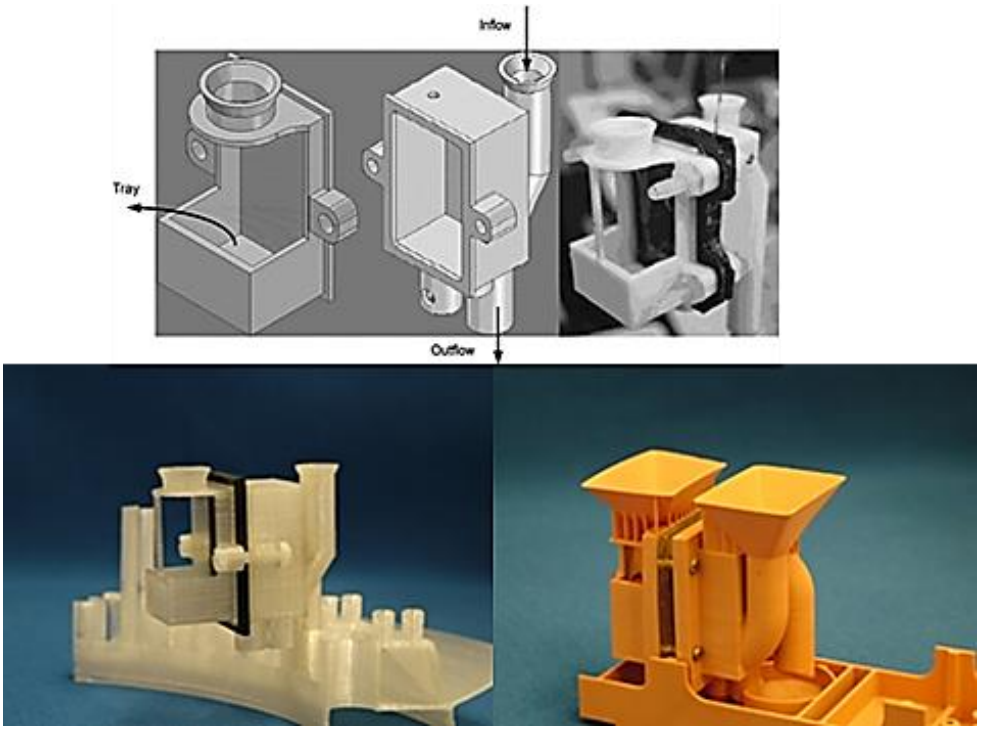

Figure 2.3. Small-MFCs developed from the Bristol BioEnergy group using in-house 3D printers.

2.2. Manufacturing materials of small MFCs

To date, most studies have been focusing on the improvement of electrode materials or the reactor's architecture [62,91–94]. The majority of MFC publications, involves MFC casings made out of glass (borosilicate) or Plexiglas (polymethyl-methacrylate, PMMA or Perspex) [38,62,95,96]. However, little is known about the selection of manufacturing materials used to build MFC reactors and only a few studies report MFC reactors made of various thermo-polymer plastics (polypropylene, polycarbonate, nanocure and acrylonitrile-butadiene-styrene) [67–69,71,97–101] where their effect on performance is examined. So far the main reason for experimenting with plastic polymers is the structural properties of thermoplastics that allow for a variety of shapes and sizes to be created and their material resistance to acidic environments.

This study focuses on the building materials and the reactor architecture of a novel MFC design (*Twist n' Play*) and highlights the fact that when developing a MFC reactor, the construction material should be biocompatible, built for electrical insulation and minimal oxygen intrusion in the anode chamber so that higher power outputs can be achieved whilst maintaining functionality with a decreased system cost.

2.3 Materials and methods

2.3.1 *Twist n' Play* MFC-chamber design and fabrication

2.3.1.1 Improvements compared to the EcoBot-III MFC casing

In order to evaluate performance standards of the new design and the materials involved, a direct comparison with an already proven small-sized MFC [69] of the same internal volume was performed. For this reason three RC25 Nanocure type EcoBot-III MFCs were used as controls so as to examine whether the architecture of the new design MFC or the materials involved in the making, can improve the performance. The new '*Twist n' Play*' MFC casing was designed using SolidWorks education Edition 2010 SP 5.0 software (Dassault Systemes, US) and maintained the same internal reactor volume (6.25 mL) as the fully tested model (EcoBot-III MFC) developed in 2008 and finalised in 2010 [69,88]. The improvements on the new MFC design comprised the following features:

a) Same internal volume with smaller external footprint (less building and support material).
b) Simple assembly without fixtures such as screws, clips or clamps.

c) Minimised exposure of the anode chamber to atmospheric O_2.

2.3.1.2 3D printing of the new design

In-house rapid prototyping facilities were employed to fabricate the new MFC (Fig. 2.4) in three different thermoplastics: PC-ISO (medical-grade biocompatible Polycarbonate; Laserlines, UK), ABS (Acrylonitrile Butadiene Styrene; Laserlines, UK) and RC25 Nanocure (ceramic-filled photo curable resin; envisionTEC GmbH, Germany). MFCs made out of RC25 nanocure were fabricated with a Stereolithography 3D printer, whereas PC and ABS MFCs were produced using the method of Fused Deposition Modelling (FDM Titan/Dimension BST, Laserlines, UK). Due to the hygroscopic nature of ABS, parts were coated with a layer of methyl-ethyl-ketone (Sigma-Aldrich, UK) so as to render the units watertight.

The selection of the above materials was based on previous studies [42,69,76,77,88,98,102–104], in which they were considered to be the most common thermoplastics used for rapid prototyping and also they could be fabricated in-house.

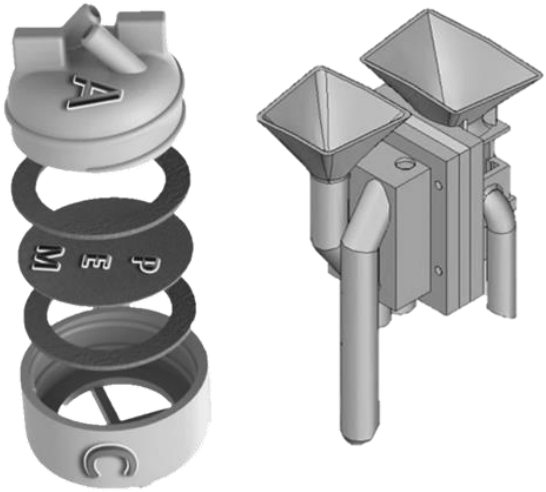

Figure 2.4. (Left) *Twist n' Play* MFC design. (Right) EcoBot-III control MFC design assembly made from RC25 Nanocure.

2.4 MFC operation and monitoring

2.4.1 Inoculation and fuel supply

Triplicates of single-chamber air-breathing MFCs were assembled for each material; both the anode and the cathode electrodes employed catalyst-free carbon fibre veil sheets 30 g/m^2. Sheets of 11 x 14 cm (155 cm^2, total surface area) were folded down five times so as to form a 1.8 cm x 2.9 cm x 1.0 cm cuboid. Titanium wire was used as a current collector, pierced through the carbon veil cuboids. An ion exchange membrane (CMI-7000, Membranes International Inc., NJ, USA) with a s.a of 12 cm^2 was placed between two silicon rubber gaskets, separating the anode from the cathode. The MFCs were initially inoculated in batch-mode with activated sewage sludge (Wessex Water, Saltford, UK). Anolyte pH was 7.3 and replenished every 24 hours with 1 mL of TYE (1% Tryptone, 0.5% Yeast extract, Fisher Scientific, UK) for the first 14 days of the experiment. A 2.7 kΩ resistor was connected to each MFC during this period for selecting an anodophilic bacterial consortium; this value was selected in order to best match the R_{int}. Following 15 days from inoculation, the feedstock was replaced with fresh non-treated human urine and all MFCs were connected to a 24-channel peristaltic pump (Watson Marlow, UK) for continuous flow, at a rate of 1 mL/h corresponding to a hydraulic retention time (HRT) of 6.8 h. Samples were received on a daily basis at fixed time of the day from a healthy individual. Measured pH on fresh urine samples ranged between 5.5 and 5.8, conductivity was 38 mS/cm average, and the mean chemical oxygen demand (COD) value from a sampling period of 20 days was 15.5 g/L. All experiments were conducted under an ambient temperature of 22 ^{o}C ± 2.

2.4.2 Power curves and data collection

Individual MFC and overall stack (triplet) voltage was recorded using a HP Agilent multiplex logging unit (34907A, HP). The performance of individual MFCs and triplets was measured by applying a range of 50 resistance values from 30 kΩ down to 3 Ω every 3 minutes using an automated variable resistor [105]. Voltage was measured in V (V), and current (μA) was calculated according to Ohm's law, I=V/R. Power in microwatts was subsequently calculated from P = V*I. Power density (P_D) was calculated by dividing the absolute power (μW) by the total electrode s.a (***α*** = 155 cm^2) and expressed in square-metres (m^2). Similarly, the current was divided by the electrode's ***α*** so as to estimate the current density (C_D). Recorded data were processed into detailed graphs using GraphPad Prism® version 5.01 software package (GraphPad, San Diego, California, U.S.A.).

2.4.3 Chemical Oxygen Demand (COD)

For measuring the COD of fresh urine, high range (0-20000 mg/L) potassium dichromate oxidation method (CAMLAB, UK) was used and COD values were calculated via colorimetric analysis (Photometer-System MD200, Lovibond). Fresh urine samples (200 μL) were filtered (0.20 μm, Minisart®) and COD content measured prior to entering and after exiting the MFCs (24-48 h). Treated urine samples were initially filtered and then centrifuged at 500 g for 5 minutes.

2.5 Results & Discussion

2.5.1 Performance from Individual new design MFCs

The materials selected in this study were based on 3D printing suitability and use in MFC work, as well as biocompatibility with respect to microbial toxicity. Specific

toxicity analyses were not performed however, implicit information could still be drawn from the MFC performance levels; possible toxic effects from the structural material, would have detrimentally affected the MFC performance.

Results shown are from 20 days (D20) and 40 days (D40) after inoculation, and there is clear evidence in terms of improvement in performance due to maturity. The 20-day point was chosen as a point in the transitory period following urine addition as the fuel, and the 40-day point was chosen as an exemplar of steady state conditions (Fig. 2.5). Polarisation runs on individual units 20 days after inoculation (Fig. 2.6) showed that the new design MFCs outperformed the control units in all three different material cases by a maximum of 74% in terms of power. The control MFCs produced a MPP of 31 μW (2 mW/m^2) at 121 μA (8.1 mA/m^2). MFCs made of PC-ISO showed the highest power and current generation amongst the different materials with values of 54 μW (3.6 mW/m^2) and 136 μA (9.1 mA/m^2) which was 74% and 12% higher than the control values respectively. The second best performing MFC material was the RC25 Nanocure, reaching 44 μW (2.6 mW/m^2) and 136 μA (9.1 mA/m^2) which was 42% higher power and 12% higher current compared to the control. MFCs built with ABS showed also 16% higher power generating 36 μW (2.4 mW/m^2) and a 7% increase in current to 130 μA (8.7 mA/m^2). To assess performance after a further period of maturity, polarisation experiments were carried out for individual units 40 days *post* inoculation, so as to examine establishment of the electro-active biofilm (Fig 2.5). With respect to the maturing between the D20 and D40 period, the control MFCs power improved to 50 μW (3.3 mW/m^2) and the current output to 210 μA (14 mA/m^2), which resulted in an increase of 61% and 73% respectively at the end of the 40 day period. As in the early stages, a similar order in performance was displayed with PC-ISO MFCs increasing their MPP by 22% to 66

μW (4.4 mW/m^2) and the average current by 160% to 354 μA (23.6 mA/m^2); RC25 Nanocure MFCs increased their power output by 29% to 57 μW (3.8 mW/m^2) and the current output to 329 μA (21.9 mA/m^2) an increase of 141%; ABS units produced a power of 50 μW (3.3 mW/m^2) and a current of 218 μA (14.5 mA/m^2) which stands for an increase of 38% and 67% respectively. In terms of performance differences amongst the examined MFCs compared to the control 40 days after inoculation, the PC-ISO, the RC25 Nanocure exhibited an increase in power by 32% and 14% respectively. The current was also higher by 68% (PC-ISO) and 56% (RC25). In the case of ABS, the power was similar to the control and the current showed only an increase of 4%. Power sweeps performed in this extended period after the inoculation presented overshoot peaks in the graph for all the examined materials and designs. This could suggest that the biofilm had yet to reach the maturity stage or the resistance value intervals rate were too large and fast for the biofilm to establish a steady state [106]. In both maturing stages all MFCs displayed a similar internal resistance of 2 kΩ, where MPP was achieved.

These results are consistent with findings from a previous study by Ledezma *et al.* (2010) that compared ABS, RC25 and PC-ISO as structural materials for a larger size (25 mL) and different architecture dual-chamber MFC [98]. Moreover, the increased outputs from the new *Twist n' Play* design when compared to the control EcoBot-III MFC casing built in 2008, suggest that the improvements made on the design led to a more functional anode chamber, which allowed for better biofilm establishment conditions and electricity generation.

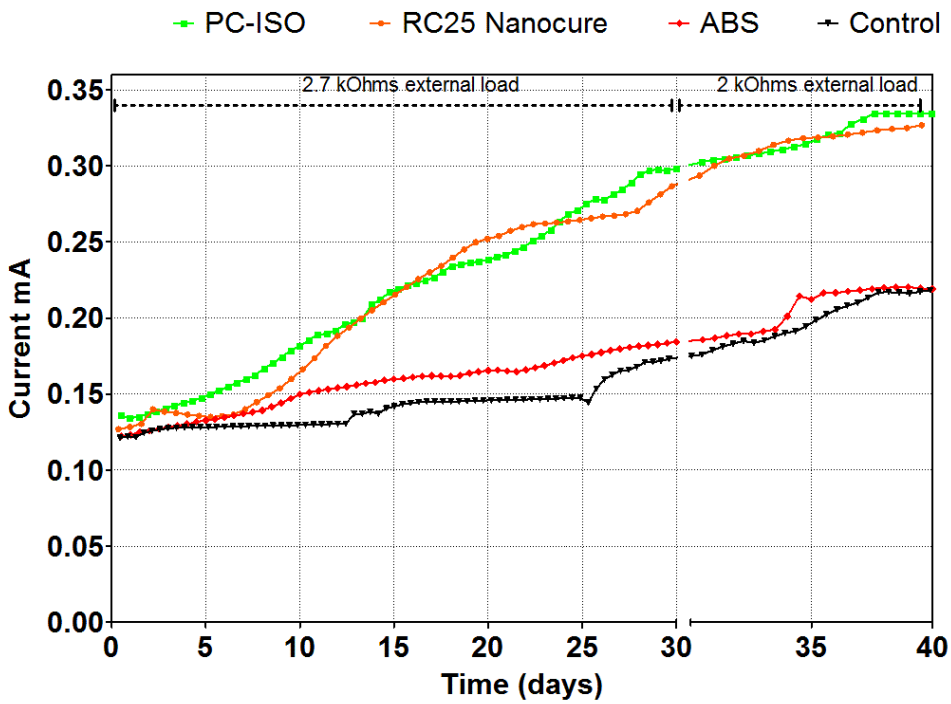

Figure 2.5. Current generation during 40 days *post* inoculation as an indication of biofilm maturity and the plateau phase near the end of this period.

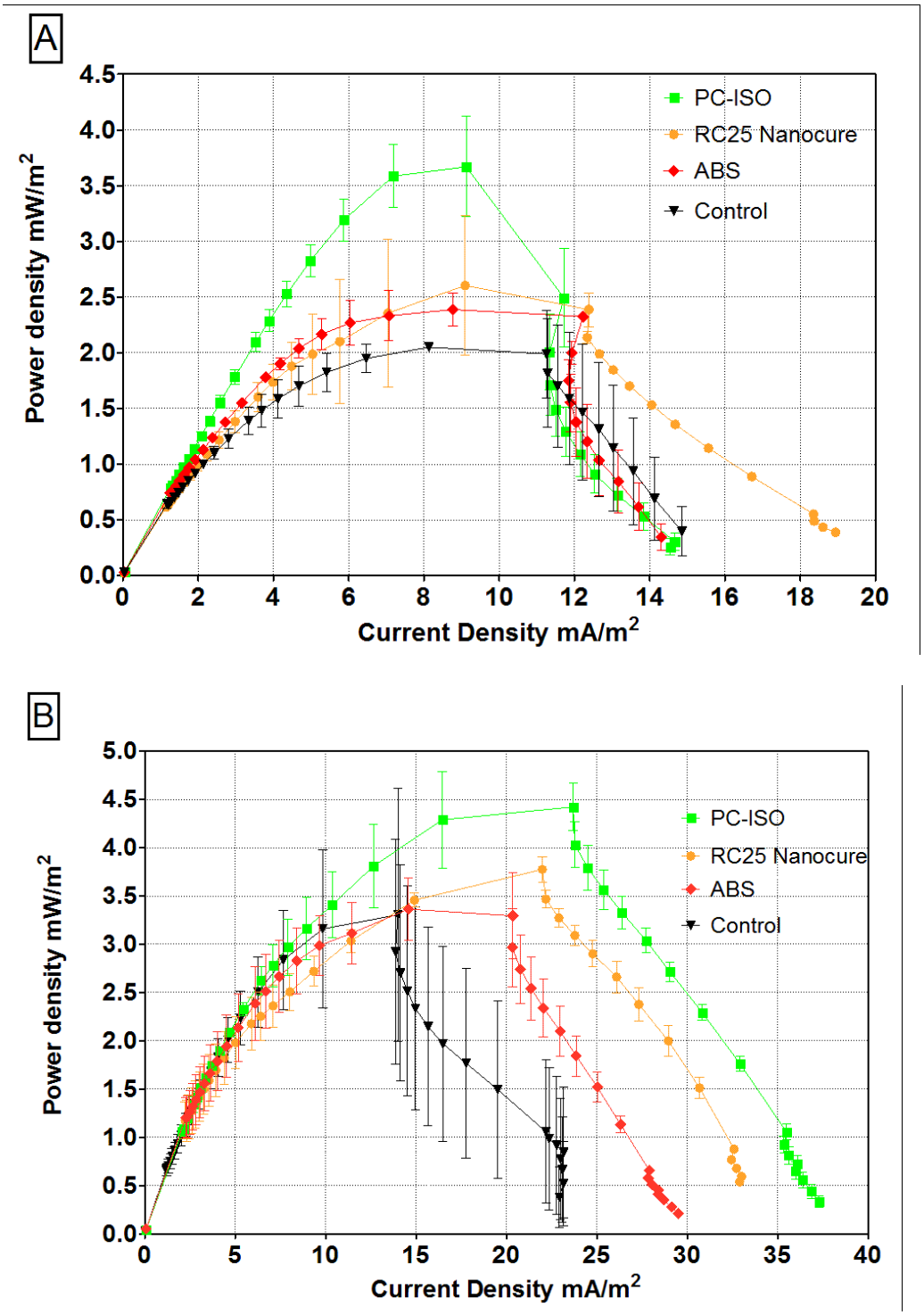

Figure 2.6. Power curves from individual units, (A) 20 days post inoculation and (B) 40 days after inoculation. (±SD n=3).

2.5.2 MFCs fluidically connected

2.5.2.1 Parallel electrical connection (n=3)

In this part of the experiments triplets made from the same material were connected electrically in-parallel, with fluidic connection between the units. Polarisation results showed a variance in performance based on the output from individual MFCs during D40 period. The control MFC triplet reached 129 μW (2.8 mW/m^2) at a current of 0.84 mA, (18.3 mA/m^2) (Fig. 2.7). The RC25 Nanocure triplet produced 203 μW (4.4 mW/m^2) and a current of 1.3mA (29 mA/m^2). ABS triplet generated 152 μW (3.3 mW/m^2) and 0.66 mA (14.3 mA/m^2). The PC-ISO MFC underperformed compared to the other new design MFCs generating 133 μW (2.9 mW/m^2) and 0.64 mA (13.8 mA/m^2).

With regard to P_D and C_D obtained from individual units, the control EcoBot-III design displayed a 15% decrease in P_D but a 30% increase in C_D. The parallel-connected MFCs made of RC25 Nanocure showed a 16% and 38% increase respectively. MFCs made of ABS, maintained similar P_D and C_D levels as the individual MFCs. Increases in C_D are to be expected due to the parallel electrical configuration of the MFCs in the triplets. On the contrary, PC-ISO new design parallel-connected MFCs decreased P_D and C_D by 34% and 40% respectively. A possible explanation for this reason could be the material's integrity, as it has the highest tensile strength of all materials but it possesses a very low endurance to fracture stress [107] especially after 40 days of operation under hydraulic pressure in the anode chambers. This led to the appearance of ductile tearing zones (Fig. 2.8) followed by ductile brittleness [108] on the external surface on all anode PC-ISO

casings, that allowed anolyte to leak, therefore allowing oxygen to penetrate into the anodes, affecting the overall performance.

The in-parallel configuration pushed the system collectively to a more optimum equilibrium which resulted in a decreased internal resistance for all tested MFCs and showed a uniform value of 105 Ω in all cases of 3 MFCs connected in-parallel, which is equivalent to a 315 Ω for an individual MFC, whereas the internal resistance from individual units at the beginning of the experiment was 10-times higher. Control MFCs exhibited a 305 Ω internal resistance which stands for a theoretical of 915 Ω in an individual unit which equals a 2.2-fold decrease compared to their resistance at the start of the of this study.

Again the newly designed MFC proved to be superior over the control MFC architecture with the exception of the PC-ISO and an overall comparison between the *Twist n' Play* and the control RC25 Nanocure highlighted the improvement of the new design.

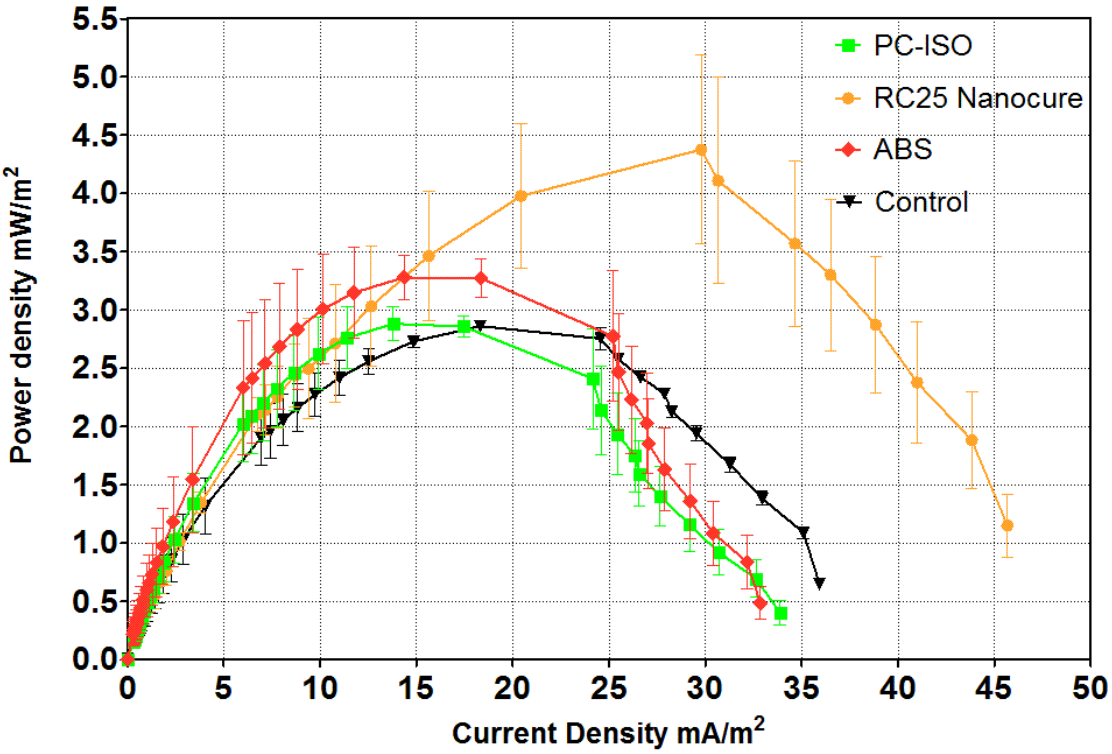

Figure 2.7. Performance of MFCs when connected in-parallel.

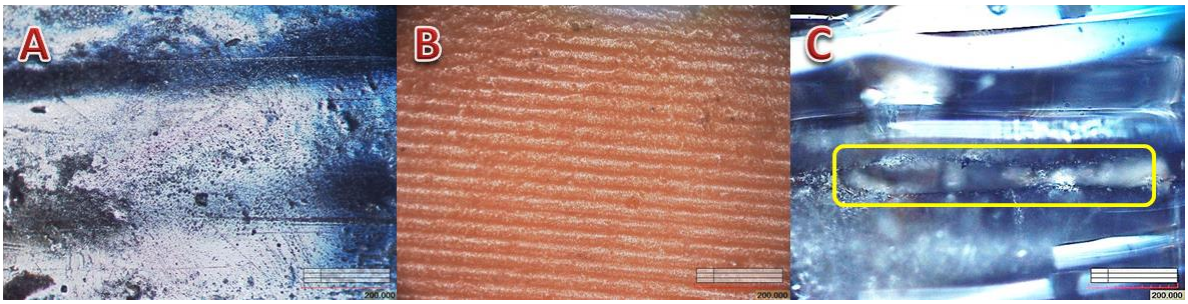

Figure 2.8. Characteristics of the (A) ABS with the porous surface, (B) the RC-25 Nanocure with the ceramic integral ruffled surface and (C) the PC-ISO with a cavity highlighted. Micrometre reference: 200um.

2.5.2.2 In-series electrical connection (n=3)

The next stage of the experiment involved triplicates from each material being connected electrically in-series and each triplet group was connected to a single feeding channel. Because of its architecture, the new MFC design, allows for tubing connection between MFC units, thus maintaining hypoxic conditions in the system, but favours fluidic short-circuiting [88] and could possibly lead to a reduced performance. Conversely, the control MFC was designed for cascade operation. This involved a vertical orientation of the MFC units placed underneath each other so the anolyte was gravitationally moved from the first unit to the next one. This set-up created an air-gap between MFCs that provided hydraulic insulation but allowed for higher oxygen presence in the system [109].

The ABS-built MFC triplet outperformed the rest and showed an increase of 38% in power (P_D= 3.18 mW/m^2) and 54% in current production (C_D= 8.21 mA/m^2) than the control. The PC-ISO triplets produced 30% more power (P_D= 2.83 mW/m^2) and 36% more current (C_D= 5.93 mA/m^2). MFC triplets constructed from RC25 Nanocure, generated 28% more power (P_D= 2.74 mW/m^2) and 51% higher current (C_D= 7.64 mA/m^2). The control MFC triplet maintained similar power density levels (P_D= 1.96 mW/m^2) as in the individual set-up and a showed a 50% reduction of current output (C_D= 3.75 mA/m^2) also (Fig 2.9.).

2.5.2.2.1 Electrical shunt losses from hydraulic conductivity

Polarisation results on the stacked triplets showed an overall increase in performance from the *Twist n' Play* MFCs compared to the control. Nonetheless, power levels were lower when compared to individual units, which in terms of power densities, the new design MFCs made of PC-ISO and RC25 Nanocure were reduced

by 30% and 14% respectively. Additionally, C_D was negatively affected in both materials by 49% in the PC-ISO and 26% in the RC25 Nanocure. The reason behind this diminution is probably due to the fluidical connection within the triplet's MFCs. This phenomenon has previously been reported in the literature [88,110] and it has been observed to decrease the performance when stacked MFCs are connected in-series electrically and feedstock is supplied through a common pathway. As such, the resistance of the anolyte acts as a load between the cathode of the first and the anode of the next MFC hence allows for a parasitic current to flow through the anolyte. However, the power from the control MFC triplet showed little difference. This can be attributed to the fact that the cascade setup (air-gaps) between MFC units prevented the feedstock cross-conduction effect (shunt losses) from further decreasing the performance.

Interestingly, the ABS triplet MFC increased by 18% its power performance and by 8% the current production even though there was a hydraulic connection opposing the performance of the other materials under the same operating conditions. A similar phenomenon was noticed from Ledezma in 2011 [111] when stacked MFCs were exposed to different wet conditions so as to investigate shunt losses in hydraulically stacked MFCs connected electrically in-series. Results from this study showed that the inconsistent behaviour of the ABS material in wet and dry conditions were in complete discordance with the other materials operated in the same manner. Therefore, this antithetic pattern suggested that it was best to avoid building MFCs from ABS for stacking purposes due to the hydroscopic effects and conductance across the material.

Finally all new design MFCs showed uniformity in their internal resistance at 1 kΩ, whereas the control EcoBot-III design produced the maximum power point at 2 kΩ. Regardless of the increased losses in this setup, new design MFCs showed a lower internal resistance and better overall output compared to the control MFC setup where no shunt losses were allowed to occur. Nevertheless, the open surfaces of the EcoBot-III design MFCs, permeated oxygen to interact with the anolyte and competed with the anaerobic biofilm limiting the biofilm's electro-genic efficiency.

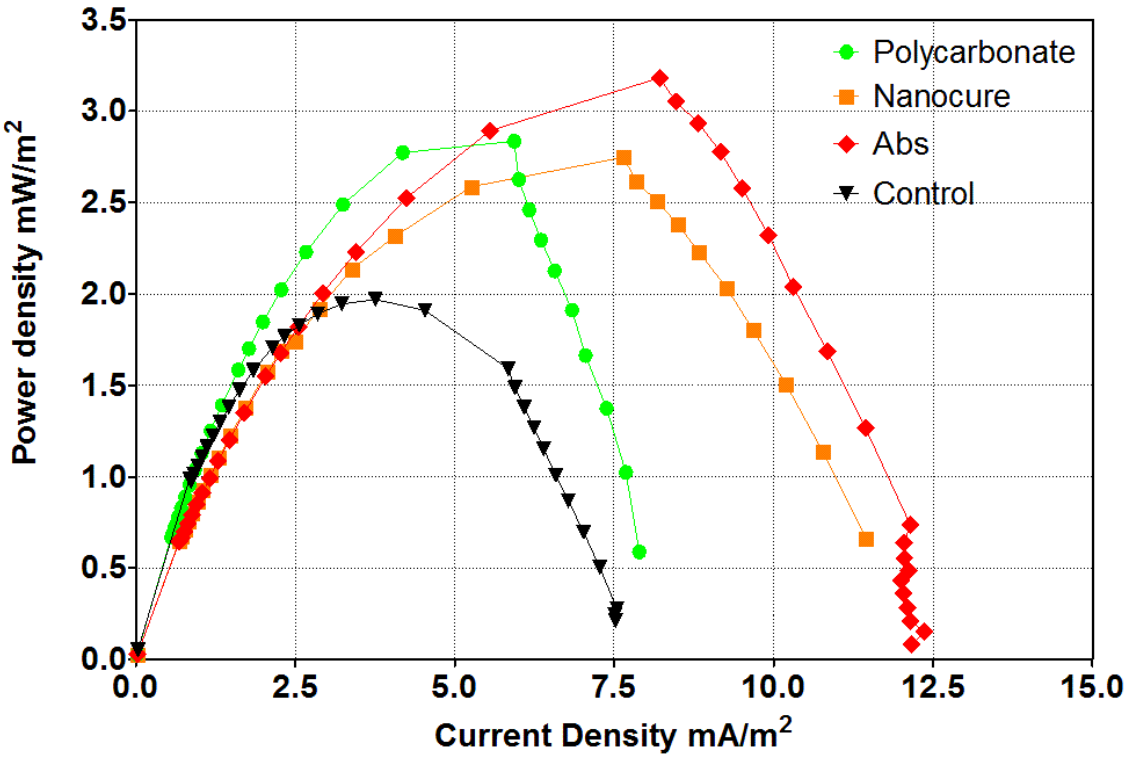

Figure 2.9. Power curves from MFCs connected electrically in-series.

2.5.3 COD reduction

2.5.3.1 Individual units

The new MFC design was tested in terms of COD reduction, both as a stand-alone unit and when in stack operation configured electrically in-parallel. For the

sake of consistency the original COD value of the urine sample used for all the individual units was 16.8 g/L on the day of the COD measurement. The control units reduced this value by 29% (11.9 g/L). MFCs made of PC-ISO achieved an average of 44% COD removal down to 9.4 g/L. RC25 Nanocure units reduced the organic content by 37% to 10.5 g/L. The mean COD treatment from ABS units resulted in 36% reduction of organic content of the original urine to 10.7 g/L. In terms of the MFCs running as individual units, the recorded COD removal was proportional to the order of power performance. It could therefore be suggested that the MFCs with the best performance characteristics are expected to achieve the highest COD removal within a number of MFCs displaying various outputs.

2.5.3.2 Stacked MFCs in-parallel (n=3)

COD values were recorded when MFCs of the same material were connected in-parallel. As it would be expected, COD remediation was increased when more elements were connected fluidically and configured electrically in-parallel [72]. In this case the initial COD content found in the supplied urine sample during the COD experiment was 19.4 g/L. The control MFC as in the individual test, showed the lowest range of removal, decreasing the COD value by 38% (7.4 g/L) to a level of 12 g/L. Again the PC-ISO triplet removed a total of 53% (10.3 g/L) which was the highest amongst the different materials. The COD value from the RC25 Nanocure stack was decreased by 46% leaving 10.6 g/L of COD in the treated sample. The ABS stack showed a similar COD treatment with the RC25, reducing the organic content by 45% down to a value of 10.7 g/L. It is important to point out, that the twist and play MFC was primarily designed to remain watertight and minimize oxygen presence in the anodic chamber when stacked in continuous flow mode, which was

not a feature of the control (EcoBot) MFC design. In all material cases besides the PC-ISO, the stacked MFCs treated the organic content of urine in line with the power outputs. Nonetheless, the high COD removal value from the PC-ISO was not in accordance with the power output, which could be related with the material's structural failure. It is expected that the failure resulted in extensive leakages and reduction/dilution of the samples, which probably affected the end-treatment product from the stack. Based on this material bottleneck, more experiments should take place to confirm the COD removal efficiency.

2.5.3.3 Stacked MFCs in-series (n=3)

Series electrical connections showed a similar ranking –as from individual MFCs- of reduction by respective MFCs. Even though shunt losses dominated the new design MFC setup, COD reduction from the PC-ISO (41%), RC25 Nanocure (31%) and ABS (29%) was higher than the control (25%). In all cases, the reduction was less than that from individual units suggesting significant energy losses because of the series connection. The new design MFCs were probably affected from the cross-conduction effect [110,112] and the control MFC was affected by the exposure to atmospheric oxygen anode.

2.6 Conclusions

In principle, a MFC's performance is affected by many variables, and behaviour of one factor may be directly influenced by other parts of the MFC. A common feature in the process that affects electricity production and COD removal is largely dependent on the materials used. It could be argued that the materials and conditions optimised for one type of MFC are not necessarily optimal for other MFC

types and structures. Several challenges need to be resolved, including high areal resistivity, high oxygen leakage and non-compatibility with micro-fabrication.

This experimental study showed how three versions of a novel MFC reactor can greatly affect their overall performance of MFCs under fluidic and electrical scenarios. The new design showed an overall increased performance compared to the control MFC reactor and depending on the electrical and the fluidic connection the RC25 Nanocure and the ABS seemed to perform better in terms of power and COD treatment of up to 15% increase whilst retaining better power and COD values than the control.

Even for rapid prototype materials, which are expected to be of a finite lifetime, RC25 Nanocure proved to be the most robust. These results demonstrate that the RP technology is a useful tool for examining various materials as structural elements for MFC reactors and the combination of the best performing plastic polymers, could possibly introduce a hybrid material that will advance miniaturisation of MFCs and provide ease of stacking, allowing for powering of real-world applications.

Chapter 3

Parts of the following results presented in this chapter have been published in:
Papaharalabos, G., Greenman, J., Melhuish, C., Santoro, C., Cristiani, P., Li, B., & Ieropoulos, I. (2013). **Increased power output from micro porous layer (MPL) cathode microbial fuel cells (MFC)**. International Journal of Hydrogen Energy, **38**(26), 11552–11558.

3. Power increase in MFCs

The second experimental chapter utilises a low-cost catalyst-free electrode as a cathode in small-size MFCs so as to improve reaction kinetics and by extension, the power output. It also demonstrates that the increase in power is sufficient enough for two small-MFCs to run for the time an off-the-shelf wristwatch.

3.1. Focus on cathode optimisation

A different approach to miniaturisation for improving power in open-to-air cathode MFCs is the efficient utilisation of oxygen on the cathode - higher ORR - by using high s.a materials with effective gas diffusion.

Oxygen is the most abundant and naturally occurring electron acceptor with a high redox potential (0.82 V). It has been suggested that the power output of a MFC can be greatly improved by increasing the surface area of the cathode electrode [40,41,113]. Greater surface area means larger number of active sites for the ORR, and the micro porous layer coating has been suggested as an efficient and inexpensive way of achieving higher active s.a [114]. A micro porous layer (MPL) is a mixture of carbon black nanoparticle powder and polytetrafluoroethylene (PTFE). Carbon black particles form a high surface area of carbon active sites, along with an extensive hydrophobic network created by the presence of PTFE. These two elements give the

ability to (i) facilitate oxygen diffusion through the inner structure and all the way to the ion exchange membrane (IEM) surface, (ii) produce water from the reaction with the incoming protons through the IEM, and (iii) avoid flooding due to the PTFE.

The present study builds on the previous work by Santoro *et al*. [114] and aims to compare the performance of small-scale MFCs incorporating MPL cathode electrodes, with control carbon veil electrode [88]. The specific aims of this study were to test (i) individual MFCs with the new electrode material, (ii) stacks of 3 MFCs in a series/parallel configuration employing the MPL electrodes and (iii) the effect that the MPL electrodes had on the hydration regime of the open-to-air cathodes. As a practical demonstration of the performance improvement from MPL, two small-scale MFCs were used to power a Texas Instruments Chronos digital wristwatch.

3.2. Materials and Methods

3.2.1. Small scale 6.25mL MFCs

Six open-to-air cathode MFCs, made from RC25 Nanocure resin in a 3D fabrication process, were used in these experiments. The internal volume of the anode compartment was 6.25mL, and the anode's electrode projected s.a was 6cm^2, as previously described[42]. All MFCs had an IEM (VWR, Leicestershire, U.K.) that was held between two rubber gaskets. For the duration of experiments, open-to-air cathodes were manually hydrated every 24 hours.

3.2.2. Electrode materials

A catalyst free carbon fibre veil (Fig. 3.1) with a carbon loading of 20g/m^2 (PRF Composites, Dorset, U.K) was used as the anode electrode for all 6 MFCs, with a total macro surface area of 156 cm^2. This was folded 5 times, in order to fit

into the anode chamber (18mm x 28mm). The same material and conformation was used for the cathode electrodes of the control-based MFCs.

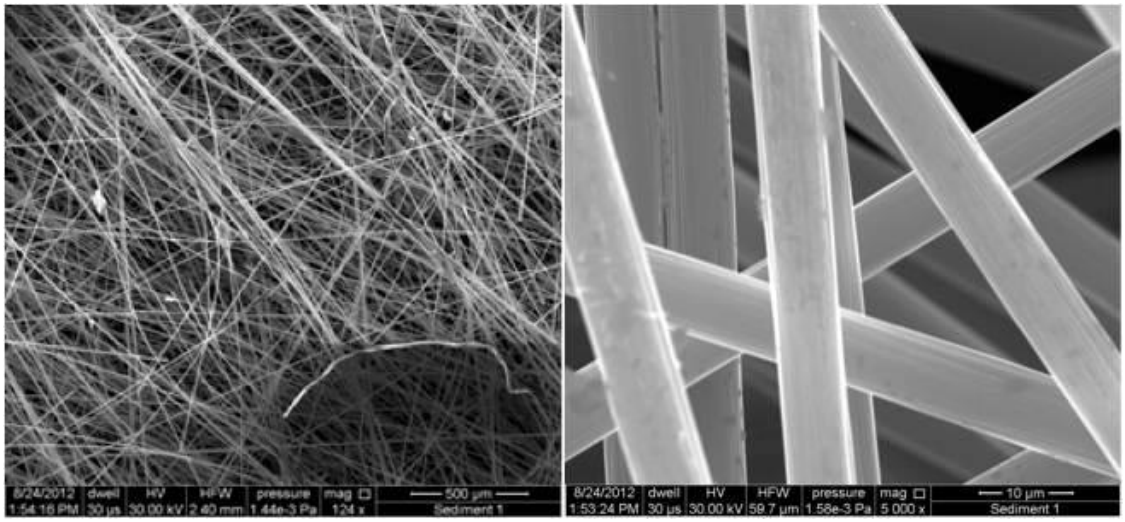

Fig. 3.1 SEM images of the control carbon fibre veil at two different magnifications (left, 120X and right, 5000X)

The scanning electron microscope (SEM) images at two different magnifications levels (Fig. 3.1) show the porous structure of the carbon veil electrode (control) as a means of comparing with the higher s.a. MPL (Fig. 3.2). The subject electrodes (2 layer carbon cloth/carbon black electrode) were made from a gas diffusion layer (GDL) and a MPL, forming a two-layer structure, 0.5 mm thick and 60 mm^2 geometric area (see Fig. 3.2). The GDL was made from carbon cloth treated with 30% by weight PTFE (FuelCellEarth) to ensure wet proofing. The MPL comprised a mixture of nano-sized carbon black particles (Vulcan XC-72R) (Cabot Corporation, Stanlow, UK) with a non-ionic surfactant (Triton X100, Sigma Aldrich), deionised water and PTFE (60% emulsion, Sigma Aldrich) [115–118]. The MPL forms a black thick paste that is applied to the GDL surface and then heated to 343^oC to allow liquefaction of the PTFE and penetration of the carbon nanoparticles in the

porous structure of the GDL [119–123]. Due to the carbon black nano-particles, the MPL consists of a high s.a, which is optimal for increased oxygen reduction [114,124].

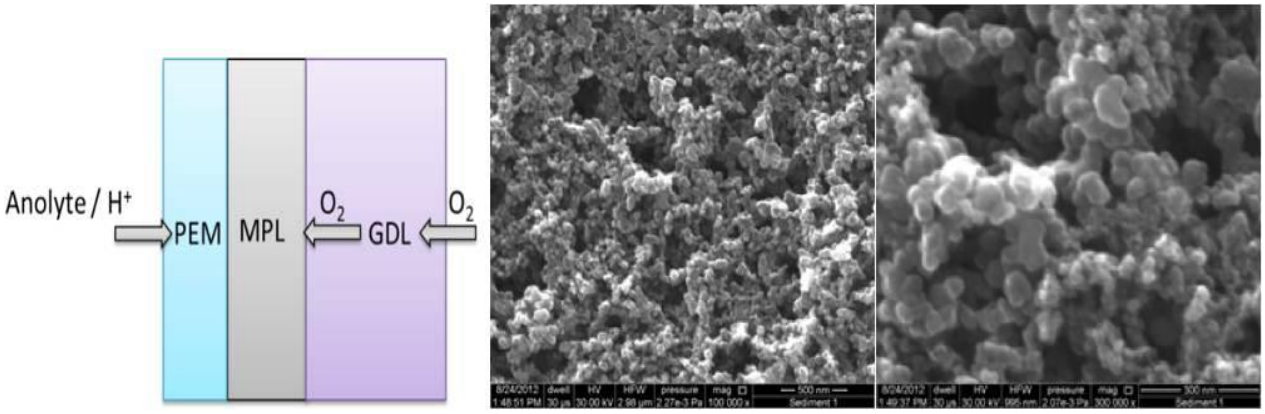

Fig. 3.2 (Left) Image of two-layer cathode with GDL and MPL; (Right) SEM images at 2 different magnification (100000X and 300000X middle and right image) levels of the active sites for ORR on a MPL surface.

3.2.3. Anolyte-Anaerobic sludge

Activated sludge supplied by the Wessex Water Scientific Laboratory (Saltford, UK), was initially used as the inoculum for these MFCs. Maturing of the biofilm inside the anodes was allowed over a period of at least 3 weeks, during which time the MFCs were frequently replenished (with sludge) and kept under a fixed load (8 kΩ). Following this maturing regime, the anaerobic sludge feedstock (pH 7.8) was mixed with TYE medium (Tryptone and Yeast Extract; 1% and 0.5%), for enrichment and batch-mode feeding took place every 4 days.

3.2.4. Data recording and processing

Real time voltage monitoring of the MFCs, was performed using an ADC-24 Channel Data Logger (Pico Technology Ltd., Cambridgeshire, U.K.). Voltage (V) was

measured in millivolts (mV) and the recorded data were processed using GraphPad Prism® version 5.01 software package (GraphPad, San Diego, California, U.S.A.). Current in amperes (A) was determined using Ohm's law, $I=V/R$, where (R) is the external resistor load in ohms (Ω). Power in watts (W) was calculated using Joule's law $P=IxV$. The power produced per electrode unit area was calculated by dividing power with the electrode's total surface area in square-metres (m^2), i.e. $P_{density} = P/\boldsymbol{\alpha}$.

3.2.5. Polarisation experiment

Polarisation experiments were performed by connecting a variable resistor, with a range between 30,000Ω-1 Ω. Resistance was changed every 3 minutes, during which time; data were recorded every 30 seconds.

3.2.6. Digital wristwatch, eZ430-Chronos

For the needs of this study, a MFC powered application was set up, using a Texas Instruments Chronos digital wristwatch (eZ430-Chronos, Texas Instruments, USA) combined with an ultra-low power boost converter with battery management (Analog evaluation module, bq25504 evm-674, Texas Instruments, USA). The power boost converter is needed to step up the operating voltage from 1.4 V (MFC output in-series) to 3 V, which is required to run the wristwatch.

3.3. Results and Discussion

3.3.1. OCV mode and power performance under a load

The OCV was close to the typical level for MFCs of 0.7V, with the control MFCs (plain carbon veil cathodes) being slightly higher than the MPL-based MFCs. Open-

to-air cathodes were hydrated every 24 hours to ensure moisture saturation throughout the experiment.

Following the open circuit measurements, all MFCs were connected to 2.7 kΩ resistors. The voltage started decreasing during the first 2 days, after which the performance of the MFCs with MPL cathodes improved, whereas that of the control MFCs continued to decline. The black arrows (Fig. 3.3) show hydration points and arrows in blue (dashed line) indicate anolyte replenishment. As can be seen in Figure 3.3, the performance from the MPL-based MFCs was in general superior to the control MFCs and continued to improve over time with the exception of one of the control MFCs, where it was shown to outperform the MPL MFCs by 25% in the later stages (after 120 h). The improvement of MPL in general over control could be attributed to the fact that MPL promotes water formation on the surface of the cathode ensuring continuous hydration. In contrast, for the control MFCs, the response to hydration was higher but at the same time shorter, decreasing significantly after 60 minutes due to drying out of the cathode. In the exceptional case, it is possible that a typical biofilm growth of cathodophilic species occurred around the cathode, acting as a moisture reservoir and maintaining a high redox between anode and cathode.

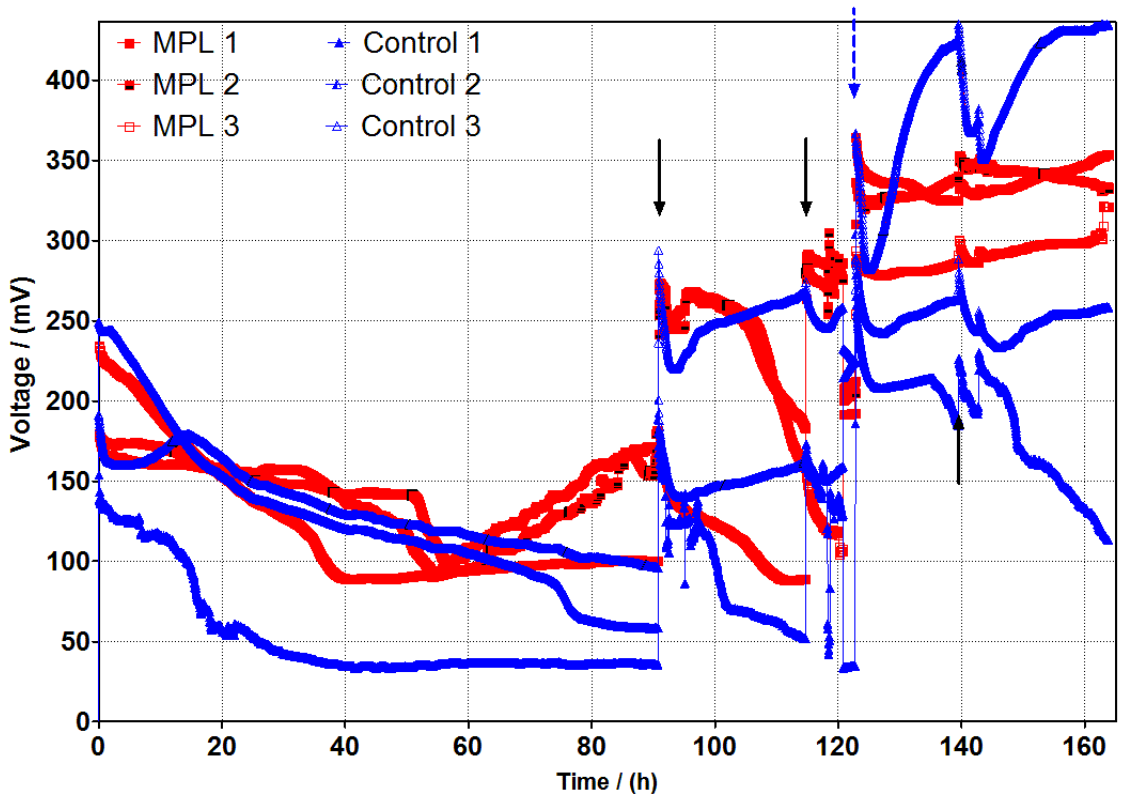

Fig. 3.3 Temporal behaviour of the MFCs under a 2.7 kΩ load.

3.3.2. Power output from individual MFCs

As can been seen from Figures 3.4a and b, despite the differences in the outputs from triplicate MFCs, which are probably due to differences in biofilm growth within those MFCs, the overall performance (Fig. 3.4b) from the MPL MFCs is significantly higher than that of the control MFCs. It is worth noting that MPP occurred in all 3 MPL MFC replicates at the same current (approx. 500 μA) (Fig. 3.4a), which suggests identical charge transfer, at different voltages. The improvement gained by the MPL was on average 38% (Fig. 3.4b).

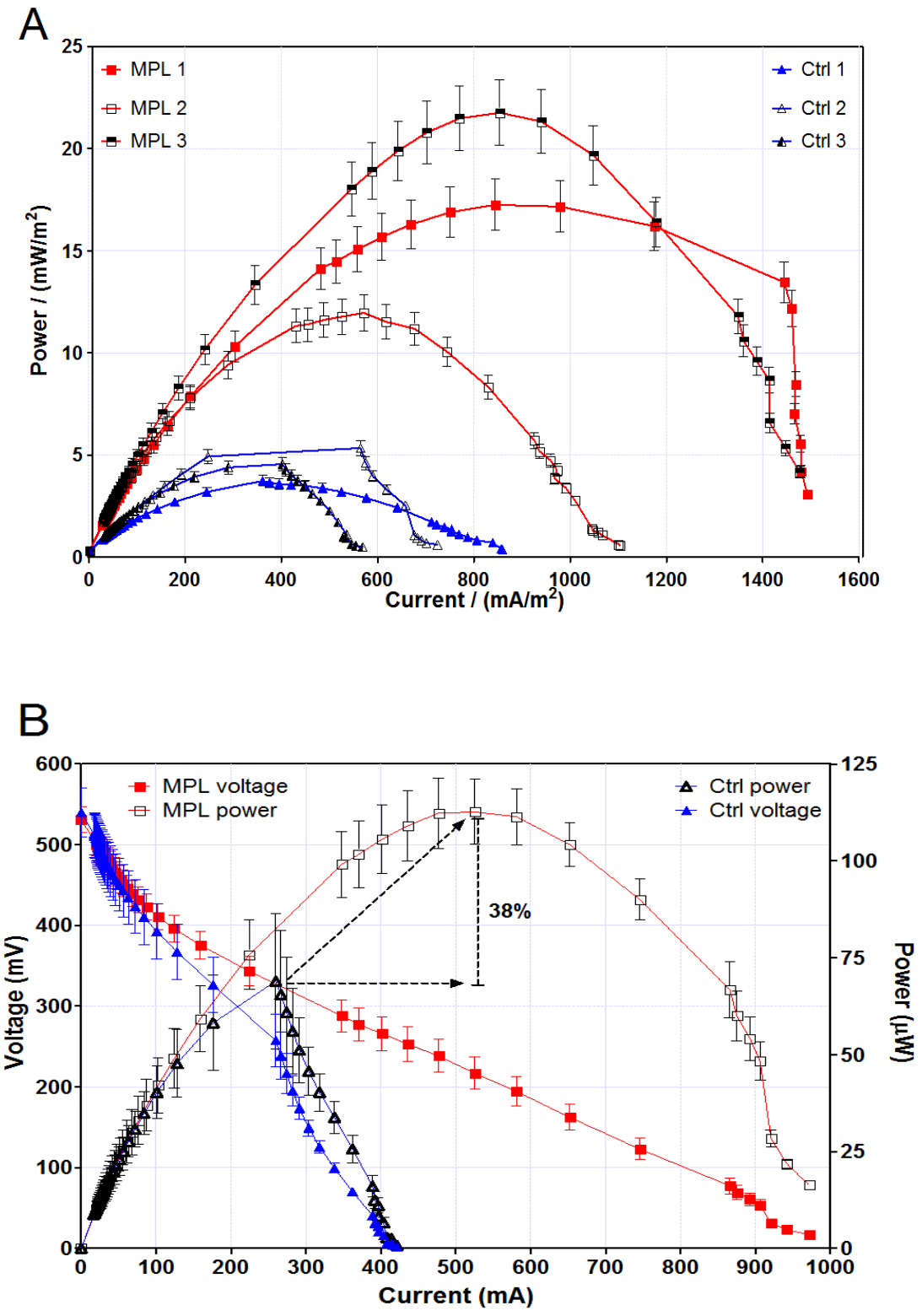

Fig. 3.4 A) Power density from 3 MPL & 3 control MFCs; B) average output of 3 individual MPL MFCs compared to 3 control ones (error bars represent standard deviation +/-).

3.3.3. MFC stacks (n=3) in-parallel and in-series

3.3.3.1. Performance and hydration regime of MFCs connected in-parallel under MPT load conditions

One method of scaling up is multiplication of small MFC which allows for improved performances [88], which was the purpose of the stacking experiment. Figure 3.5 shows the power and polarisation curves produced when the two groups of replicate MFCs were connected as stacks in-parallel; the 3 MPL MFCs were connected together and similarly the 3 control MFCs were also connected in-parallel. The MPL stack produced a maximum of 249 μW [41.6 mW/m^2] and 1867 μA [3112 mA/m^2], whereas the control MFC stack produced 129μW [27 mW/m^2] and 1087 μA [1576 mA/m^2]. Once again, the stacked MFCs with MPL electrodes improved the performance by 48%, which further supports the findings from individual units.

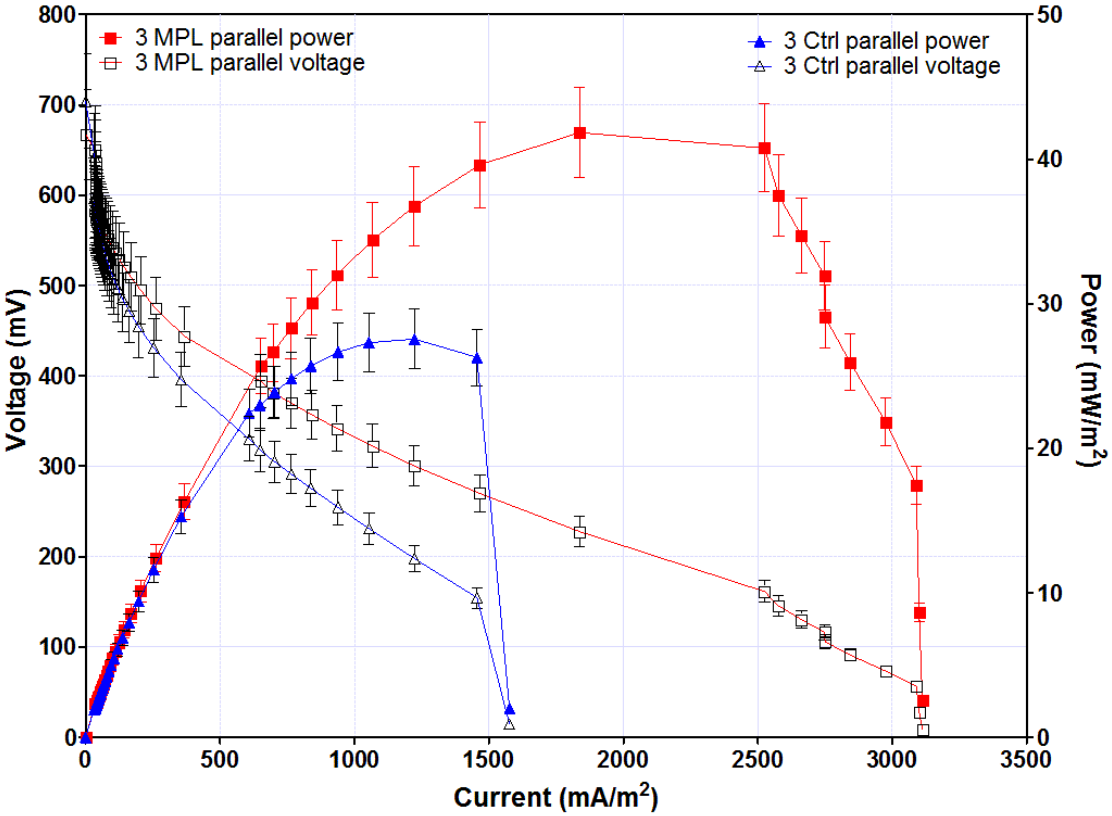

Fig. 3.5 Comparison between 2 MFC stacks with different cathode materials (MPL & carbon veil). Error bars represent standard deviation +/-.

The findings from the polarisation experiments indicated that the maximum power transfer points of the stacked MPL MFCs and control MFCs were at 500 Ω and 1000 Ω, respectively. Hence, these loads were applied to the MPL and control MFC stacks, for a period of 4 days (see Fig. 3.6). Black arrows indicate the hydration intervals and the blue arrow (dashed line) shows anolyte replenishment. Initially, the performance of the control stack, connected to a 1000 Ω load, was decreasing, but this quickly changed after the first manual hydration. On the contrary, the MPL MFC stack showed little response to water, probably because the material temporally inhibits the balance between the gas and liquid phases on the active sites. In this period, the MPL MFCs showed a decreasing trend in power generation, whereas the

control MFCs displayed an increasing trend, but still producing less overall power. The decline in the general trend of both types of MFC was undoubtedly related to the batch mode operation; however the tendency to decrease the performance in the case of the MPL MFC stack might have been the result of induced flooding, due to the frequency of hydrations. This was further confirmed when both MFC stacks were subjected to a 7-day dehydration regime whereby the MPL MFC stack continued to exhibit higher levels of power, whereas the control MFC stack decreased significantly (Fig. 3.7).

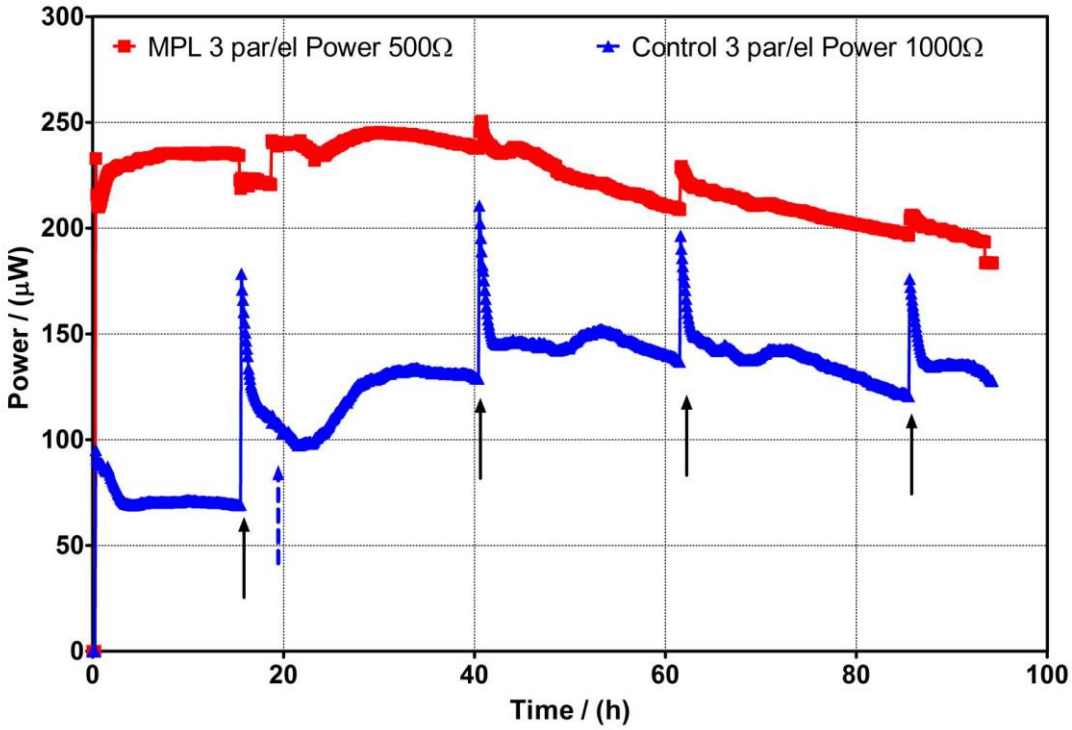

Fig. 3.6 Performance of MPL stacks under a 500 Ω load, and control stack under 1000 Ω.

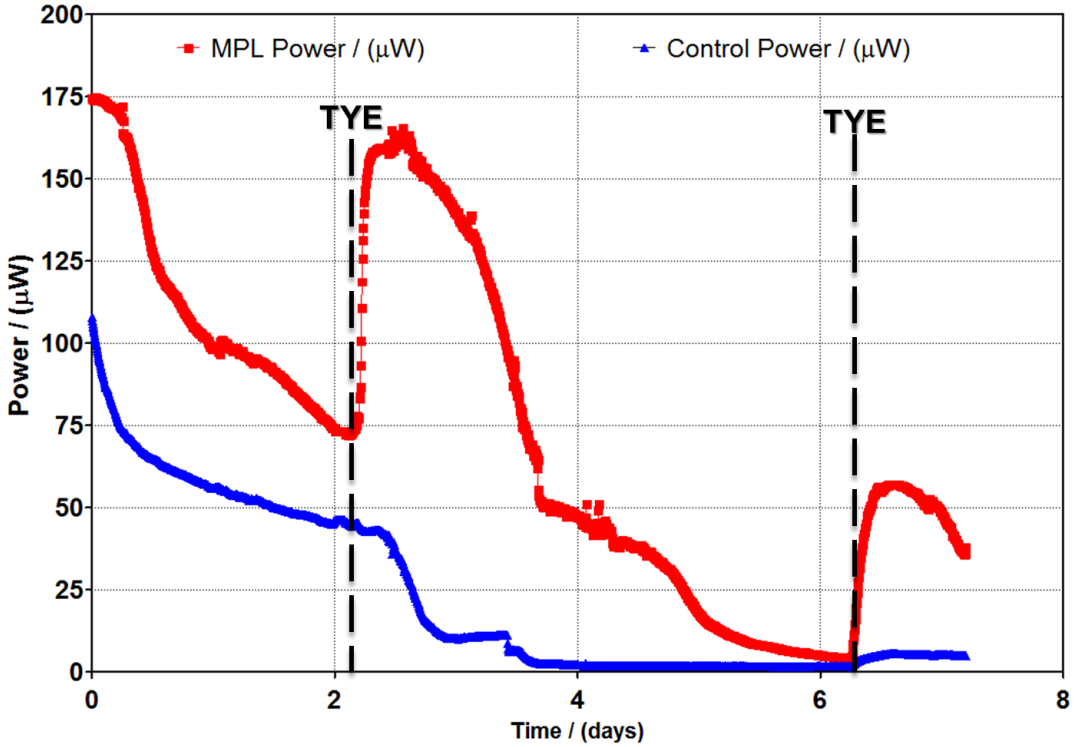

Fig. 3.7 Performance of the stacks under a dehydration regime. Dashed lines indicate feeding points with TYE.

3.3.3.2. Performance of MFCs connected in-series

As a final step in this line of experiments, the two types of MFC were connected in stacks of 3 in-series, and where then compared under polarisation sweeps. Figure 3.8, shows that the power and current generated by the MPL stack reached a maximum, of [43 mW/m^2 and 593 mA/m^2, which were two-fold higher than those produced by the control stack, 22 mW/m^2 and 247 mA/m^2. Results here designate that the MPL stack continued to be superior to the control stack, by approximately 52% (Fig. 3.5).

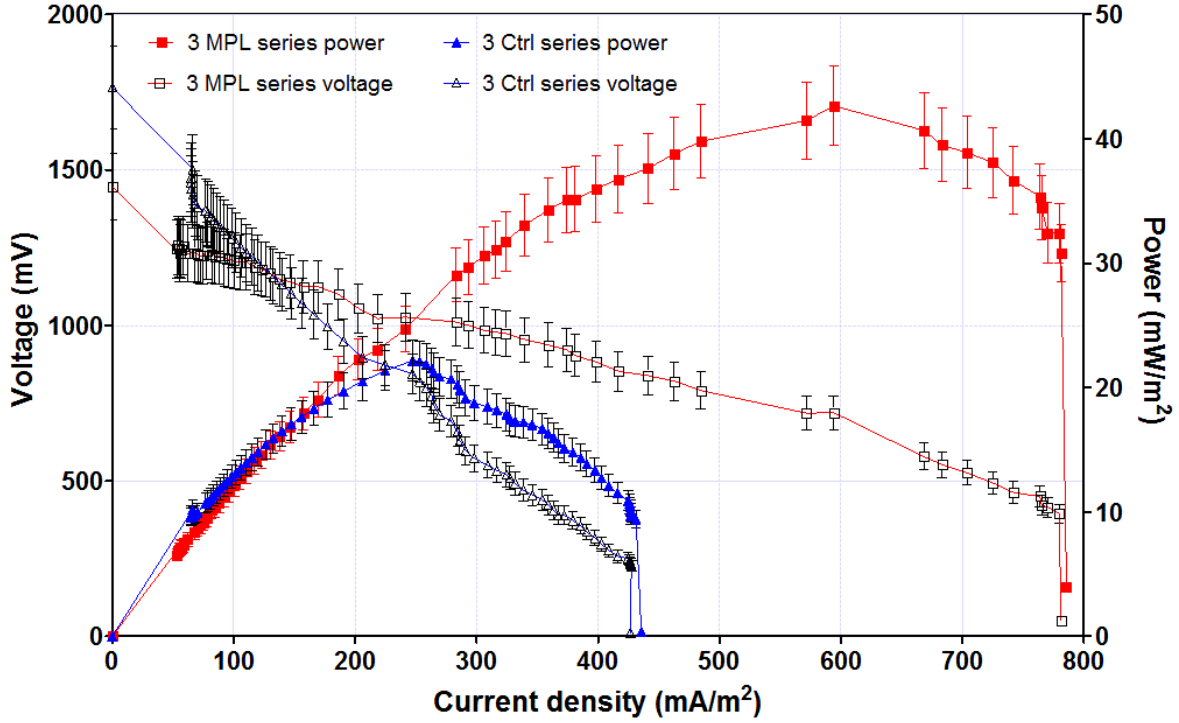

Fig. 3.8 Performance of MPL and control MFC stacks in-series. Error bars represent standard deviation +/-.

3.3.4. MFC stack (n=2) powering a practical application

This study investigated the effects on the performance of small-scale MFCs, when the control carbon veil electrodes were replaced with MPL coated electrodes. Results showed that the performance increased significantly and this is closely related to the electrochemical and physiochemical properties of MPL. The key to improve energy production in a MFC is to increase the surface area of the active sites where gas reactions easily take place, and at the same time, create a structure, which facilitates the removal of the produced liquids, that decrease the available s.a for ORR. MPL seems to be an excellent cathode, which combines all of the above features.

During the last decade, in conjunction with the development of low power electronics, MFCs have matured as a viable technology for energy production with a positive environmental impact. As a result, the MFC technology has already been implemented in low power practical applications [67–70,125,126]. The use of MPL in the present study has, for the first time, allowed for the continuous energising of a commercially available digital wristwatch (eZ430-Chronos) by 2 MFCs in-series, connected through an energy harvesting module (Fig. 3.9). The harvesting device steps up the operating voltage from 1.4 V (MFC output in-series) to 3 V, which is required to run the wristwatch. This is an efficient way of using the MFCs, since the energy harvesting module is drawing only 20% of the energy extracted by the 2-MFC stack, thus facilitating the continuous operation of the wristwatch, provided that fuel (organic waste) is periodically supplied. The wristwatch has been running for at least 4 months (video documentation available).

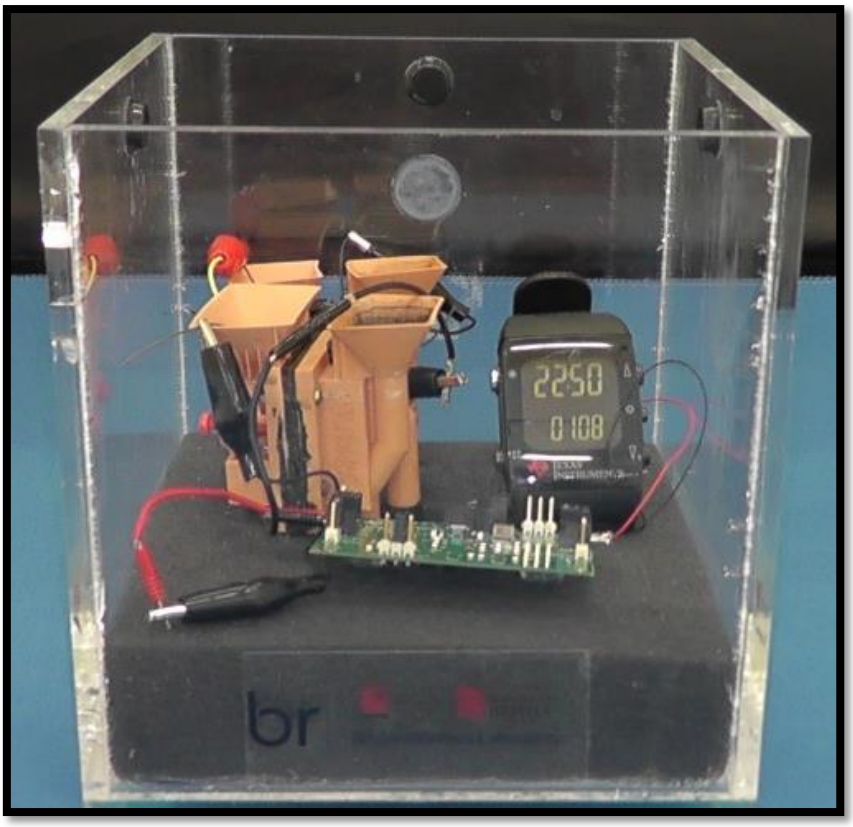

Fig. 3.9 Two MFCs with MPL cathode electrodes connected in-series, powering the TI Chronos wristwatch.

3.4. Conclusions

The experiments presented in this chapter show that the use of materials that facilitate the reaction kinetics on the cathode can greatly increase power without the use of high-cost catalysts. In the following chapters, experiments will focus onto multiplication of MFCs in stacks incorporating MPL cathodes whereby the inherent advantages of this effective cathode material are fully exploited. In this context, recent advances in MPL carbon materials will also be investigated and implemented in comparison to standard carbon veil electrodes. That, combined with active (or passive) energy harvesting techniques, such as the one used above, will become integral parts for running and even managing the essential peripherals in MFC stacks.

Chapter 4

Parts of the following results were presented in the 4th International Conference on Bio-Sensing Technology in Lisbon (2015):

Papaharalabos, G., Greenman, J., Stinchcombe, A., I., Melhuish, C., & Ieropoulos, I. (2015). **Microbial Fuel Cell stack for human urine remediation and synchronous energy harvesting**.

4. MFC stacks for energy harvesting and wastewater treatment

4.1. Operational versatility of MFC stacks

4.1.1. Challenges in wastewater treatment

On a daily basis the 624,200 kilometres of UK's sewer network, is filled with 11 billion litres of urban waste water. Even though urban waste water contains generally less than 0.1% solid materials (11 million litres per day) this waste is adequate to poison aquatic environments. Biodegradation of organic matter oxygen which can lead to anoxic waters. Additionally water eutrophication and the presence of water-borne pathogens are promoted by the high amount of nutrients found in waste water and human recreational activities respectively, which can cause chronic damage to an ecosystem [127]. In order to provide remediated waste safe-to-release to the environment, the UK government spends on an annual basis approximately £2.5 billion on the national electrical grid for wastewater treatment. To date, significant efforts are taking place into implementing anaerobic digestion technologies for potential reduction of excessive sewage sludge and treatment costs, and the concomitant utilisation of biogas which is mostly used in the production facilities to increase the temperature in the anaerobic digestion process chambers [128].

4.1.2. Urine: an energy source in abundance

Urine is a by-product of human and animal metabolism and is in abundance globally. On a daily basis, a healthy individual produces approximately 2.5 litres of urine, and a cistern toilet uses about 10-15L of water every time it is flushed. The UK uses almost 1.5 billion litres of fresh water every day to flush urine down the sewage pipes. Human urine is water-based comprising mostly nitrogen (urea), phosphate, potassium, urinary calcium and carbon [129]. It is estimated that urine is responsible for 75% of the nitrogen, 50% of the phosphorous and 10% of the COD content found in municipal wastewater and these concentrations are primarily responsible for water eutrophication and poisoning of the water horizon [130]. Hence, if urine is processed separately from municipal waste, it could greatly decrease the need for high cost segregation and breakdown chemicals[131]. Because the composition of urine reflects also the average requirement of nutrients for plant growth [132] many studies have attempted nutrient removal from urine for industrial usage, such as ammonia and struvite ($MgNH_4PO_4$) [131,133–139] and their use as fertilizers in agriculture [130,134,139–142]. Urine has also been demonstrated to work as an efficient fuel for direct electricity generation, via the microbial fuel cell technology; this is presented in more detail below.

4.1.3. MFC stacks: a wastewater processor for urine

The ability of MFCs to generate electricity from domestic waste water [143,144] with the concomitant removal of COD has received the attention of the research community due to its advantages over aerobic treatment processes [145]. Many studies, demonstrated that the addition of MFC units in a continuous flow of organic substrate, allows for a better effluent utilisation because of the higher active surface

area of microbial communities (biodegradation factor) that the effluent is exposed to as in a trickling filter treatment process (i.e volcanic rocks, lava, coke, gravel). This concept was adopted for reducing the organic content of glucose solutions [146]; sucrose [99]; landfill leachate [56] and human feces [147] by using relatively large MFC ranging from 0.25 L to 1.5 L. Similarly, due to the advantages of small MFCs in terms of diffusion, mass transport and energy density, previous workers [148] used a seven-MFC stack to demonstrate a small-scale scenario whereby the power output from each MFC was directly correlated with the availability of organic content (acetate concentration) down the effluent stream. It was also suggested that the higher the carbon concentration of the effluent, the less affected the power levels were in the MFCs close the effluent exit point.

Many substrates have been examined as fuel for anodophilic bacteria [46–59,149], but great interest has been shown lately in the use of neat human urine for electricity production and by-product removal [102,150–154]. MFCs consist of microorganisms capable of reducing the organic content and other elements found in urine whilst generating useful amounts of electricity[128,143,155] with the added feature of recycling elements deleterious for the environment [150]. Elements such as N, P, K can be transferred via bacterial metabolism into new biomass, thus removed from solution, resulting in element reuse. Moreover, the MFC technology has the added bonus of generating hydrogen through the electrolysis of urea in urine [151].

4.1.4. MFC stacks and energy extraction from urine

An effective way to increase the performance of individual MFC units is through the connection of multiple MFCs in stack configurations [67–69,71–73,125]. A study in 2008 showed that small-sized MFCs can generate higher power densities compared to

larger MFCs [88] and that scaling-up is the way forward [42]. In 2013, the use of a 24 small-scale MFCs stack using human urine as a substrate, demonstrated the charging of a mobile phone [77], and the applicability of the MFC technology in waste recycling and utilisation.

The present study uses a 24 MFC unit stack fed with urine and examines the possible electric and fluidic combinations under 8 different cascade formations and 23 electrical configurations. Each scenario investigates the impact that a set of electrical configurations with sequential units into the same waste stream have on (i) COD removal; (ii) power and current generation; and (iii) internal resistance, by gradually adding units in a cascade. The hypothesis is to simulate a real-time scale-up scenario whereby a MFC stack is reconfigured electrically or fluidically so as to meet either the energy or remediating demands –or both- of a wastewater treatment facility.

4.2. Materials & Methods

4.2.1. Microbial Fuel cell Stack

Twenty four RC25 Nanocure open-to-air cathode MFCs were used for the experimental setup as previously described [42] (see chapter 2). The internal volume of the anode compartment is 6.25 ml, and the anode's electrode projected s.a is 6 cm^2. A catalyst-free carbon fibre veil was used for the construction of the anode (168 cm^2), five times folded down so as to fit the chamber and for the cathode, a single MPL assembly was used (7 cm^2) based on previous work [76] (see chapter 3). An IEM (12 cm^2) was used as a separator (Membranes International, Ltd) that was held between two rubber gaskets. Throughout the experiments, open-to-air cathodes were hydrated every 24 hours, to ensure sufficient liquid bridging between the IEM

and the cathode electrode surface. Titanium wire was used for current collection (50 mm long, 0.5 mm thickness).

4.2.2. Switch box for electrical configurability

To control the connections between MFCs within the stack, a novel device for manually switching the connections between MFCs from series to parallel was developed. The switch box also provided the ability of electrically isolating MFCs within the stack (Fig. 4.1).

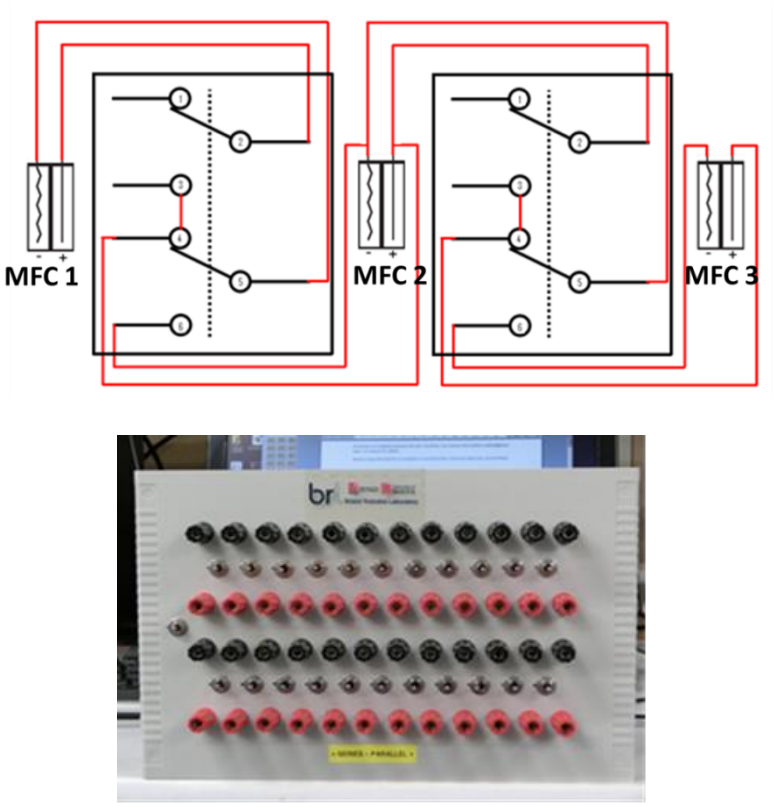

Fig. 4.1 (Upper) Schematic diagram and (lower) photo of the switch box for controlling the electrical connections in a stack of 24 MFCs.

4.2.3. Cascade setup and isolated hydraulic scenarios

All 24 MFCs were attached to supportive rods via adjustable clamps, allowing an air gap between sequential units (Fig. 4.2), therefore eliminating the substrate cross-conduction effect [110] that resulted in losses when MFCs were connected in-series

(see chapter 2.5.2.2.1). In the following paragraphs, the term fluidical/hydraulic connection is also used to describe succinctly the cascading of sequential units under the same feedstock line and taking into consideration the air-gap (liquid isolation) between MFC units for preventing electrons from travelling through the feedstock. MFCs were designed in such a way that the pumping system completely fills the anode chamber with anolyte, where an overflow tube then removes used substrate, directing it to the next MFC unit that is placed underneath the first unit, creating a gravitational feeding regime [156] allowing for stable HRT and higher coulombic efficiency [157].

Table 1 summarises the different cascade set-ups along with the electrical configurations, starting from individual MFCs when they were not in cascade, and looked at their performance when connected electrically in-series and/or in-parallel. The following stages looked at the MFCs set up in different cascade formations where an upstream MFC fed into a downstream MFC which in turn fed into to another (depending on how many were in the cascade). Figure 4.2 shows three such cascade set-ups as performed in real lab situations. During the cascade stages, the electrical configurations were chosen that matched the physical set-up of the stack and never more than four were used (see table 1). This prevented overcomplicating the experiment whilst helping to maintain the physical/electrical balance.

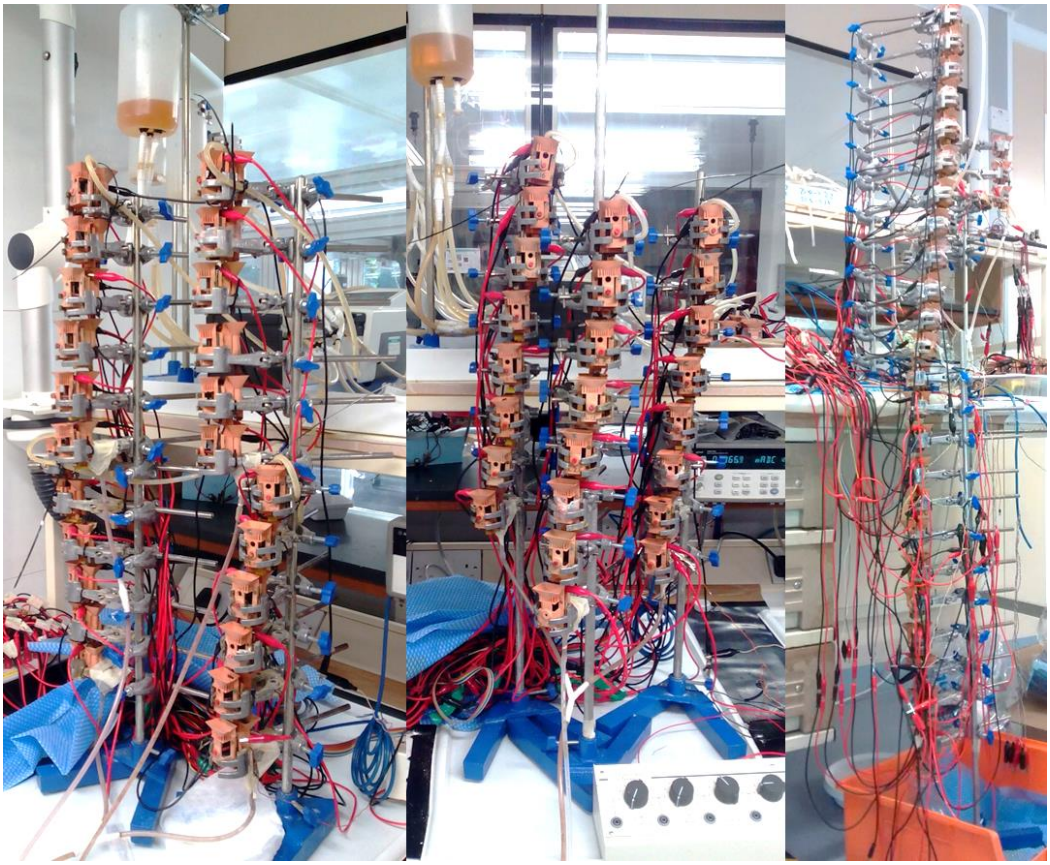

Fig. 4.2 Example of stacked MFCs in different cascade configurations as operated in the BRL facilities. (Left) Four groups of 6 MFCs hydraulically connected. (Middle) Three groups of 8 MFCs in cascade. (Right) All 24 MFCs fluidically configured as one cascade

24 MFCs	Electrical configurations			
Cascaded elements (x number of groups)	In-series elements	In-parallel elements	In-series MFCs/ in-parallel groups	In-parallel MFCs/ in-series groups
Single unit	24	24	-/-	-/-
2 (x 12 groups)	24	24	2/12	2/12
3 (x8)	24	24	3/8	3/8
4 (x6)	24	24	4/6	4/6
6 (x4)	24	24	6/4	6/4
8 (x3)	24	24	8/3	8/3
12 (x2)	24	24	12/2	12/2
24	24	24	24/0	24/0

Table 1. Available electrical and hydraulic combinations in the stack

4.2.4. Operational parameters

All experiments were performed under constant room temperature of 22 ±3 ^{o}C. The supplied fuel for the start-up of MFCs was activated sludge waste, courtesy of Wessex Water Scientific Laboratory (Saltford, UK), mixed with TYE medium (Tryptone and Yeast Extract; 1% and 0.5%). A 24-channel peristaltic pump (Watson Marlow, UK) was used to provide substrate at a flow rate of 1 mL h $^{-1}$ corresponding to a HRT of 6.8 h. All MFCs were operated in bach-fed mode for a period of 3 weeks. During this time all MFCs were connected under an external load of 2.7 kΩ until stable power outputs were reached and no power overshoots [106] were observed. Following maturity period, substrate was switched to neat human urine. Samples were received on a daily basis at fixed time of the day (morning) from a healthy individual. For the first stage of the experiments all MFCs were fed independently (Fig.4.3). Thereafter, the fresh feedstock channels decreased in number as more MFCs were fed in cascade from the preceding unit(s) along the waste stream. The later stages of the experiment involved after every stage the repositioning of extra unit/s to the lower part of the stacked groups. At the beginning of each stage and every time that the number of units increased in a cascaded group, the stack was isolated electrically and left open circuit for 2 hours with fresh urine being pumped into the system. Voltages were logged for 3 hours until the OCV had reached a steady state. Polarisations were then performed in triplicate, to examine the power, current and the internal resistance value where maximum power transfer occurred.

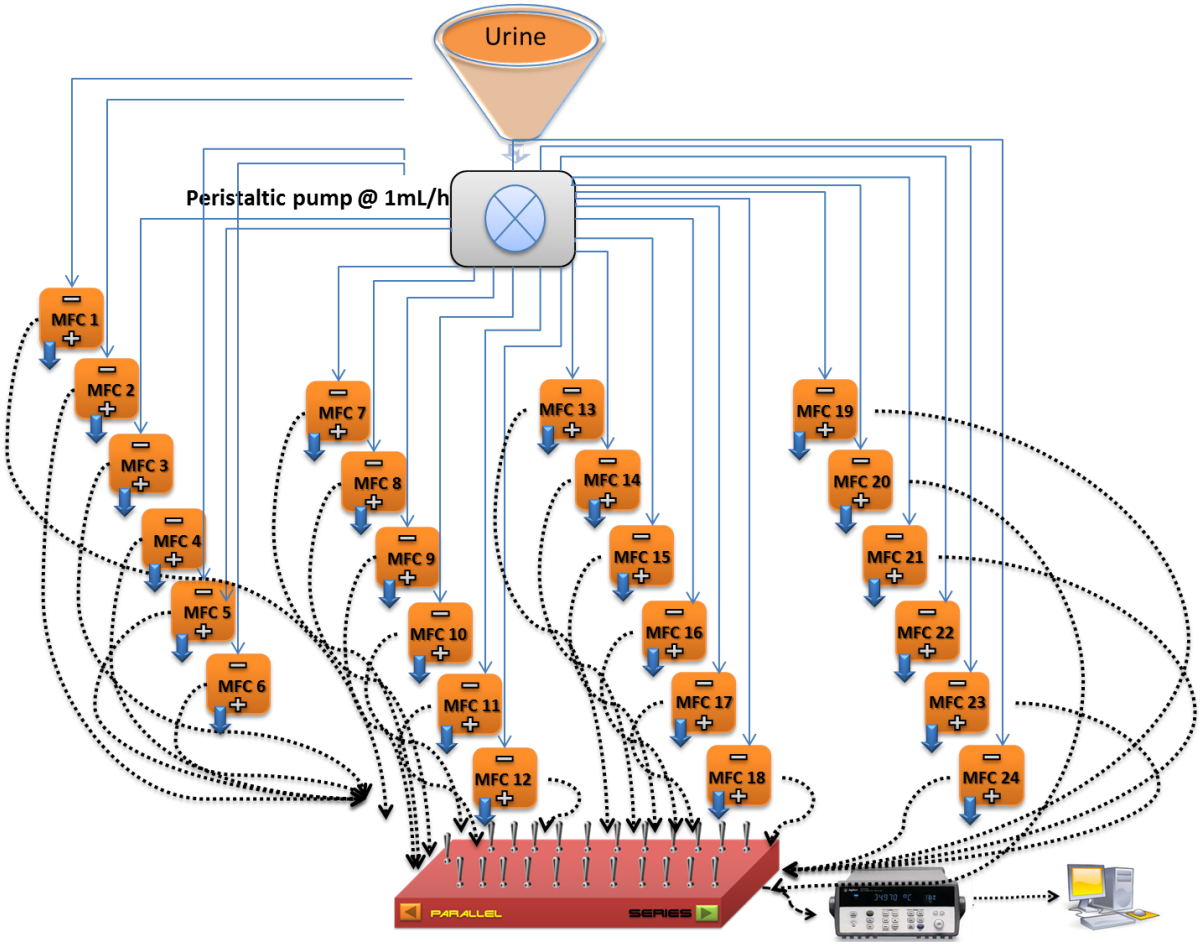

Fig. 4.3 Stage 1: All 24 MFCs individually fed and electrically independent

4.2.5. Data logging

MFCs' voltage and overall stack voltage was recorded using a HP Agilent multiplex logging module (34907A, HP). Voltage was measured in Volts and the obtained data were further transformed into detailed graphs using GraphPad Prism® version 5.01 software package (GraphPad, San Diego, California, U.S.A.). The Agilent logger was also used to calculate current and power output from the stack according to Ohm's law, I=V/R. Current was measured in mill amperes (mA) and power was measured in milliwatts (mW). The power being produced per unit surface area was calculated by dividing power by the electrode's surface area in square-metres (m^2).

$$P_{density} = P/\alpha$$

4.2.6. COD, pH and conductivity measurements

For measuring the COD of fresh urine, high range potassium dichromate oxidation method vials (CAMLAB, UK) were used and COD values were calculated via colorimetric analysis (Photometer-System MD200, Lovibond). Fresh urine samples (200μL) were filtered and their COD content measured prior to entering and after exiting the MFCs (24-48 h). Additionally urine samples were left exposed to air and in closed bottles on the bench, for examining the effect that atmospheric oxygen has on the oxidation of urine, without the process from MFCs. Treated urine samples were initially filtered and then centrifuged to 2500 rpm for 5 minutes [158]. The pH was measured with a Hanna 8424 pH meter (Hanna, UK) and the conductivity with a 470 Jenway conductivity meter (Camlab, UK). Due to the high conductivity of urine, the instrument's measuring capabilities were out of range, thus urine was diluted with deionised water in a 1:4 ratio. Measured pH of fresh urine samples ranged between 5.5 and 5.8, conductivity was ca. 38 mS from a total of 24 samples and COD ranged between 11-16g/L (the large variance was due to the daily nutritional conditions of the donor).

4.2.7. Polarisations sweeps

Performance of individual MFCs was measured by applying a range of 50 resistance values from 30 kΩ down to 3 Ω every 3 minutes. This process was done either with the use of an automated variable resistor[105] for stack voltages did not exceeding 2.5 V, or with the use of a variable resistor box (Centrad Boite A Decade De Resistances DR07) for higher voltage outputs.

4.3. Results and discussion

4.3.1. Individual/stacked units fed independently (Stage 1)

4.3.1.1. Performance readings

Polarisation sweeps on all 24 MFCs showed an average power density of 6.6 mW/m^2 and a current density of 18 mA/m^2 from a single unit (Fig. 4.4). The average internal resistance (R_{int}) that matched the impedance of the external load at the maximum power transfer (MPP) occurred was 800 Ω. According to this value the theoretical R_{int} of 24 MFCs connected in-series or in-parallel is estimated to be 19.2 kΩ and 33 Ω respectively. However the actual R_{int} of the stack connected in-series was 11 kΩ, which equals 458 Ω per MFC, 43% less than the expected value. Similarly the MFCs connected in-parallel showed a lower internal resistance (22 Ω) than the theoretical R_{int}.

Following this, all MFCs were connected in-parallel and in-series configurations. Parallel connections showed a P_D of 5 mW/m^2 and a C_D of 24 mA/m^2 with a R_{int} of 21.7 Ω (Fig. 4.3). As previously reported [72], P_D from electrically connected MFCs is likely to be lower than individual unit performance. In this case power was lower by 25% from the power density of single MFC units. However, due to a lower R_{int} in the stacked MFCs C_D from in-parallel exceeded the overall current density from individual units by 25% which concurs with findings from another study [88].

When MFCs were connected in-series, P_D was 5.2 mW/m^2, and a C_D 1.1 mA/m^2 which was 4% higher and 23-times lower respectively, than that of equivalent number of MFCs in-parallel. Nevertheless, the actual generated current from the in-series connection was 438 µA compared to the 314 µA from equivalent number of individual units, which can be attributed to the lower R_{int} of the series configuration.

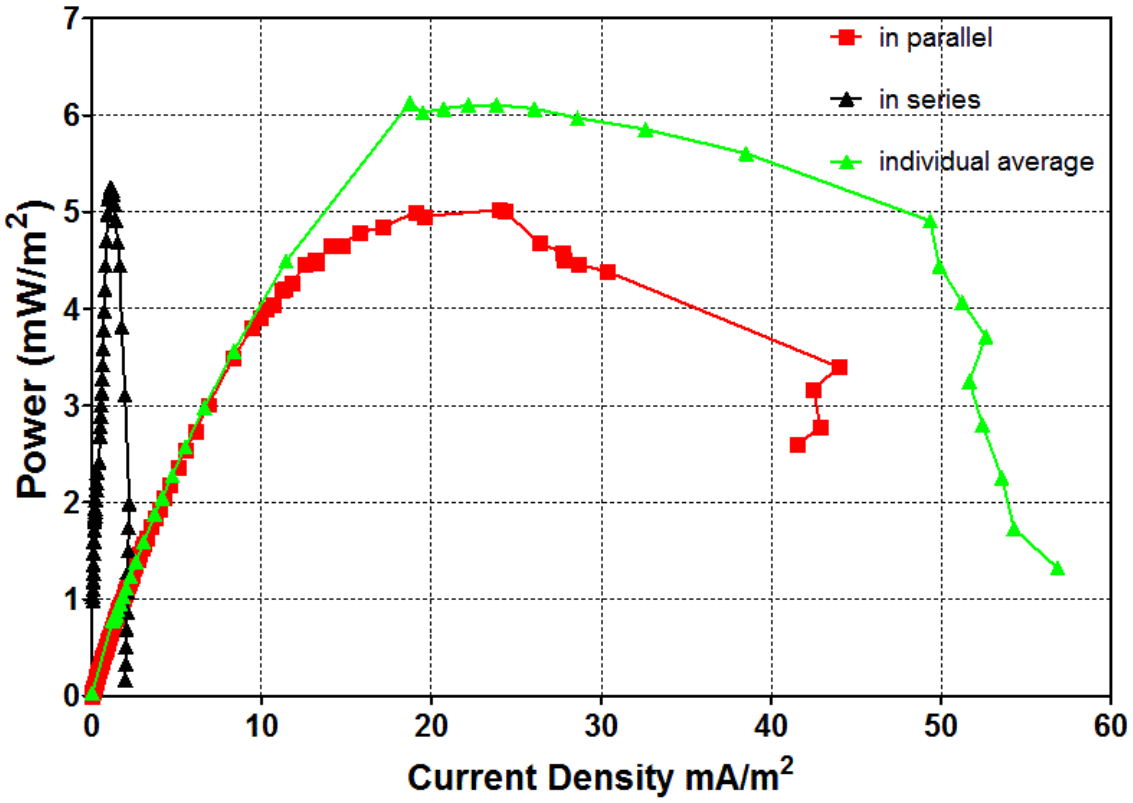

Fig. 4.4 P_D from individual units, stacked in-series and in-parallel electrical configuration

4.3.1.2. COD removal

COD of fresh urine ranged between 11 g/L to 16 g/L. Samples from treated urine that had passed through individual MFCs showed a COD removal of 19%. When connected electrically in-series and in-parallel, COD removal was 17% and 23% respectively. Even though MFCs in-parallel produced a lower power density from the in-series connection, the current density was 23-times higher which resulted in higher COD removal, matching findings from Aelterman *et al.* in 2006 [72].

4.3.2. Cascade operation scenarios

4.3.2.1. Cascades of 2 sequentially fed MFC units (**Stage 2**)

4.3.2.1.1. Power (P_D) and current (C_D) densities

The first cascade configuration involved MFCs arranged in cascade pairs, forming 12 hydraulically isolated groups (Fig. 4.5). The stack was initially connected in-parallel configuration and the rest of the electrical combinations that followed were 12 serially connected groups of 2 MFCs in-parallel, 12 in-parallel groups of 2 MFCs in-series and lastly all 24 MFCs connected in-series. Urine was first being pumped in the odd numbered MFCs and then gravitationally moved into the even numbered MFCs. Results from polarisations showed that the in-parallel configuration produced 7.21 mW/m^2 and 29.2 mA/m^2 increasing its performance by 30% and 18% respectively compared to single fed MFCs connected in-parallel and even exceeding the individual P_D by 8% (Fig. 4.20) and the C_D by 38% (Fig. 4.6).

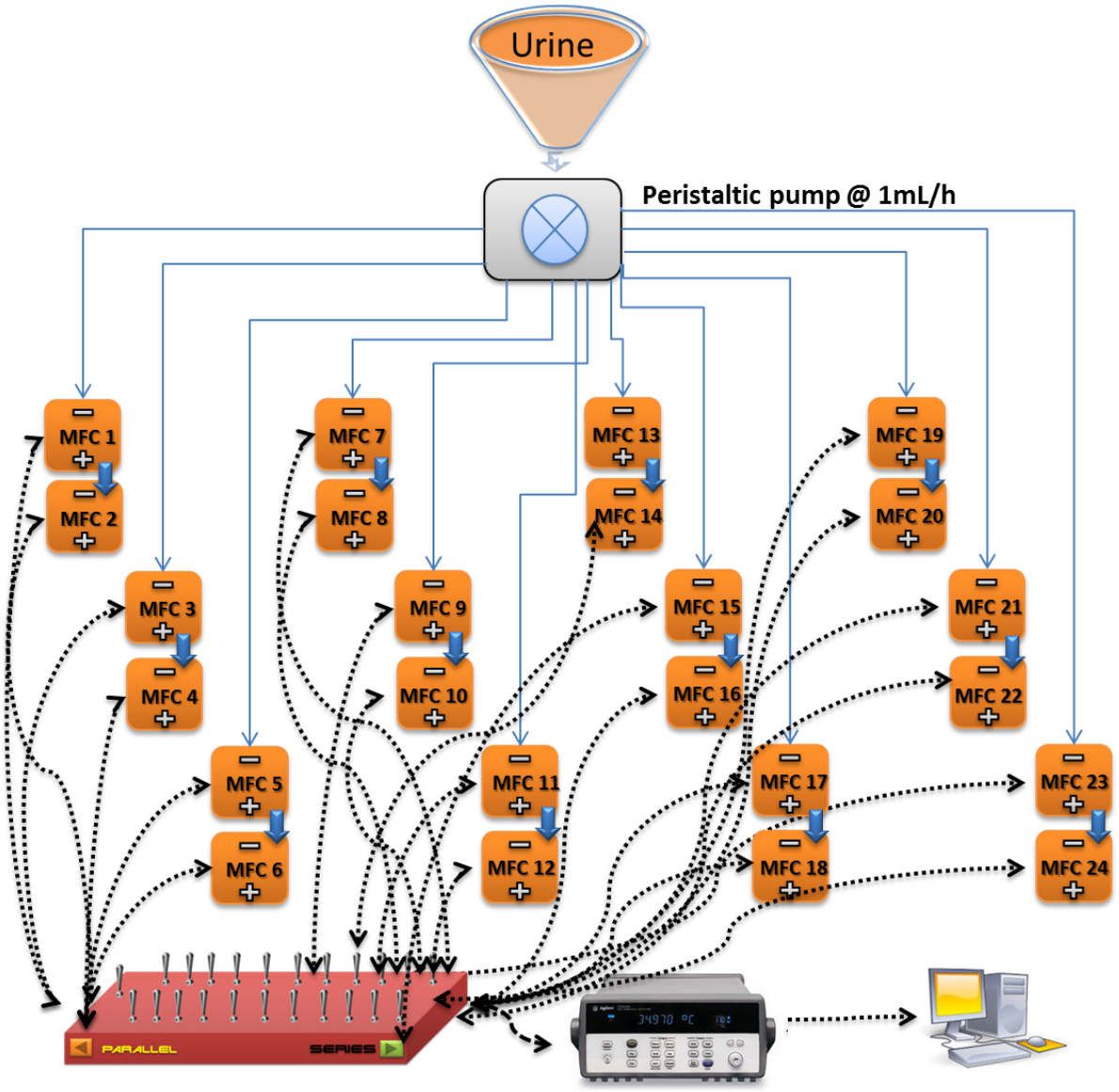

Fig. 4.5 Stage 2: setup of pairs in cascade

The introduction of 2 electrical in-parallel elements and 2 in-series elements, showed an increase of 5% for the first case and an 8% decrease in P_D for the latter configuration, compared to purely parallel or series formation of the cascade. The 12 in-series by 2 in-parallel (electrical) produced 6.75 mW/m^2 and the 12 in-parallel by 2 in-series generated 6.58 mW/m^2. The addition of parallel elements electrically, exceeded expectation, based on previous work [72], producing 2.9 mA/m^2, an increase of 61%. Conversely, the introduction of in-series elements (electrically) in

the parallel connection decreased the C_D by 77% giving 6.7 mA/m^2 (Fig. 4.7; cascade n=2).

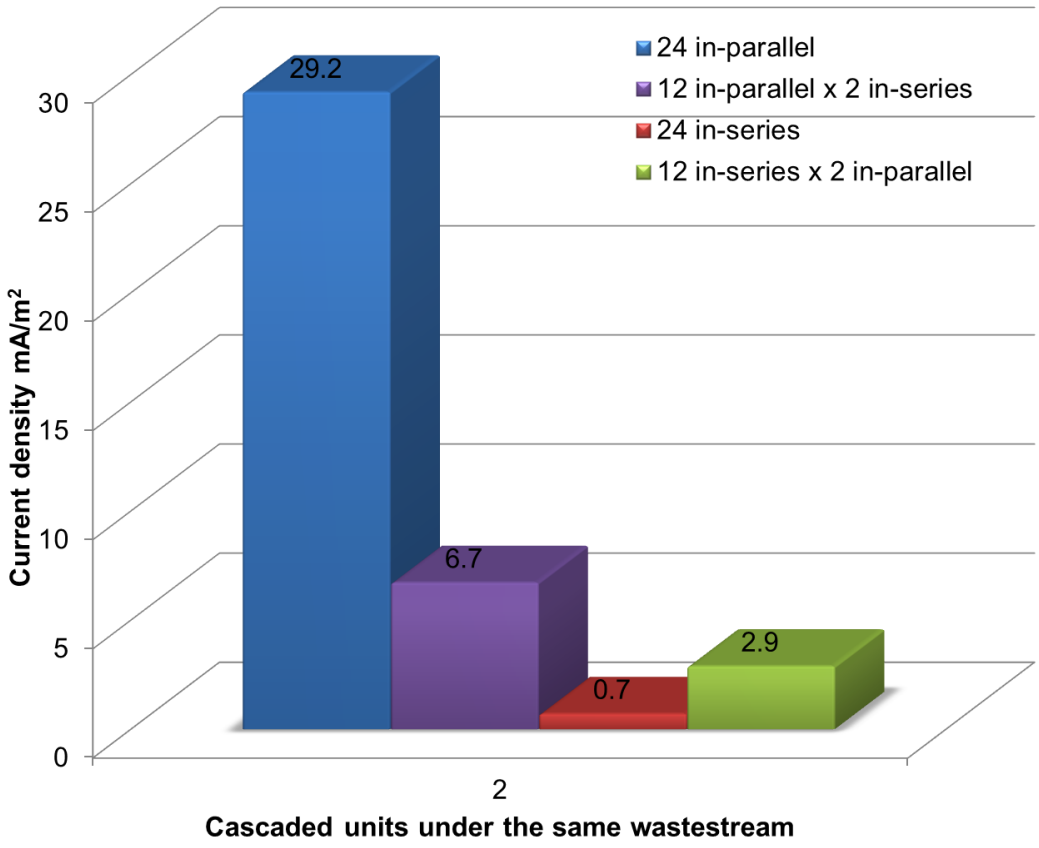

Fig. 4.6 Current density from cascades of 2 MFCs x12 groups in 4 different electrical configurations

The increase in the overall performance of the two-element cascade can be attributed to the fact that the availability of organic content in urine, which is being supplied in the first MFC, is superabundant, which concurs with findings from a recent study [148]. This combined with the low retention time, allows for adequate nutritious substrate to reach the nether MFC [56] increasing the overall performance in the stack. Furthermore, previous studies have shown that the metabolic activity of

bacteria in the upper MFC provides by-products or shorter chain compounds easily accessible for the lower MFC to process [56,100,147].

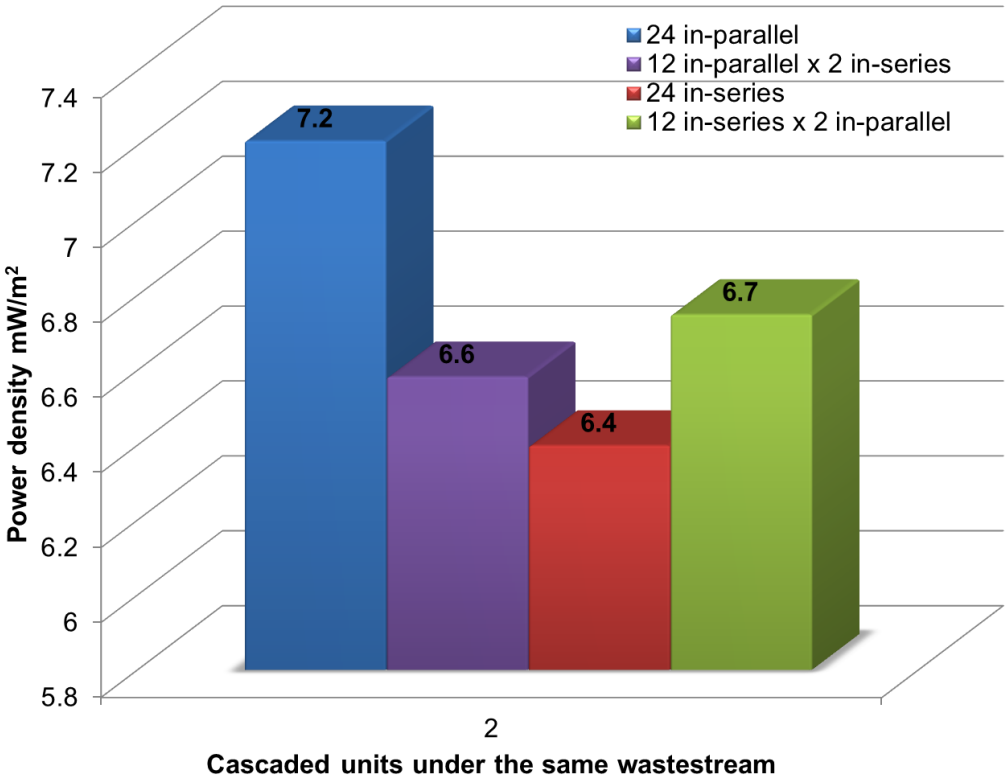

Fig. 4.7 Power density from cascades of 2 MFCs x12 groups in 4 different electrical configurations

4.3.2.1.2. COD treatment and R_{int}: 2-unit cascade regime with electrical reconfigurations

MFCs in-parallel achieved a 31% removal of organic content, 8 % higher than individually fed units connected electrically in-parallel. By reconfiguring the stack in-series, a 16% COD treatment occurred, showing a 1% decrease in urine treatment compared to solely in-seris fed units (17%). The presence of series elements in the

12 in-parallel by 2 in-series electrical formation, resulted in a 23% COD treatment (8% drop), which shows the negative impact that series elements caused on the COD remediation. Adversely, the presence of electrical in-parallel elements in the 12 in-series by 2 in-parallel increased the COD treatment by 3%, reaching a value of 19% (Fig. 4.8). The above results agree with the results from the current densities, and confirm the hypothesis that a majority of MFCs connected in-parallel, optimises both current density and COD removal that a specific number of stacked MFCs can provide [72].

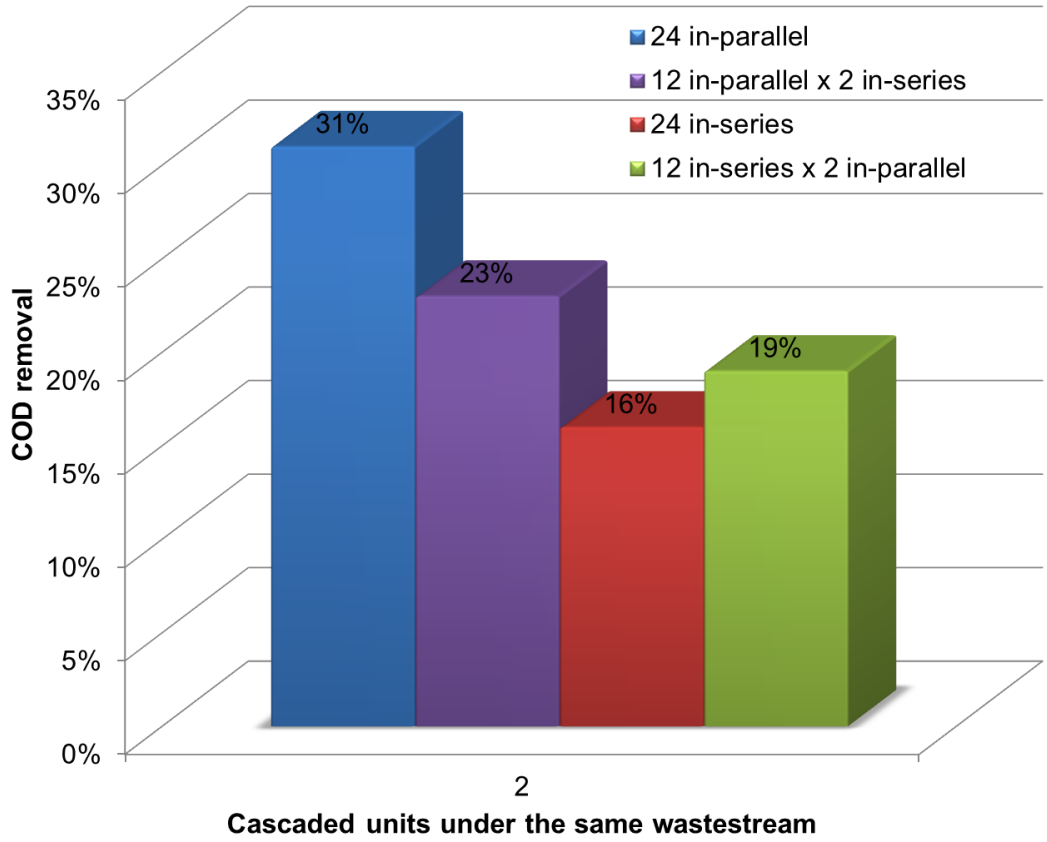

Fig. 4.8 COD treatment from MFC pairs sequentially fed and electrically connected in four possible electrical configurations

Even with the stack's overall performance increased, R_{int} showed a gross increase. The R_{int} of MFCs connected in-parallel maintained the same value (21 Ω)

as when individually fed, the R_{int} reached 25kΩ when connected in-series increasing 2.5-times compared to the equivalent from previous stage, and doubled its value when in 12 parallel by 2 series (166 Ω) based on a theoretical equivalent of one MFC's R_{int} (504 Ω) in the same configuration. In contrast, the 12 in-series by 2 in-parallel lowered its R_{int} by 33% (2.8 kΩ) compared to the theoretical projection from a single unit connected in the same configuration (504 Ω) (Fig. 4.9). Nonetheless, it can be suggested that the parallel elements seemed to play a key role in containing the resistance at usable levels and withstanding the pressure of the series elements to large increments above 50%. It could be suggested that the internal resistance of a stack connected in-parallel or containing in-parallel elements with large variations in resistance within the system, will tend to acquire the lowest resistance values, as it is the less impeded way for the current to flow.

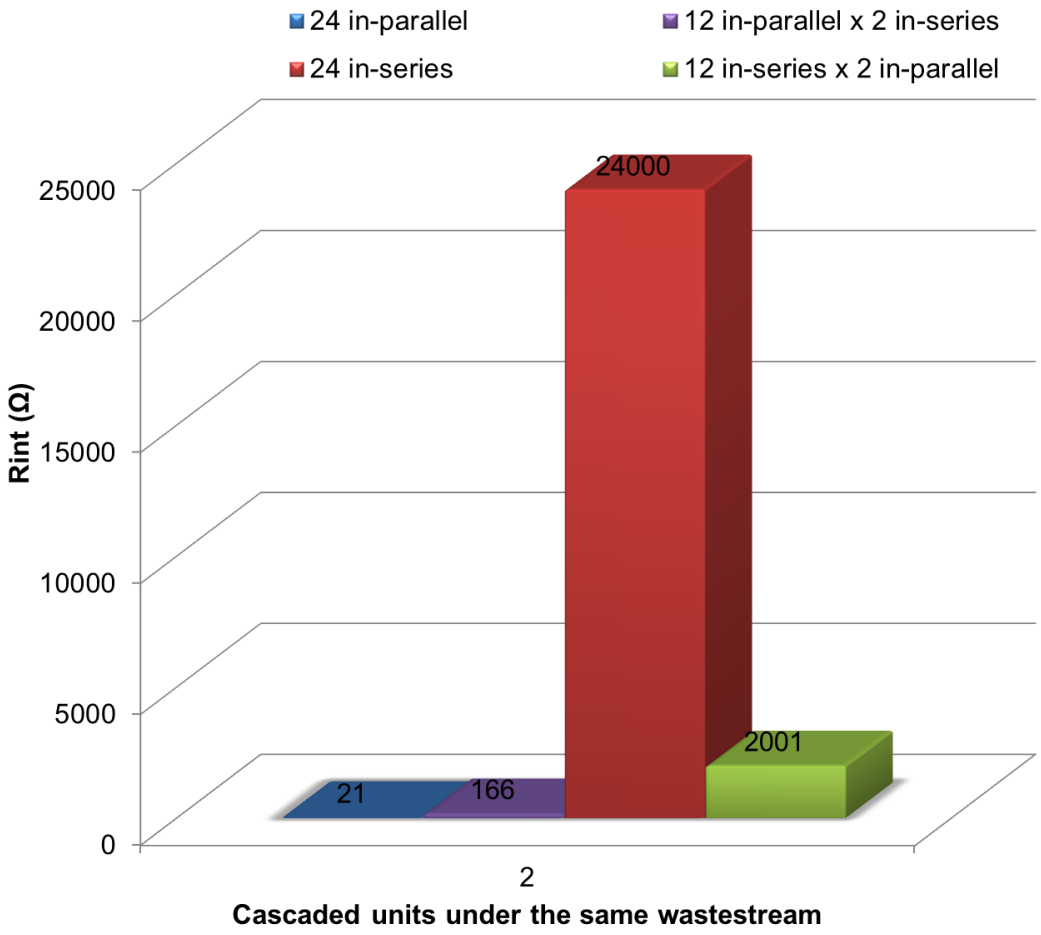

Fig. 4.9. R_{int} values based on MPP measurements from pairs of MFCs in cascade and different electrical configurations

4.3.2.2. Cascades of 3 sequentially fed MFC units (**Stage 3**)

4.3.2.2.1. Performance readings

The third stage of the experiment featured sequential triplets of MFC units in cascade, forming 8 hydraulically insulated groups (Fig. 4.10), connected electrically to the switch box for electrical reconfiguration. Similarly, 4 possible electrical configurations were examined for power and current densities. MFCs connected in-parallel produced a P_D of 3.47 mW/m^2 and a C_D of 11 mA/m^2. When connected in-

series, the stack achieved a P_D of 4.08 mW/m^2 and a C_D of 0.6 mA/m^2. The 8 in-parallel connected groups of 3 MFCs in-series produced a P_D of 3.57 mW/m^2 and a C_D of 5 mA/m^2. The 8 in-series connected groups of 3 MFCs in-parallel showed a P_D of 3.97 mW/m^2 and a C_D of 1.9 mA/m^2 (Fig. 4.11 and Fig. 4.12).

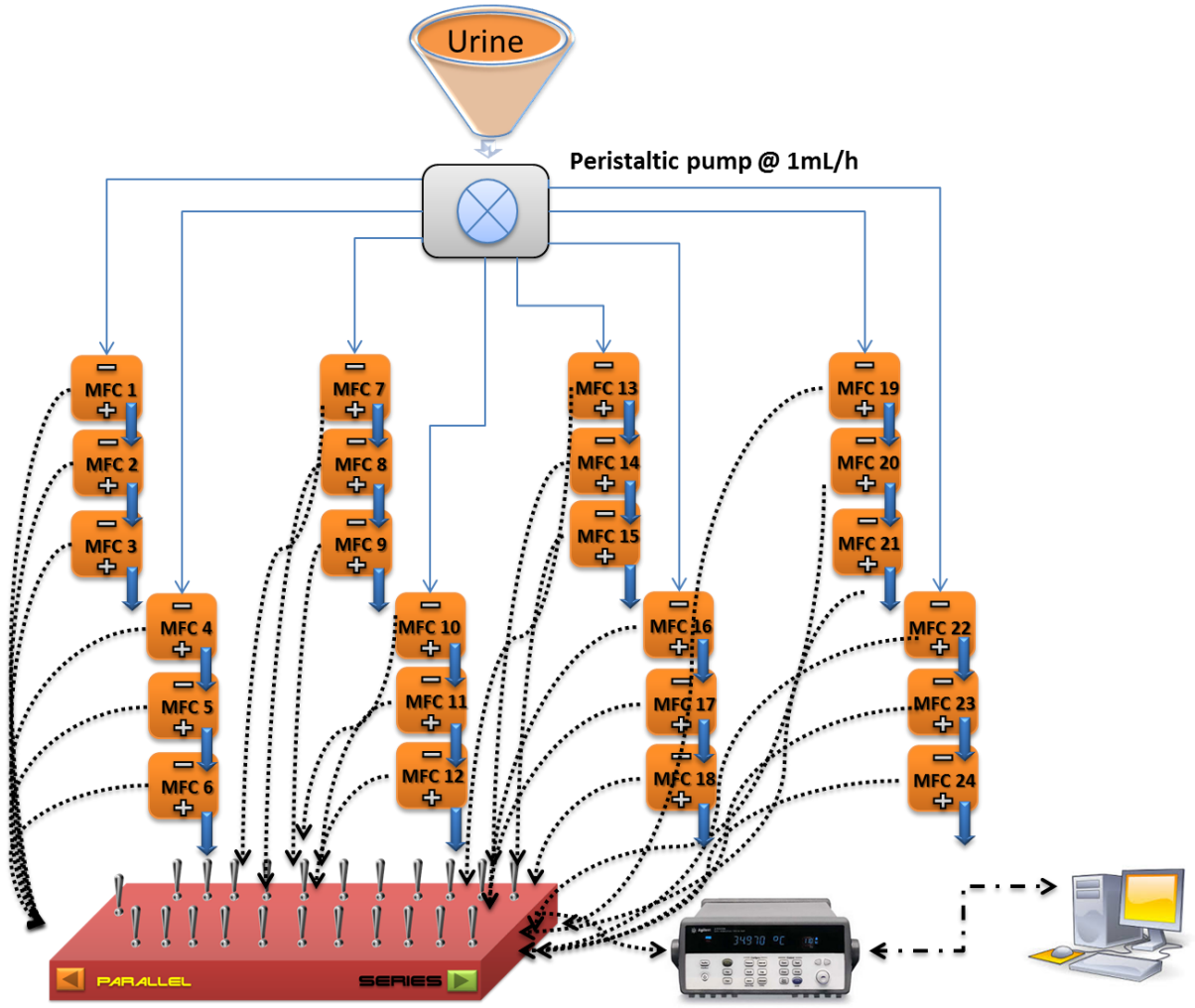

Fig. 4.10 Stage 3: Setup of eight groups of MFC triplets sequentially fed and electrically connected

Even though, the stack showed an increase in its performance with the introduction of the second unit in cascade, in this stage the addition of a third MFC unit in the waste stream resulted in a reduced overall performance. This may be due to the fact that the pre-processed substrate that derived from the preceding MFC

affected the power output of the following which had an adverse impact on the overall performance regardless the in-parallel connections within the stack. This is also pictured in the similarities of the P_D amongst the four different electrical configurations and it can be suggested that an increase in the flow rate is more likely to recover the stack to higher levels of power. However, the flow rate had been determined based on the idea that high COD removal is directly correlated with (a) low flow rates, (b) HRT and (c) loading rate [158], thus it remained the same throughout the experimental procedure.

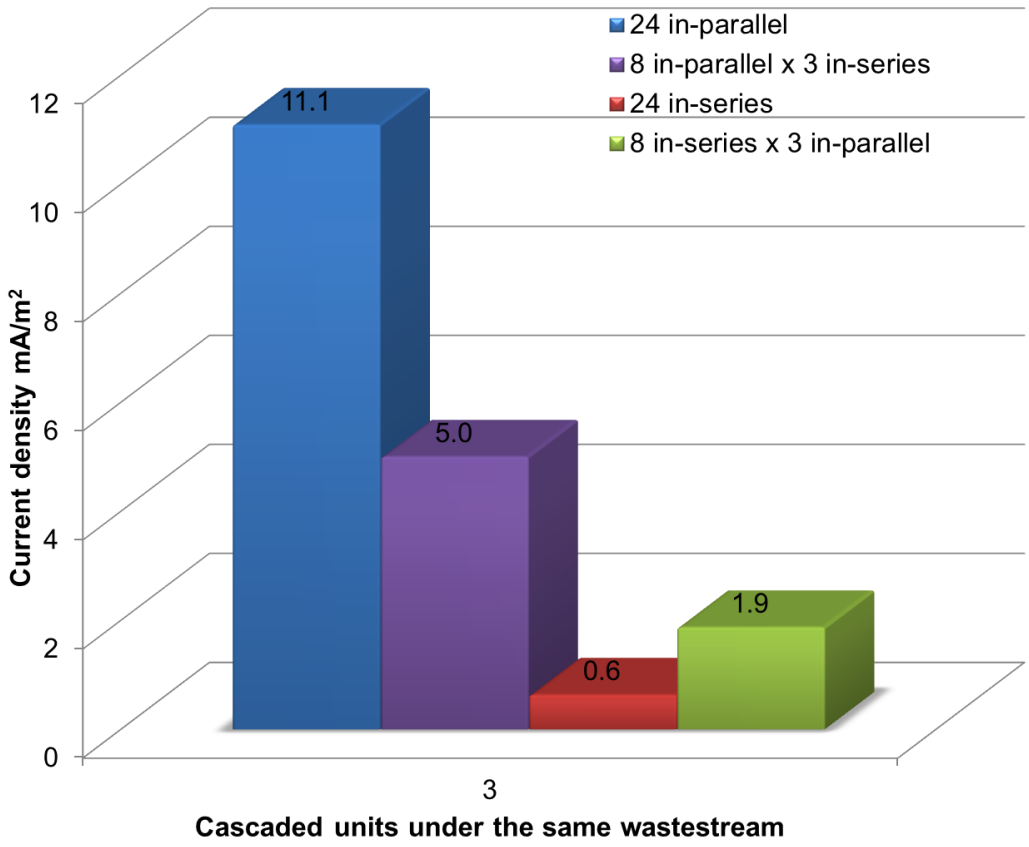

Fig. 4.11 Current density from cascades of 3 MFCs x8 groups in 4 different electrical configurations

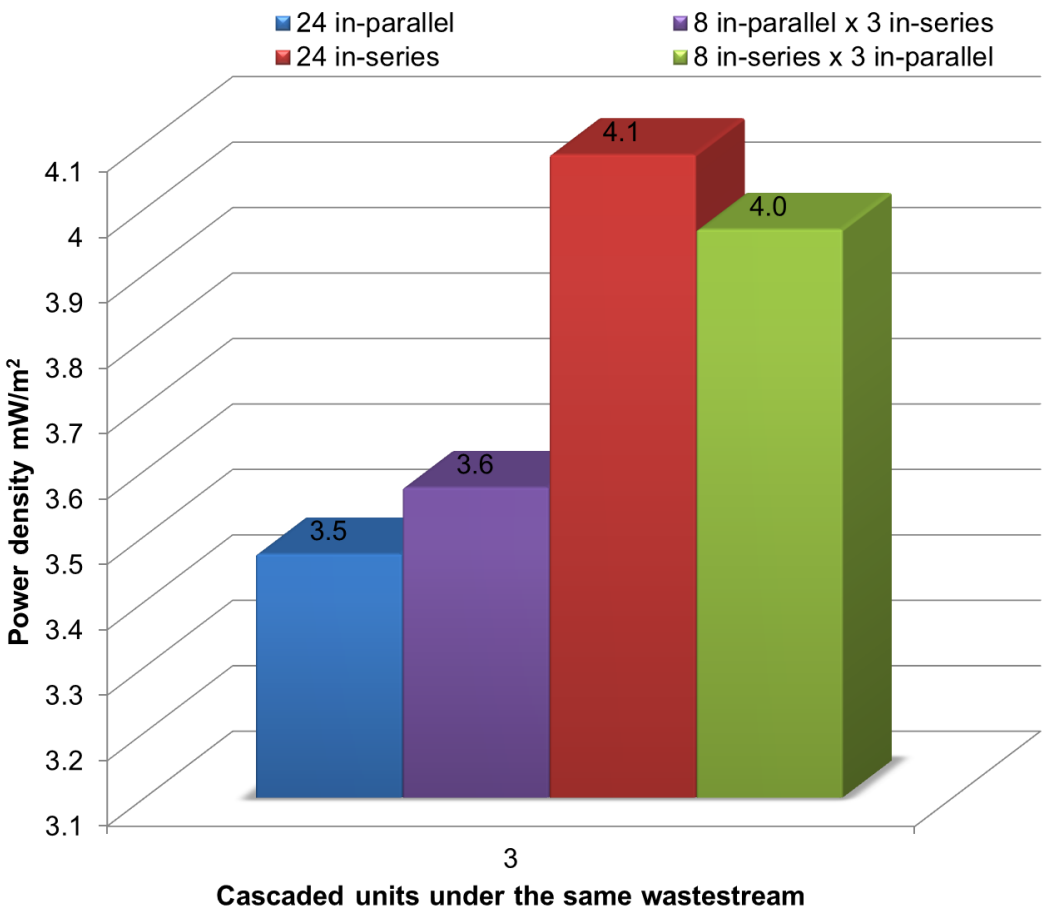

Fig. 4.12 Power density from cascades of 3 MFCs x8 groups in 4 different electrical configurations

4.3.2.2.2. COD treatment and R_{int}: 3-unit cascade regime with electrical reconfigurations

Following the decrease in current densities, COD values from three electrical configurations showed a similar decreasing trend. The in-parallel connection managed to treat 29%, decreasing its remediating capability by 3%, whereas the in-series connection maintained the same treatment outcome which it can be correlated with the small decrease in the series' C_D (5%). Both the 8 in-parallel by 3 in-series and the 8 in-series by 3 in-parallel stack connections showed a reduction in COD efficacy by 3%, to 20% and 16% respectively (Fig. 4.13). According to the above

results, the drop in COD removal is part of the suboptimal performance due to the malnutrition that governs each MFC on the end of each group in the stack.

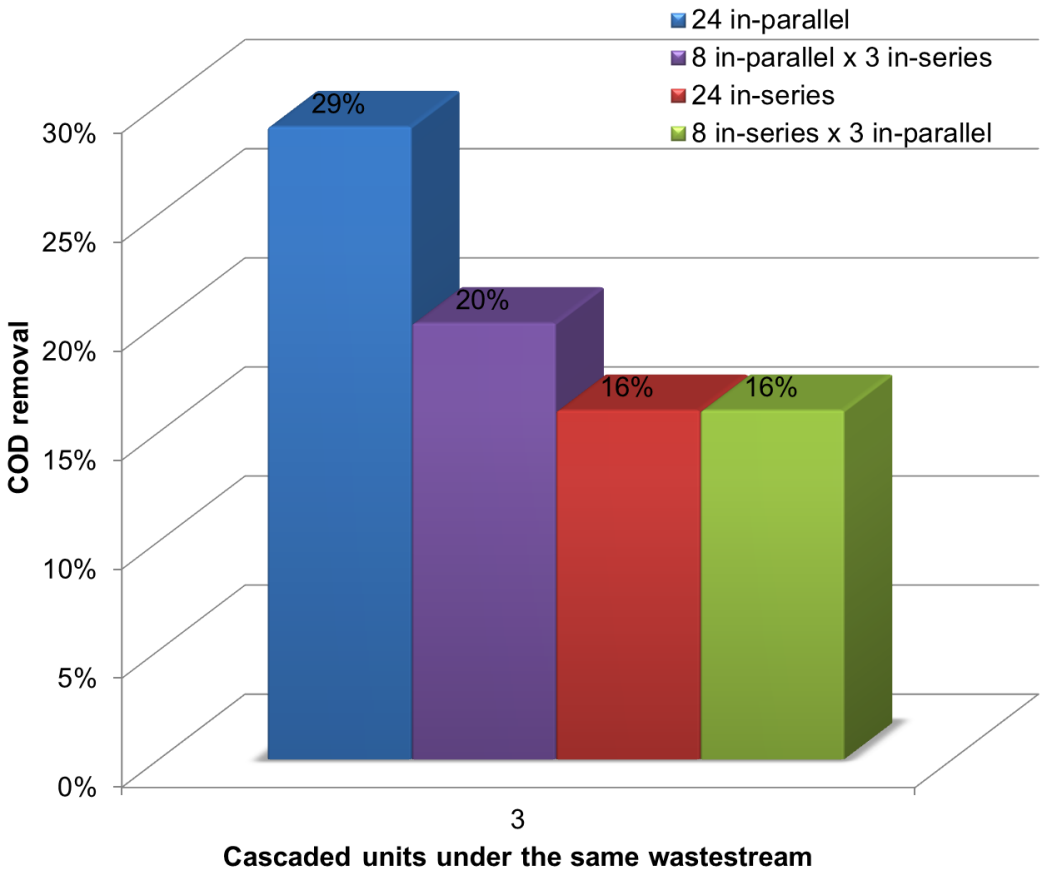

Fig. 4.13 COD treatment from MFC triplets sequentially fed and electrically connected in four possible electrical configurations

The negative effect on the performance, affected in a similar way the R_{int} in three electrical configurations. The R_{int} in-parallel increased by 70% (70 Ω), but in the series stacking decreased by 20% (20 kΩ). The 3 in-parallel units by 8 groups in-series increased its R_{int} by 28% (2.8 k) and the 3 in-series units by 8 in-parallel groups showed a rise of 53% (350 Ω) (Fig. 4.14). These results indicate that the lack of carbon energy in the third MFC in the cascade caused a large decrease in performance and the overall resistance but interestingly enough, did not affect the in-series resistance.

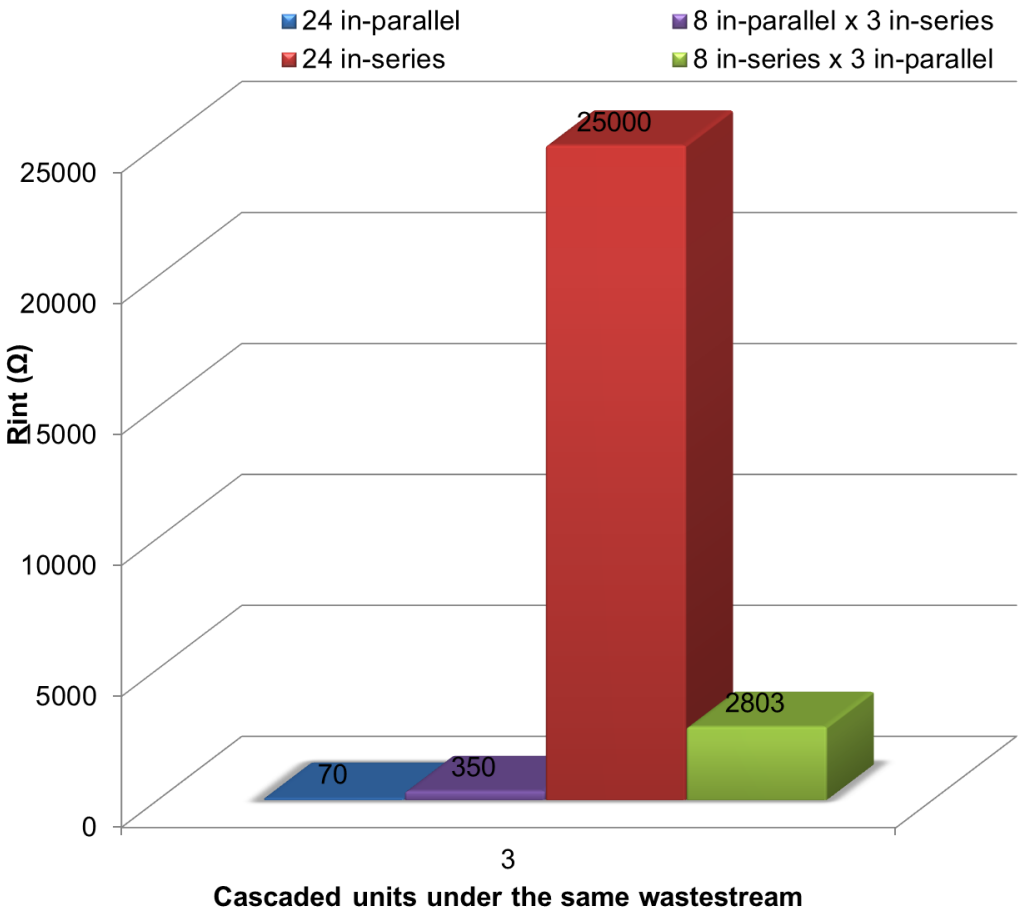

Fig. 4.14 R_{int} values based on MPP measurements from triplets of MFCs in sequential feeding regime and different electrical configurations

4.3.2.3. Cascades of 4 sequentially fed MFC units (**Stage 4**)

4.3.2.3.1. Performance readings

The fourth stage of the experiment comprised quadruplets of MFC units in cascade, forming 6 hydraulically insulated groups (Fig. 4.15). The substrate supply channels were now six and the total amount pumped fed to the stack was 6 mL/h (6x 1mL/h, HRT=6.8mL/h). Stacked MFCs connected in-parallel produced a P_D and a C_D of 3.75 mW/m^2 and 10.7 mA/m^2 subsequently (Fig. 4.17 and 4.16), which shows that power and current outputs compared to the previous stage, were not

affected significantly from the addition of a fourth unit in cascade and decreased by 3% and 4% respectively.

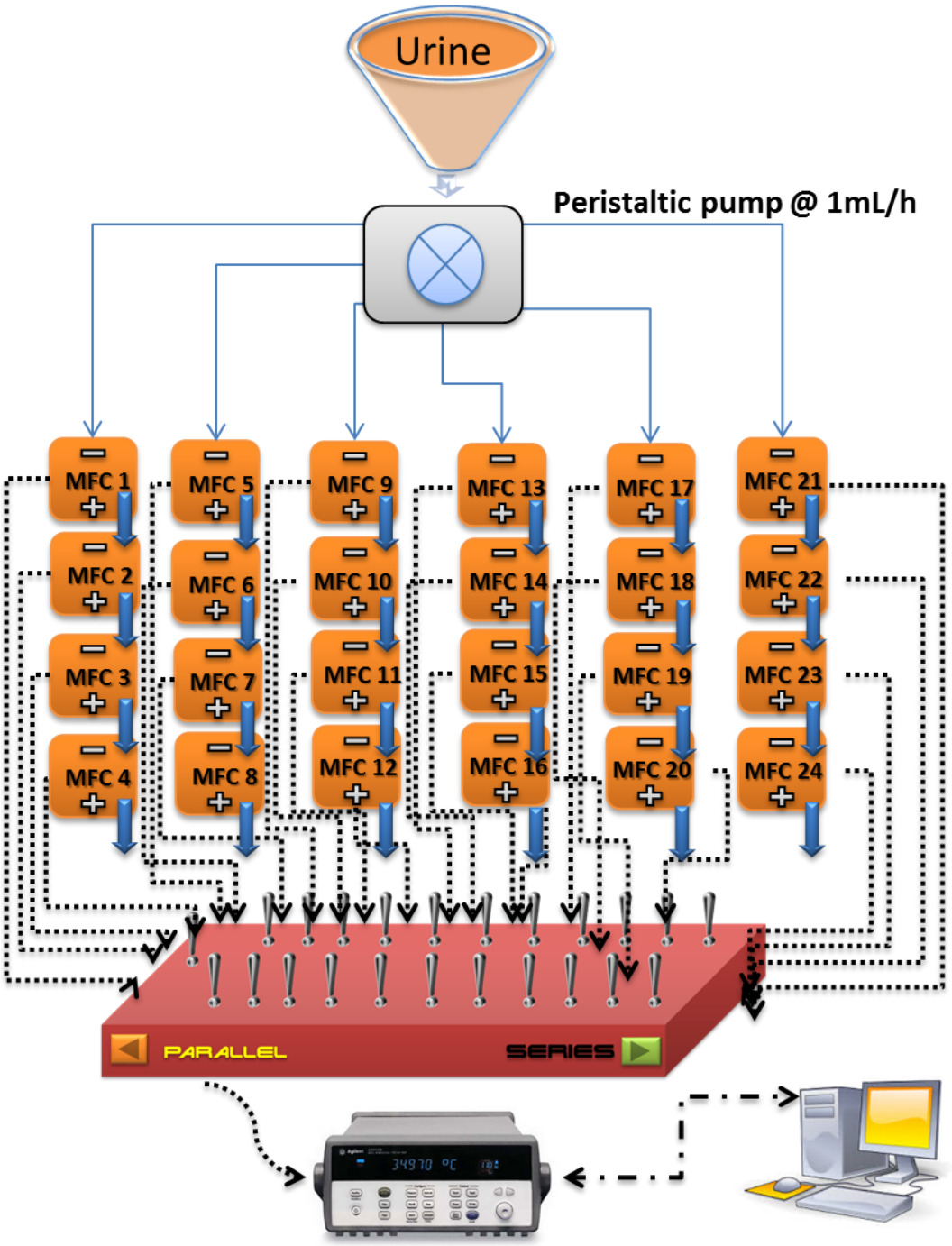

Fig. 4.15 Stage 4: setup of tetrads in cascade

The in-series electrical configuration produced 2.73 mW/m^2 and 0.56 mA/m^2, a 12% and 18% reduction in respect to the previous cascade setup. The electrical formations of 4 units in-parallel by 6 in-series produced 2.36 mW/m^2 and 1.57 mA/m^2 whereas the 4 units in-series by 6 in-parallel delivered a 1.98 mW/m^2 and 2.02 mA/m^2. In both cases the P_D showed a similar pattern in decrease by 42% and 45% accordingly. This can be attributed to the fact that the last MFCs on the cascade were running under suboptimal feeding conditions, affecting even more the already underperforming stack from stage three.

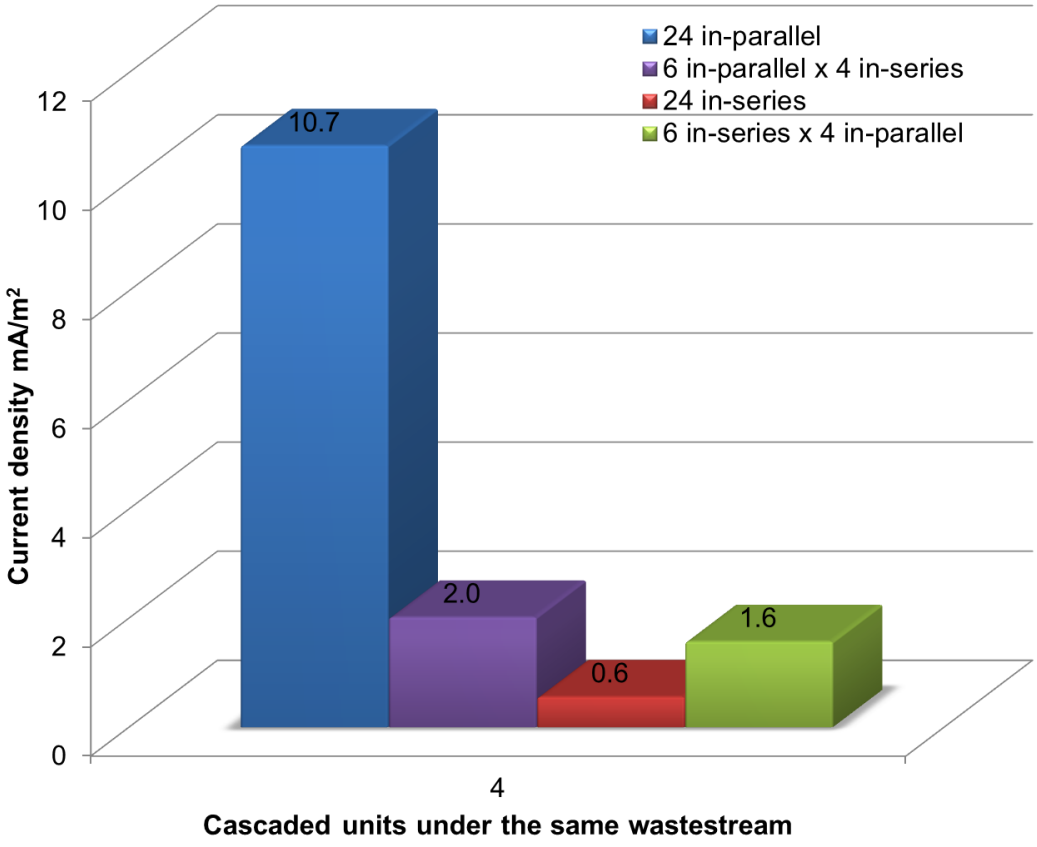

Fig. 4.16 Current density from cascades of 4 MFCs x6 groups in 4 different electrical configurations

However, a positive remark, are the results from the C_D which revealed that the increase of electrical in-parallel units in a plurality of in-series (electrically) connected elements may have given the stack resilience since the stack dropped by

only 16% and could possibly withstand further deterioration. Adversely, the configuration whereby an additional in-series element was introduced in the stack, showed a decrease of 60% in C_D. This large discrepancy in performance could be related with the addition of previously fed units directly from the feedstock bottle, underneath the first MFC on the cascade. This resulted in a cascade where only MFCs 1 and 13 were kept fed by the original substrate. The rest of the top MFCs in the cascade groups had previously been in a poor feeding position. That, combined with the fact that MFCs connected in–series show the same current flow for all elements, may be the reason for this large declination.

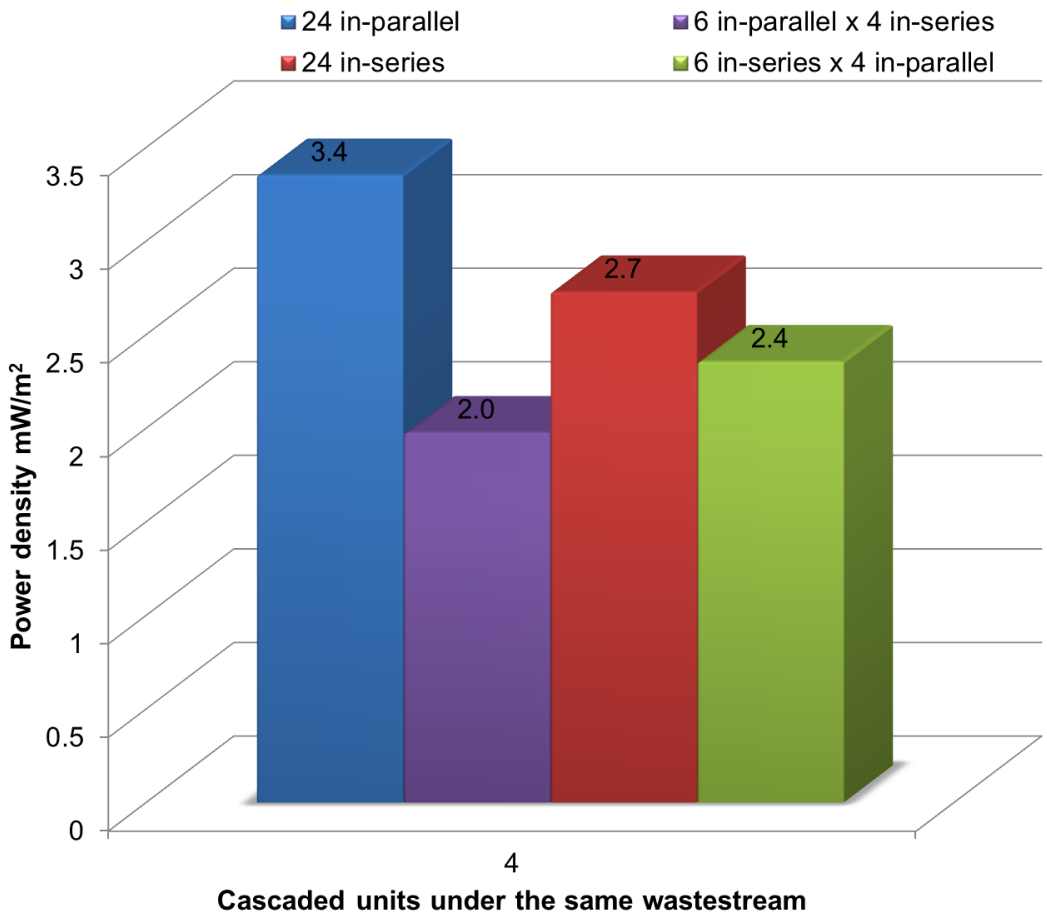

Fig. 4.17 Power density from cascades of 4 MFCs x6 groups in four different electrical configurations

4.3.2.3.1. COD treatment and R_{int}: 4-unit cascade regime with electrical reconfigurations

With the cascade having all MFCs in-series, the cascade achieved an 18% COD removal, 2% higher than stage 3. All MFCs connected in-parallel (electrically), showed a 27% COD treatment, 2% lower than in stage three, yet maintaining a sufficient organic load removal. The configuration of 4 in-series by 6 in-parallel managed a 17% COD treatment of urine, 3% lower from the previous stage (Fig. 4.18), pointing out the crucial role of additional in-series elements in waste treatment. On the other hand, the electrical combination of 4 in-parallel units by 6 groups in-series achieved a 28.6% COD remediation, so far the highest value from this cascade scenario.

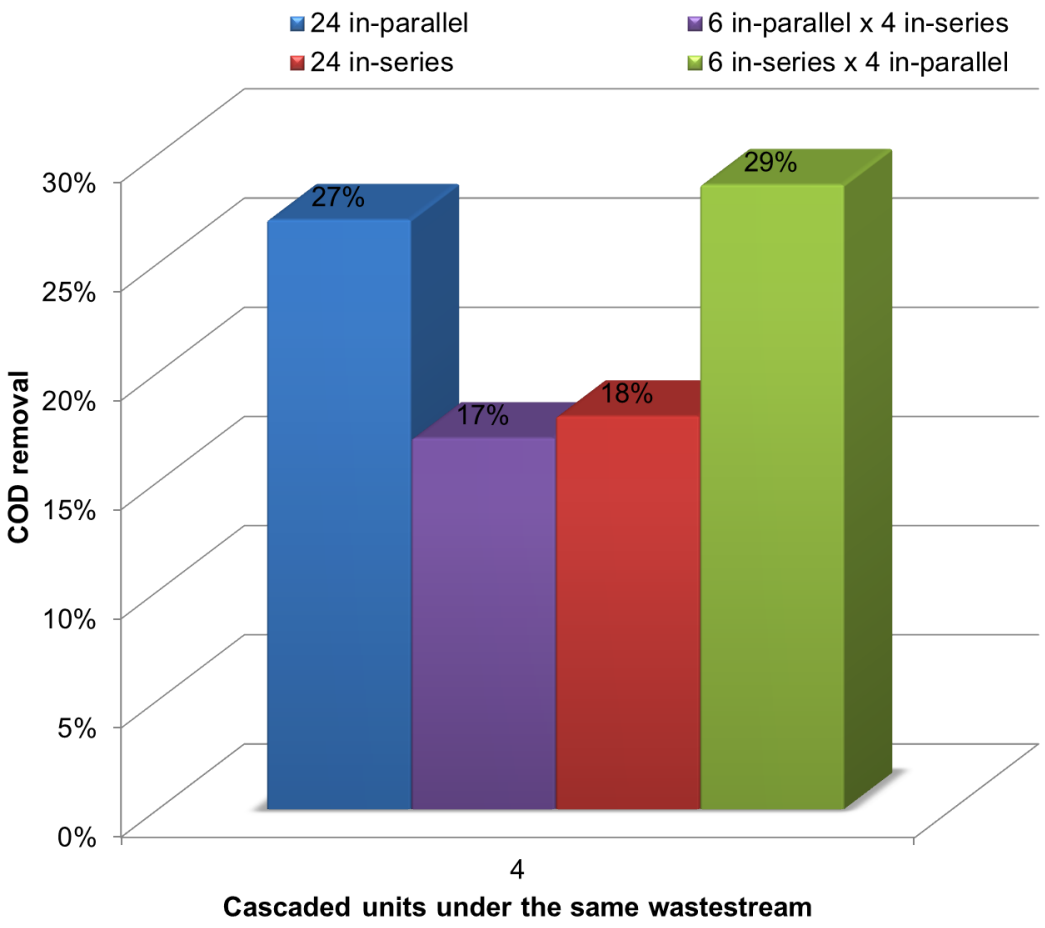

Fig. 4.18 COD treatment from hydraulically connected of MFC tetrads in four electrical configurations

The internal resistance in a stack losing power would be expected to rise due to variances in substrate concentration feeding into the cascade MFCs. In fact the in-series configuration doubled its value (42 kΩ) (Fig. 4.19) and similarly the 4 in-series units by 6-in-parallel groups increased by 70%. Nevertheless, the parallel connection maintained the same value as in stage three (70 Ω) and the 4 units in-parallel by 6 groups in-series showed a 6% decrease (2355 Ω). The parallel connections in conjunction with the best fed MFCs from the cascade groups in the stack with the lowest R_{int} were able to maintain a steady overall resistance of the system thus facilitating ease of charge transfer to the external load.

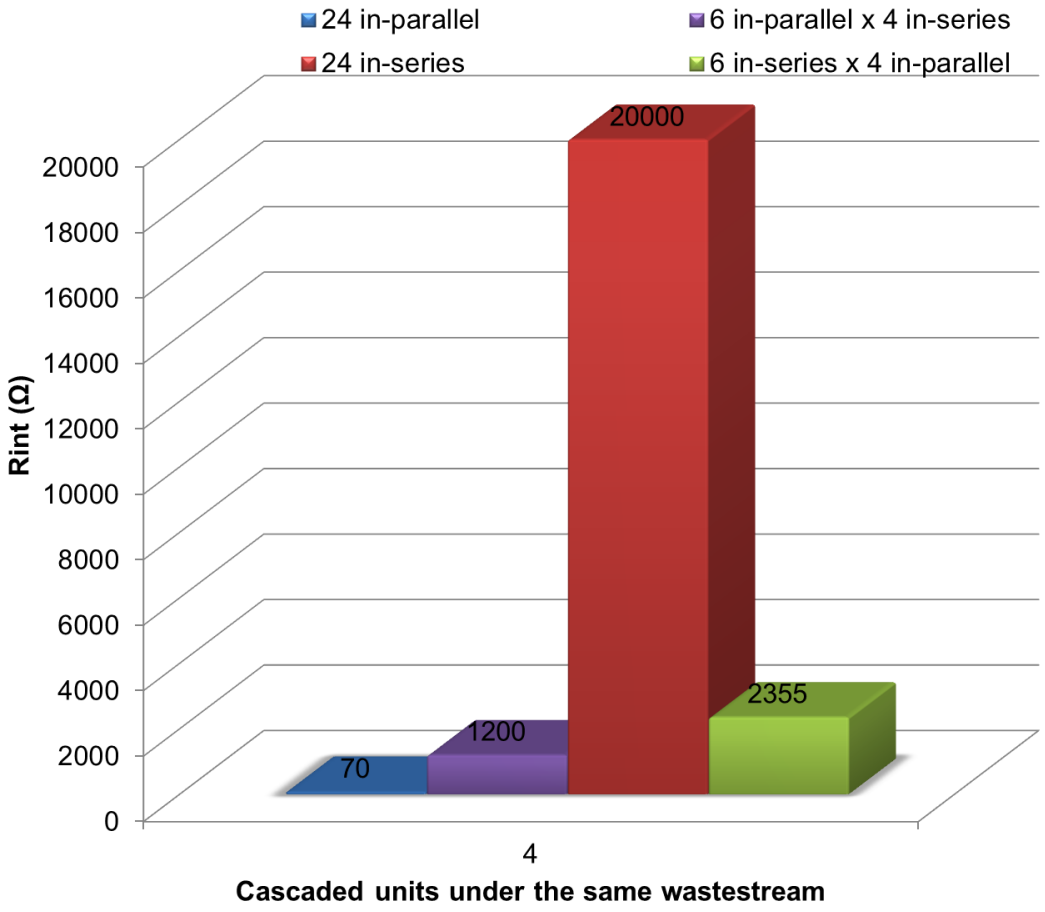

Fig. 4.19 R_{int} values based on MPP measurements from six groups of 4 MFCs sequentially fed and configured in different electrical configurations

4.3.2.4. Cascades of 6 sequentially fed MFC units (**Stage 5**)

4.3.2.4.1. Performance readings

The fifth stage of the experiment included the addition of two more MFC units in the existing cascade, forming 4 hydraulically insulated groups (Fig. 4.20). Four substrate channels were pumping a total amount of 4 mL/h (4x 1mL/h) of fresh urine to the stack.

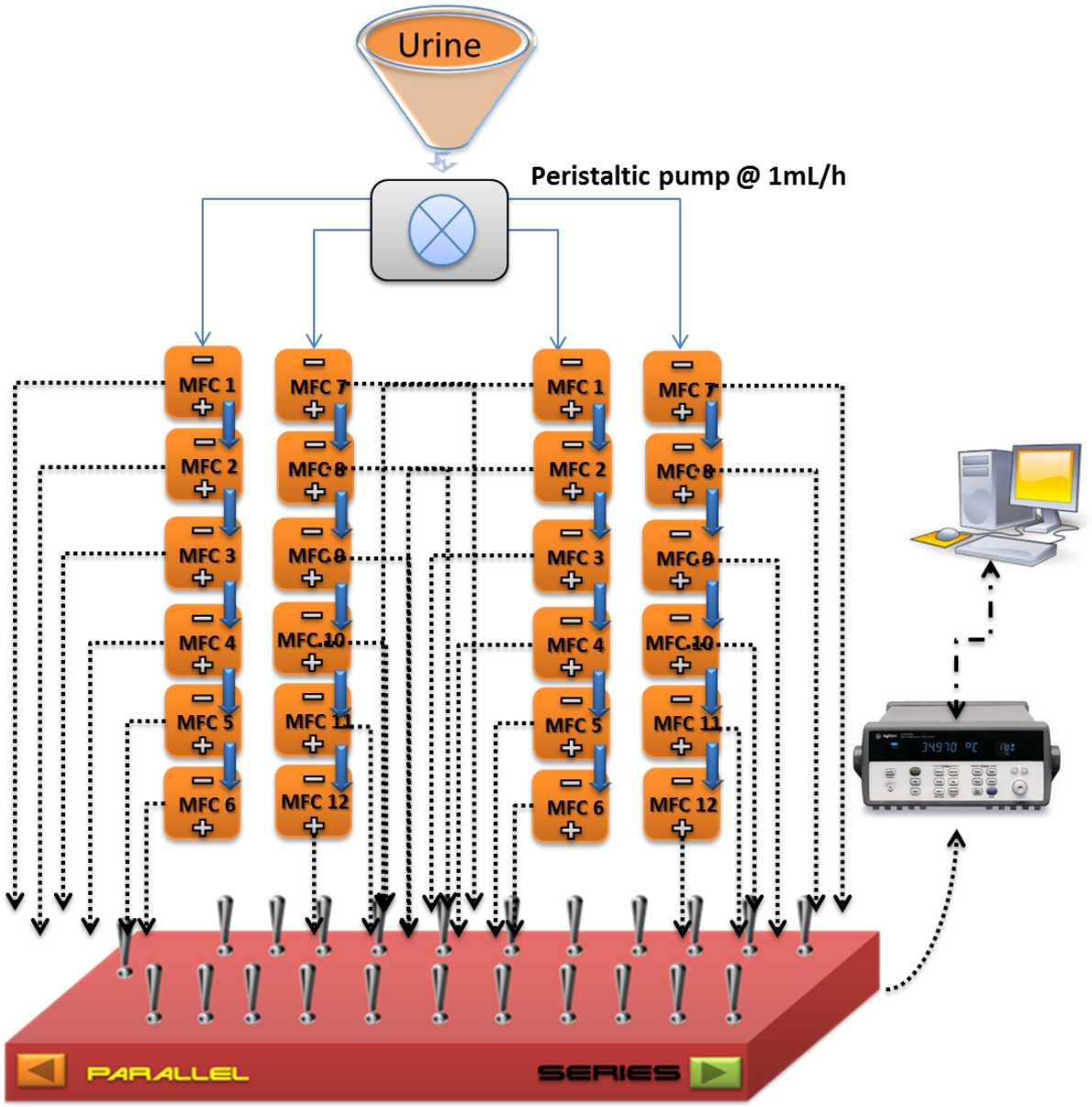

Fig. 4.20 Stage5: setup of the sixfold cascade groups

Stacked MFCs connected electrically in-parallel produced P_D and C_D of 2.05 mW/m^2 and 11 mA/m^2 (Fig. 4.22 and 4.21). The P_D continued its decreasing trajectory, strengthening the effect of cascading multiple units in the stack and reached a decrease of 39%. Contrariwise, the current output compared to the previous stage, was slightly increased with the addition of two more units by 3%. The in-series configuration produced 1.76 mW/m^2 and 0.32 mA/m^2, a 35% and 43% reduction in respect to the previous cascade setup.

The combined electrical formation of 6 units in-parallel forming 4 groups in-series resulted in P_D and C_D of 2.22 mW/m^2 and 2.34 mA/m^2. In this case, even though power was decreased by 6% the current density showed an increase of 33%. The phenomenon of increased current densities from the presence of in-parallel electrical elements at this stage of the cascade is mainly attributed to the shuffling of previously positioned MFCs in upper parts of the cascade to the lower parts of the cascade, giving the advantage of maintaining the C_D to high levels whilst the P_D dropped. However this is expected to cause a drop in the stack's voltage, as V=P/I.

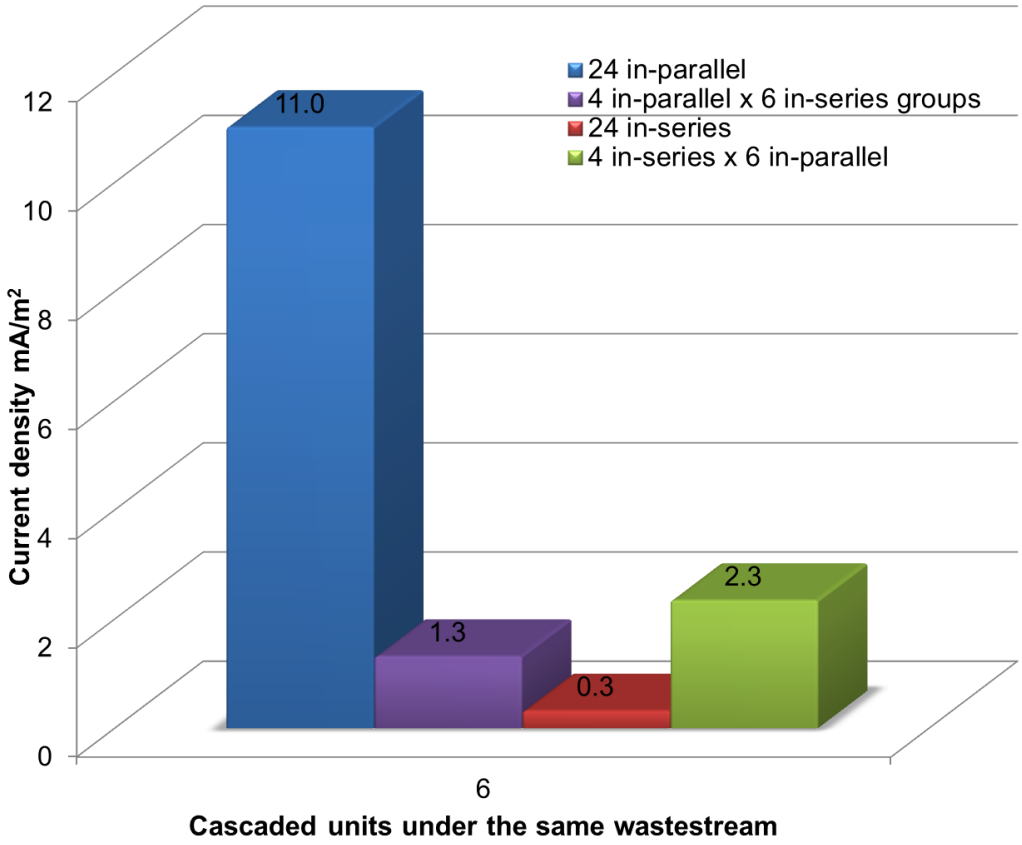

Fig. 4.21 Current density from cascades of 6 MFCs x4 groups in 4 different electrical configurations

The electrical formation of 6 units in-series by 4 in-parallel groups, showed a negligible 0.5% decrease in P_D (1.97 mW/m^2) and a 35% decrease in C_D (1.32

mA/m^2). Again, the presence of in-series elements in the cascade played a negative role in current generation but managed to balance the power output with the increased voltage that renders in-series connections.

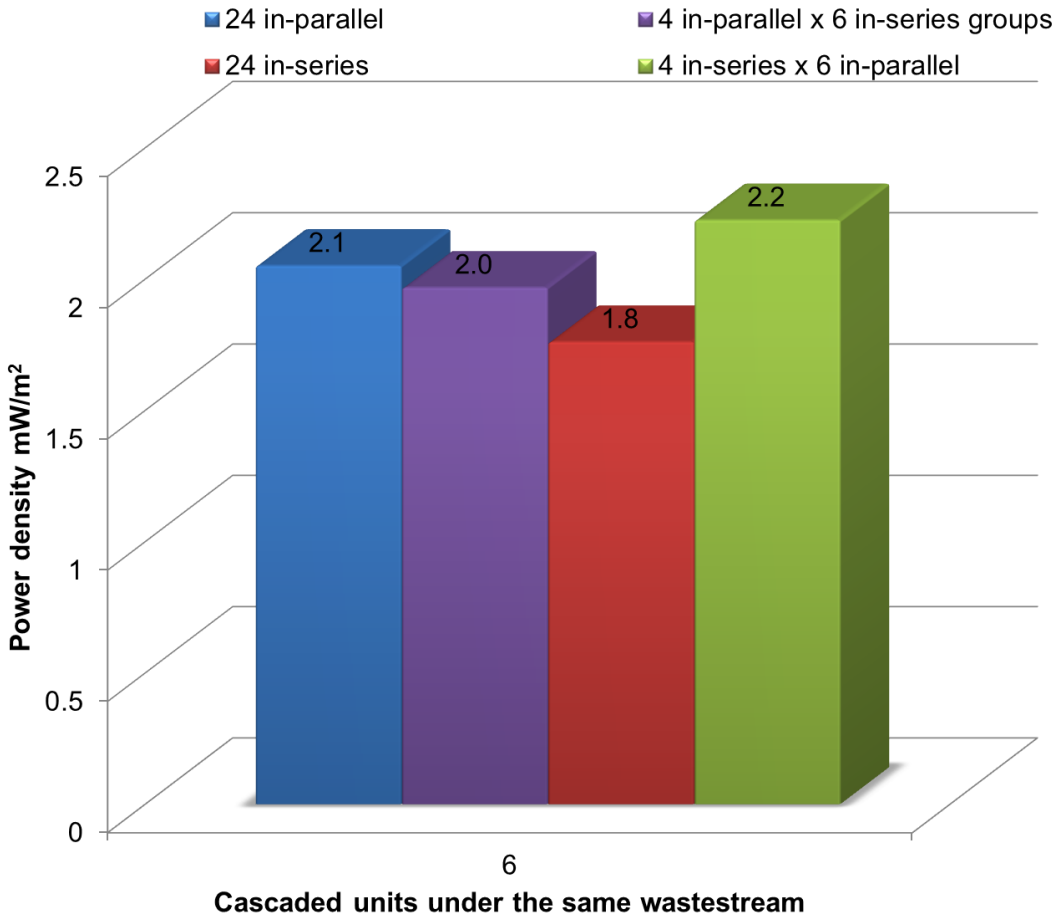

Fig. 4.22 Power density from cascades of 6 MFCs x4 groups in four different electrical configurations

4.3.2.4.2. COD treatment and Rint: 6-unit cascade regime with electrical reconfigurations

The cascade MFC stack when connected electrically in-parallel managed to remediate 33.6% (Fig. 4.23) of the provided feedstock showing the highest levels of treatment to this point of the experiment. As mentioned before, the removal

benefited not only from the increased number of MFCs down the waste stream but also from the insertion of more electro-active biofilms parenthetically along the cascade as time progressed. In-series connection of the whole cascade MFC stack resulted in a reduced COD value of 12%. COD reduction from 6 units in-parallel by 4 in-series groups was 30% and the other configuration, 6 units in-series by 4 in-parallel groups, managed to remove an 18% of COD.

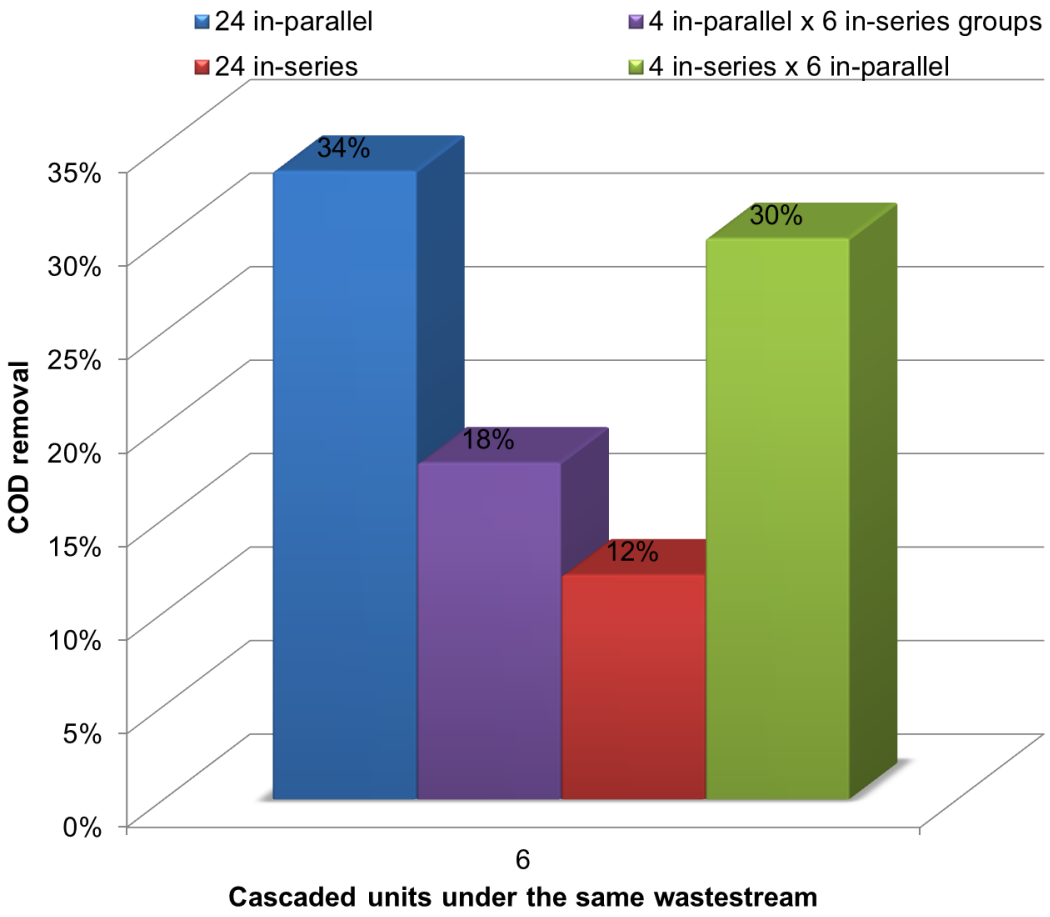

Fig. 4.23 COD treatment from sequentially fed MFC hexads in four electrical configurations

The electrical configuration with all units in-parallel showed a R_{int} decrease to 40 Ω, and it seemed to be closely related with the C_D values seen in the parallel and mixed parallel configuration (Fig. 4.24). The R_{int} from the in-series connection

exhibited a 30% increase, to 60 kΩ and in the 6 units in-parallel by 4 in-series groups decreased by 58% to 1 kΩ. The next configuration, 6 units in-series by 4 in-parallel groups increase the stack's R_{int} by 57% (2.8 kΩ).

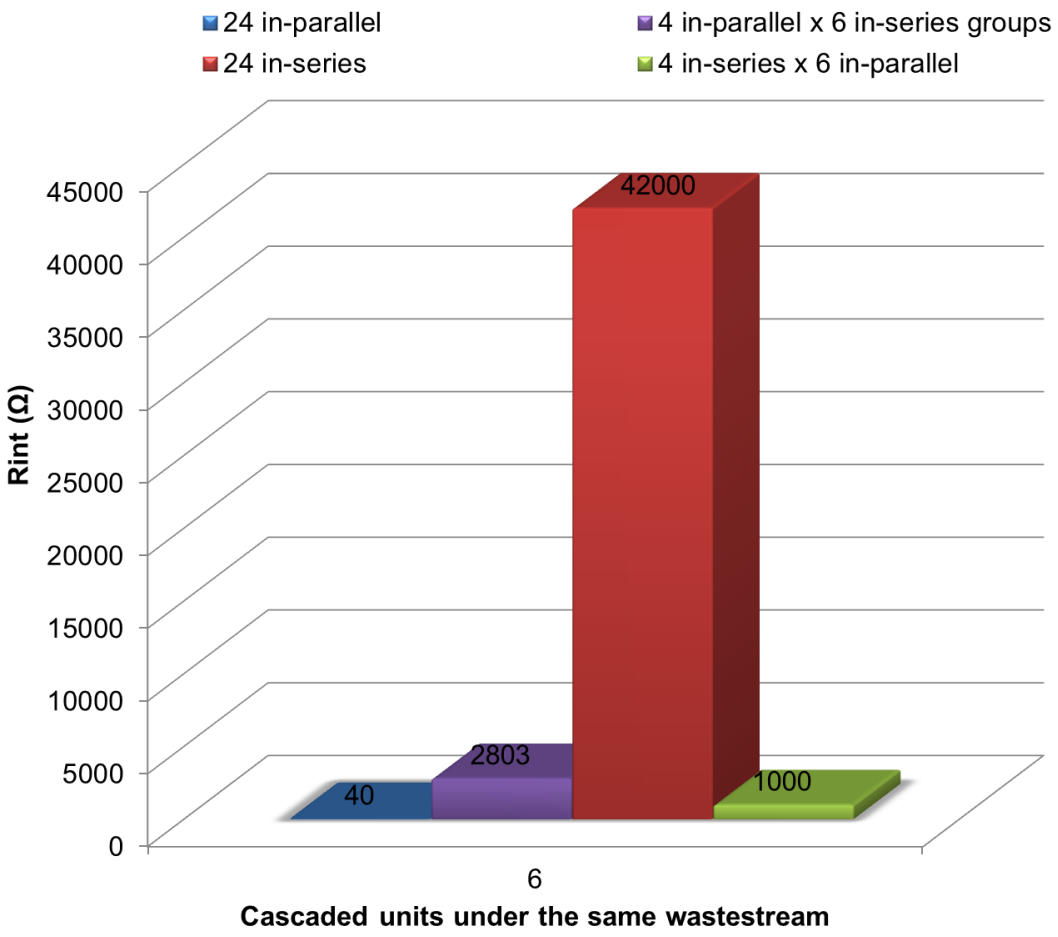

Fig. 4.24 R_{int} values based on MPP measurements from four groups of 6 MFCs in fluidical cascade and different electrical configurations

At this stage, the shuffling of two more MFC units at the end of the cascade combined with in-parallel elements, showed a decreased R_{int}, high COD removal and rebounded the current densities to higher levels. In-series configurations exhibited an opposite behaviour speculating that the shuffling of MFCs alone might be sufficient to maintain performance characteristics albeit electrical configuration is also pivotal for cascade robustness and longevity.

4.3.2.5. Cascades of 8 sequentially fed MFC units (Stage 6)

4.3.2.5.1. Performance readings

Stage 6 of the experimental setup examined the addition of two more units in the cascade, now forming octets of hydraulically connected MFCs in 3 groups of different electrical connections (Fig. 4.25).

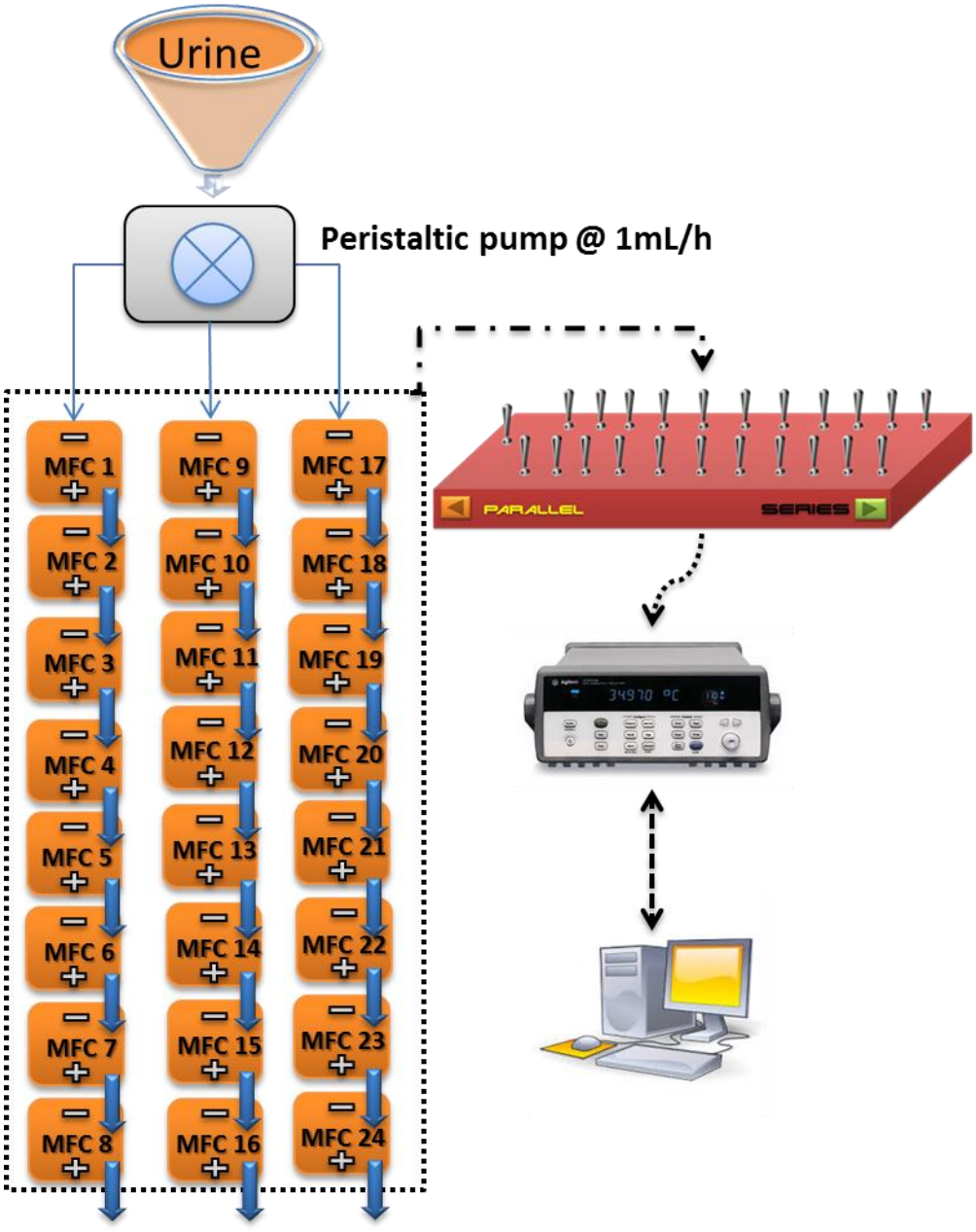

Fig. 4.25 Stage 6: setup of the MFC stack with 3 groups of octets in cascade mode

Results from all MFCs electrically configured in-parallel showed a P_D of 2.19 mW/m^2 and a C_D of 8.8 mA/m^2 and the MPP occurring at 70 Ω. MFCs connected in-series produced a P_D of 1.61 mW/m^2 and a C_D of 0.26 mA/m^2 with the MPP occurring at 24 kΩ. The configuration of 8 units in-parallel by 3 groups in-series reached a maximum of 2.21 mW/m^2 and a C_D of 2.34 mA/m^2 (Fig. 4.27 and Fig. 4.26) at 1 kΩ. The last electrical configuration comprised 8 in-series units by 3 in-parallel groups, delivered 1.86 mW/m^2 and 1.06 mA/m^2 at 4 kΩ.

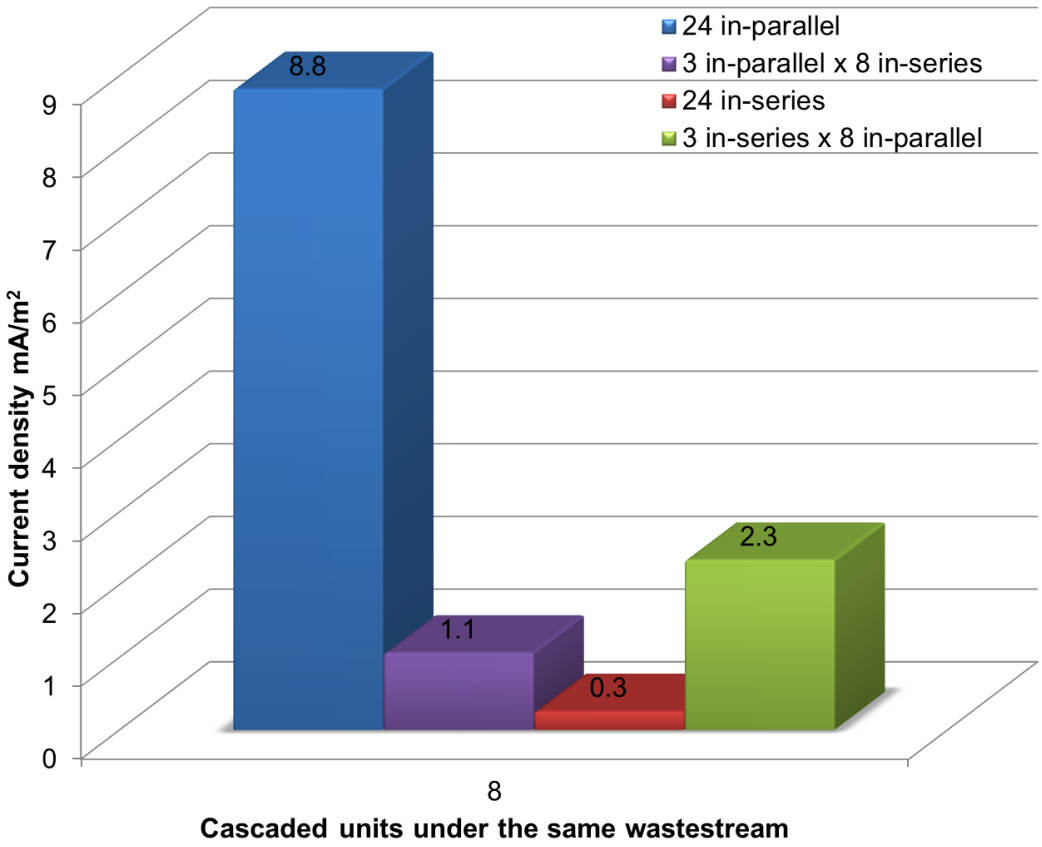

Fig. 4.26 Current density from cascades of 8 MFCs x3 groups in 4 different electrical configurations

Power outputs from the in-series, 8 in-parallel x 3 in-series and 8 in-series x 3 in-parallel configurations showed a decrease of 8%, 0.5% and 5.5% respectively. The configuration with the highest number of units connected in-parallel demonstrated a more stable performance compared to the other formations with plethora of in-series elements. However the increase in power density that was observed in the in-parallel connection could be a case of stronger units previously found on the top of a cascade group increasing the overall voltage after entering the bottom of the cascade.

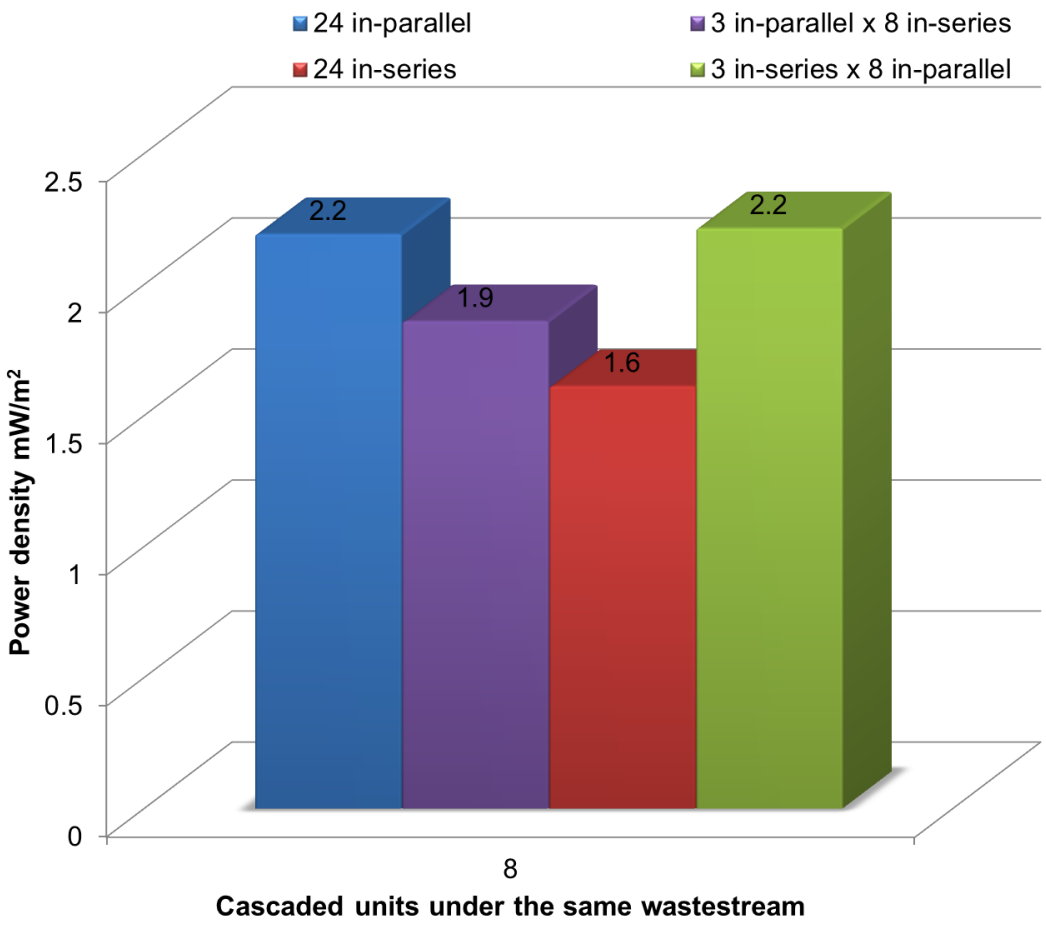

Fig. 4.27 Power density from cascades of 8 MFCs x3 groups in four different electrical configurations

4.3.2.5.2. COD treatment and R_{int}: 8-unit cascade regime with electrical reconfigurations

The ability of each electrical configuration to treat urine was examined by measuring the COD sample that ran off the last MFC of the cascade in a sterilised collection bottle. Due to the low flow rate speed (1mL/h, HRT= 6.7 h) and the high number of MFCs down the waste stream, COD was performed after 48 hours, when the collection bottle was starting to fill up with processed urine. The MFCs connected all in-parallel managed to reduce 33.2% of total COD in fresh urine, 1.2% less than in the six-unit cascade previously (Fig. 4.28).

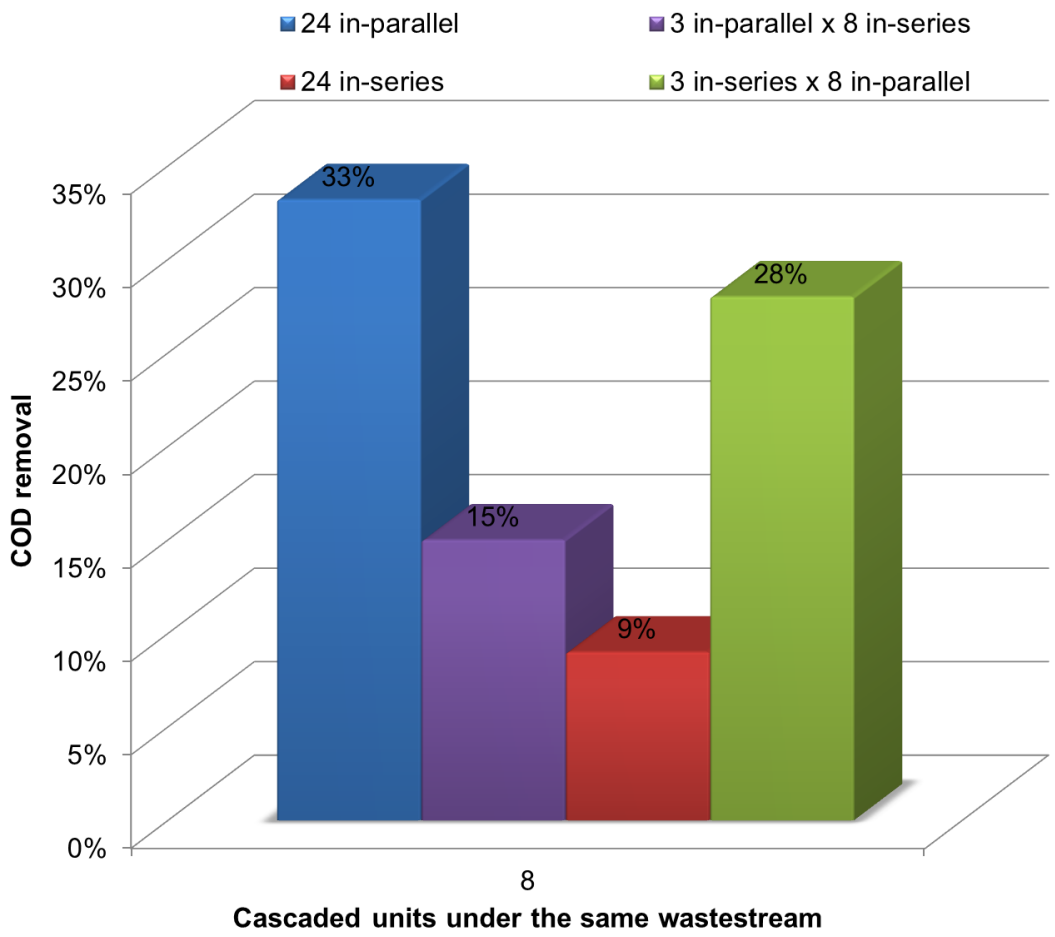

Fig. 4.28 COD treatment from hydraulically connected of MFC octets in various electrical configurations

The R_{int} was increased from 40 Ω to 70 Ω (Fig. 4.29) and it could be suggested that elements with previously low R_{int} were under feeding-stress and the overall resistance increased further. MFCs connected in-series managed to remove 9% of COD decreasing their performance by 3% compared to the previous stage. The internal resistance of the in-series connection, showed a significant increase of 42% (60 kΩ). The 8 units in-parallel connected with 3 groups in-series achieved a 28% decrease in COD whilst maintaining a R_{int} of (1 kΩ). Finally the 8 in-series units by 3 in-parallel groups reduced COD by 15% and continued to increase its internal resistance to 4 kΩ.

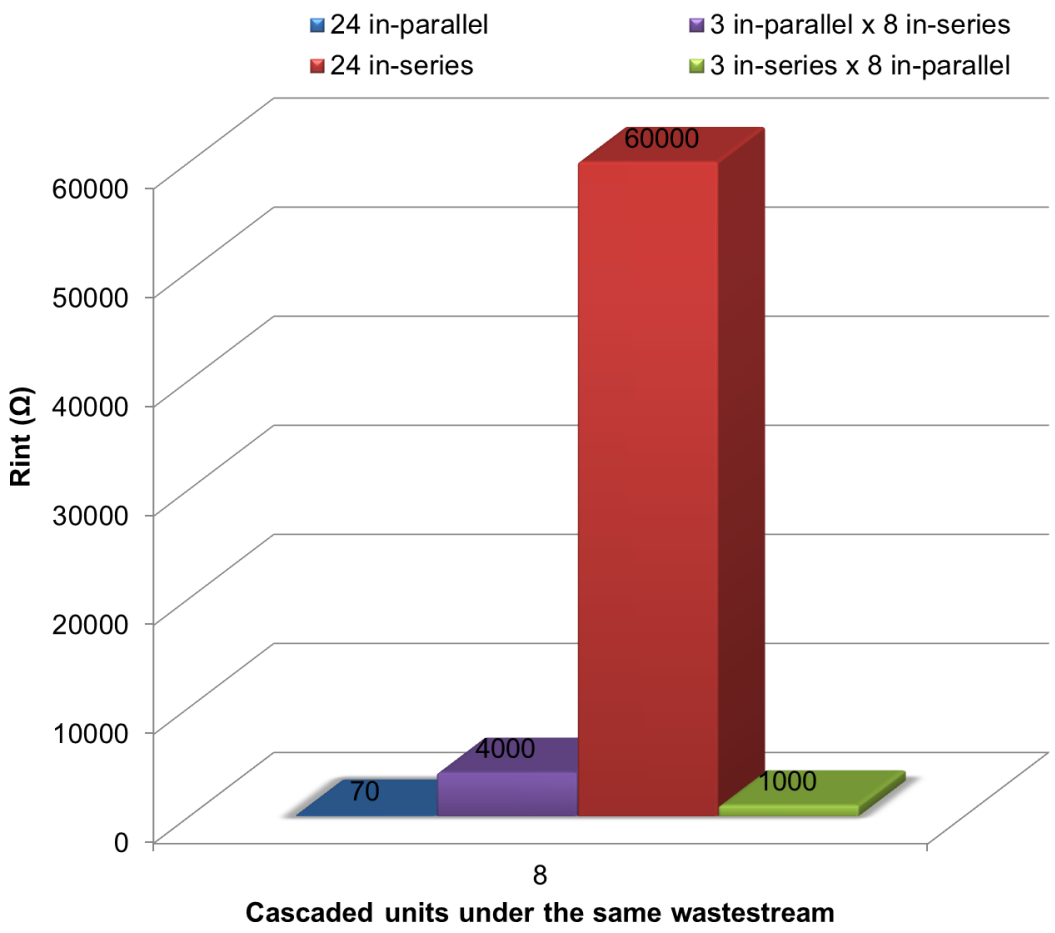

Fig. 4.29 R_{int} values based on MPP measurements from three groups of 8 MFCs in sequentially cascaded and connected different electrical configurations

4.3.2.6. Cascades of 12 sequentially fed MFC units (**Stage 7**)

4.3.2.6.1. Performance readings

The penultimate stage of hydraulic configuration of the stack involved two cascaded rows consisting of twelve units each connected electrically (Fig. 4.30).

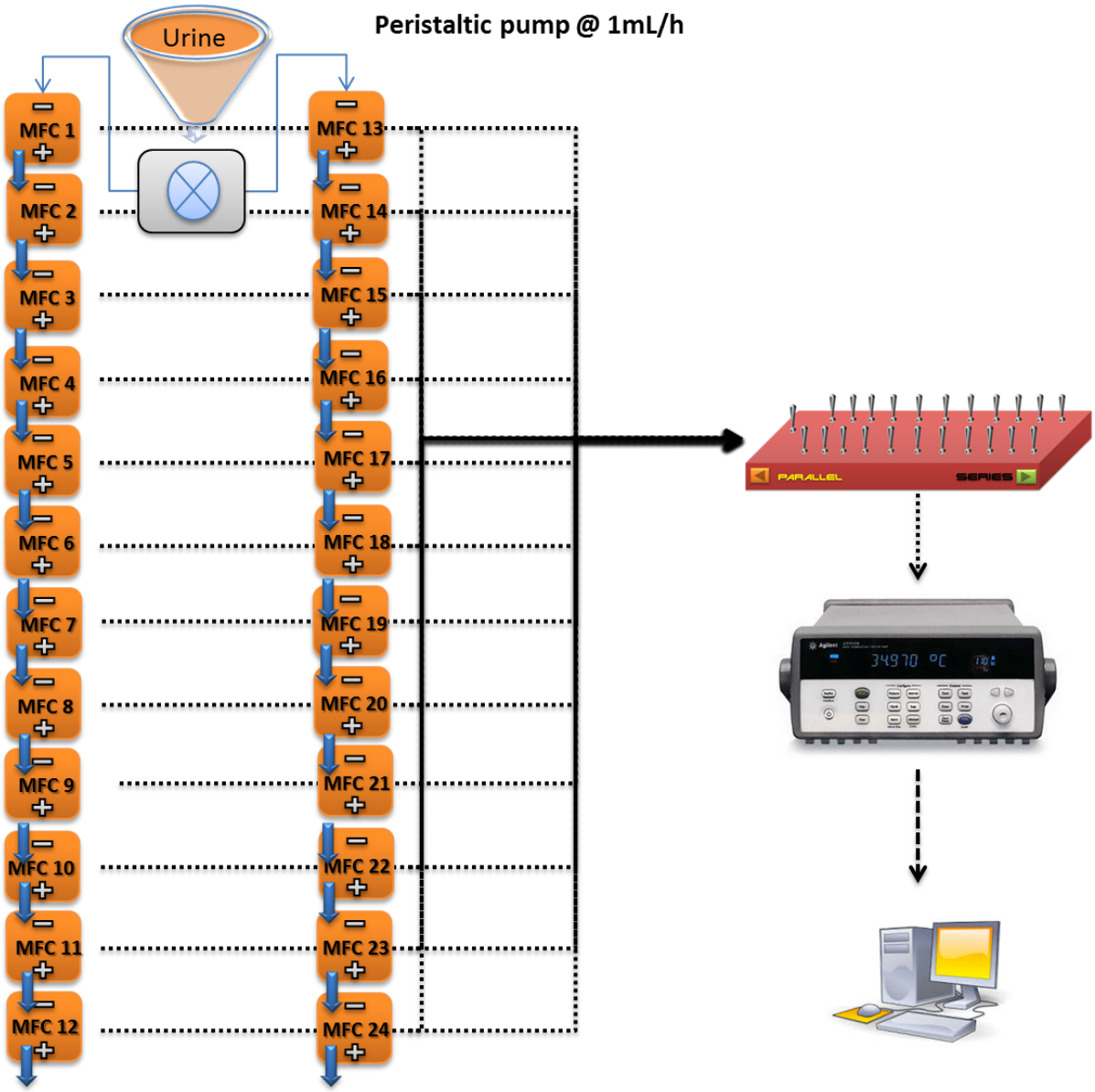

Fig. 4.30 Stage 7: setup of the MFC stack with 2 groups of MFC dozens in cascade mode

Polarisation experiments in the stack when all MFCs were connected in-parallel showed a P_D of 2.4 mW/m^2 and a C_D of 10.2 mA/m^2, an increase of 9.5% in power and 16% in current compared to the performance in stage 6. In-series stacked MFCs generated a P_D of 1.7 mW/m^2 and a C_D of 0.4 mA/m^2; increased by 5.6% and 53% respectively from the previous stage. The configuration of 12 parallel units by 2 groups in-series produced 2.53 mW/m^2 and 5.2 mA/m^2, an improvement of 15% for P_D and a 2.2-fold enhancement for C_D. The remaining configuration of 12 serially MFCs in 2 parallel groups generated a P_D of 2 mW/m^2 and a C_D of 1.11 mA/m^2, which was a 7.5% increase in power and 5% in current (Fig. 4.32 and 4.31).

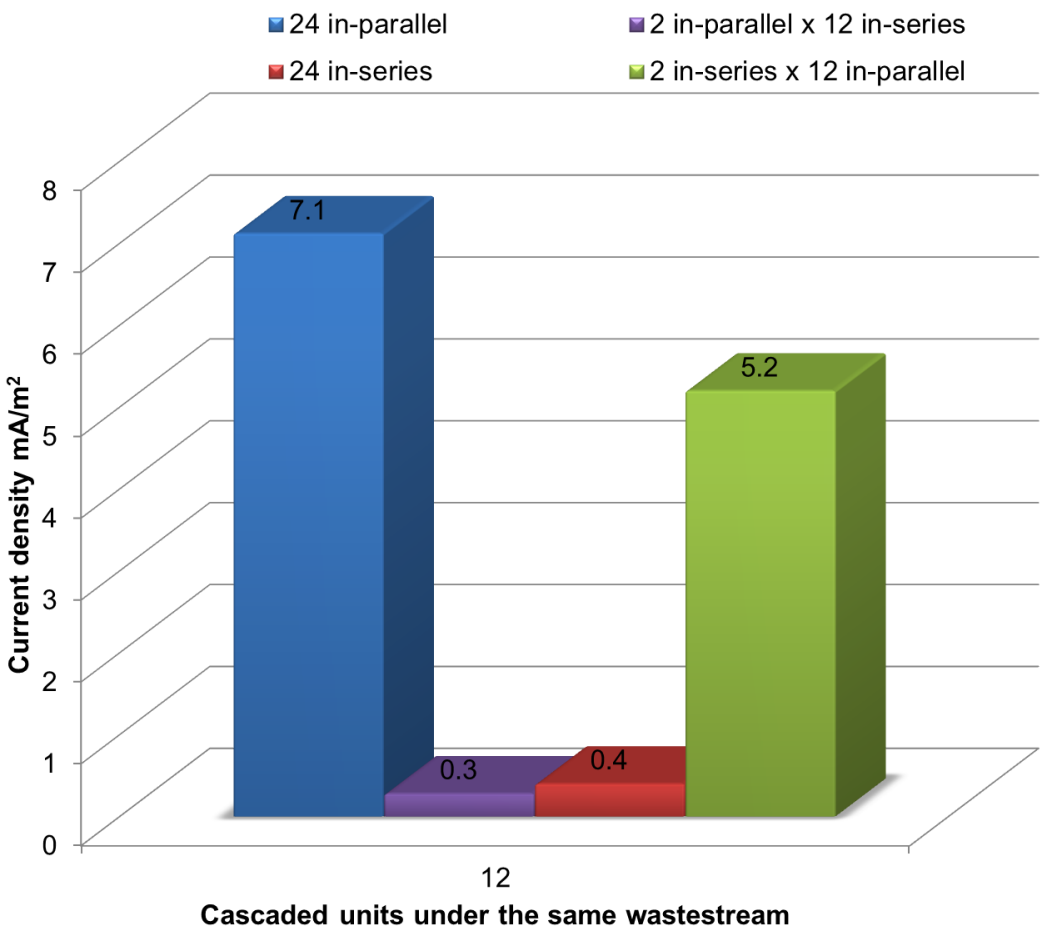

Fig. 4.31 Current density from cascades of 12 MFCs x2 groups in 4 different electrical configurations

In this stage it is the first time that more than two units were transferred away from positions near the feeding source. It could be suggested that this shuffling may affect the overall performance adversely, continuing the decreasing pattern in power and current from the previous four stages. However, all the electrical configurations improved their power and current outputs.

The reason behind this could be found when closely tracing back the repositioned MFCs in the cascade. MFCs number 9, 10, 11, and 12 previously found near the feeding port were transferred below MFC 8, which is further away from the inlet. At the same time MFCs 17 to 24 were positioned below MFC 13 to 16, a cascade already away from the inlet. Hence the new two groups of cascades remained with only the array of MFCs 1 to 8 with a fixed feeding regime. Thus, if all parameters remained the same, then these biofilms would be expected to sustain similar electro-active activity. Furthermore, the biofilms previously deprived of unprocessed urine and now being provided with richer feedstock, are likely to recover to a previous state of metabolic activity that allows for a better electro-genic performance [148].

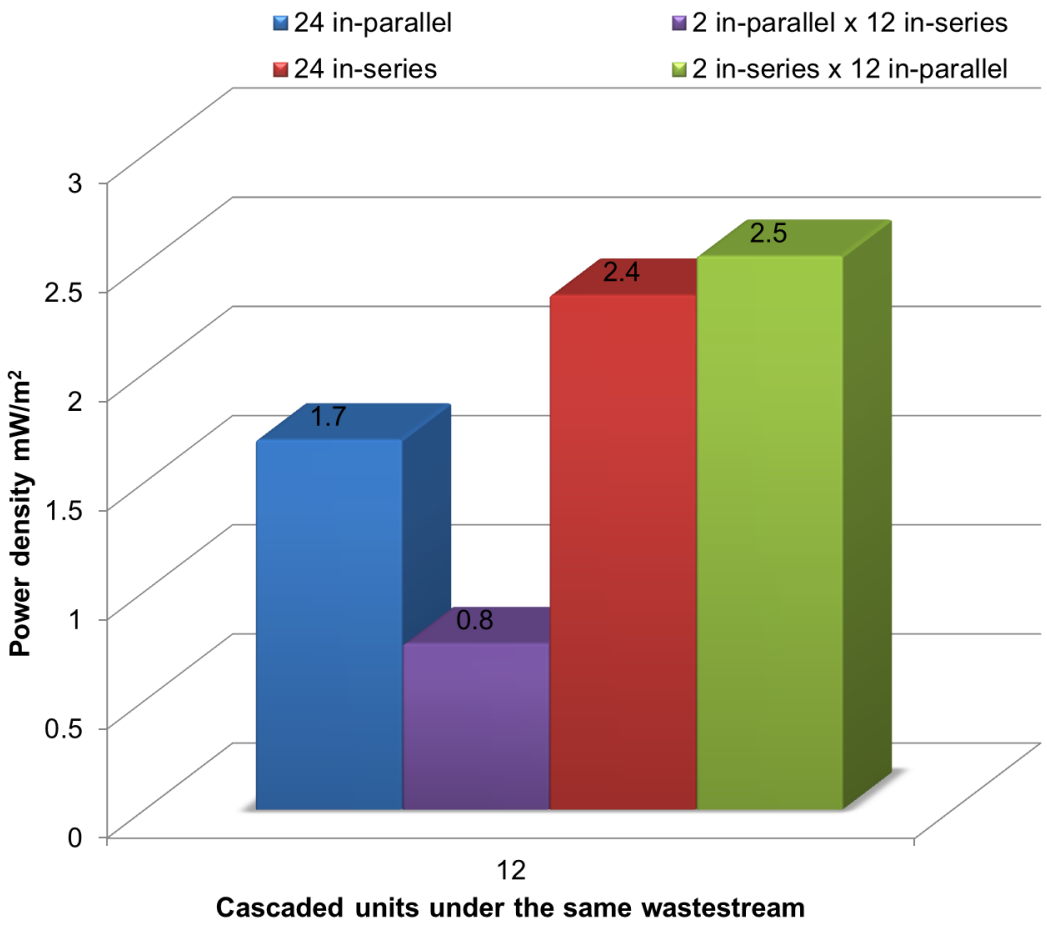

Fig. 4.31 Power density from cascades of 12 MFCs x2 groups in four different electrical configurations

4.3.2.6.2. COD treatment and R_{int}: 12-unit cascade regime with electrical reconfigurations

The two groups of 12-units cascades removed 26% of the urine's organic content when configured in-parallel, 7% less COD reduction than with the 8-unit cascade (Fig. 4.32) but still maintaining sufficient removal efficiency for that retention time [159].

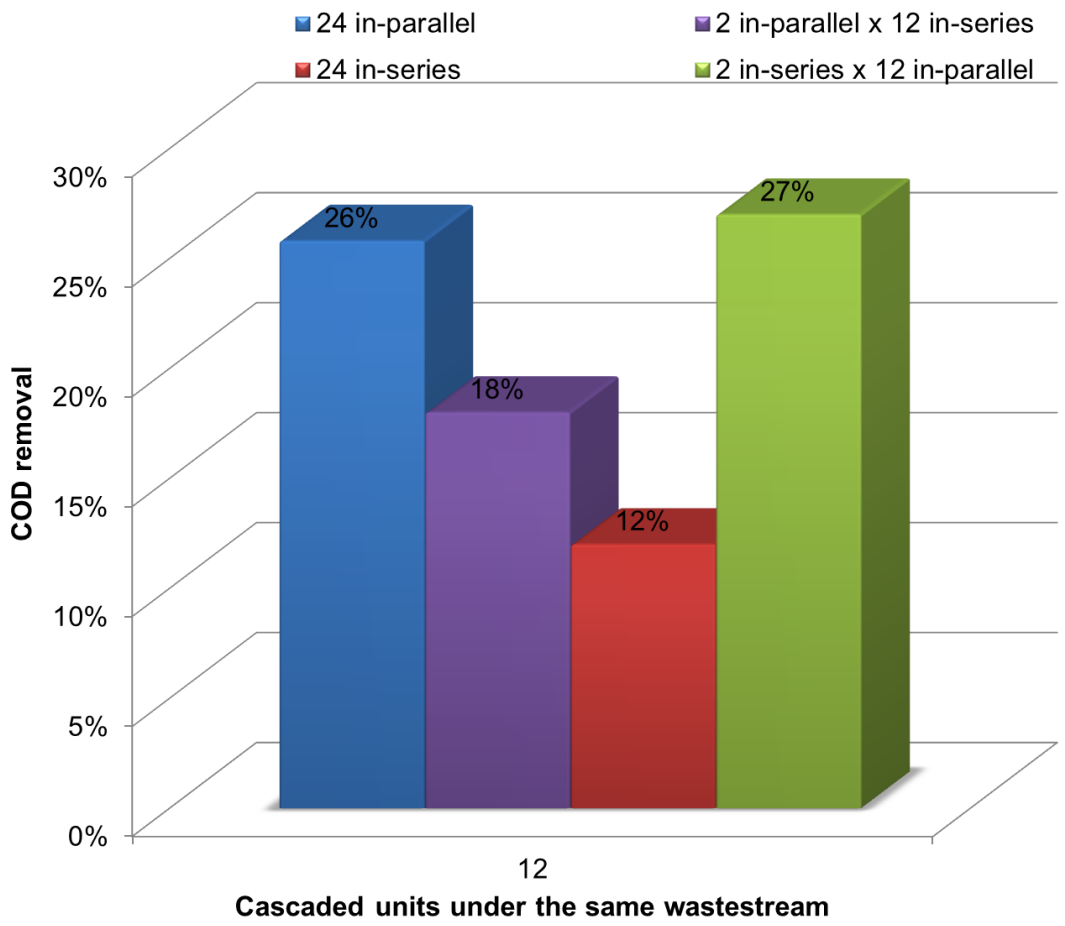

Fig. 4.32 COD treatment from 12 hydraulically connected MFCs in two groups under four electrical configurations

The R_{int} increased from 70 Ω to 80 Ω. MFCs connected in-series increased to 12% the COD removal (Fig. 4.33) and displayed a R_{int} of 38 kΩ. The formation of 12 units in-parallel of 2 in-series groups achieved a 27% decrease in COD whilst maintaining a R_{int} of 1 kΩ. Lastly the 12 units in-series by 2 groups in-parallel reduced COD by 18% and continued to increase its internal resistance to 22 kΩ.

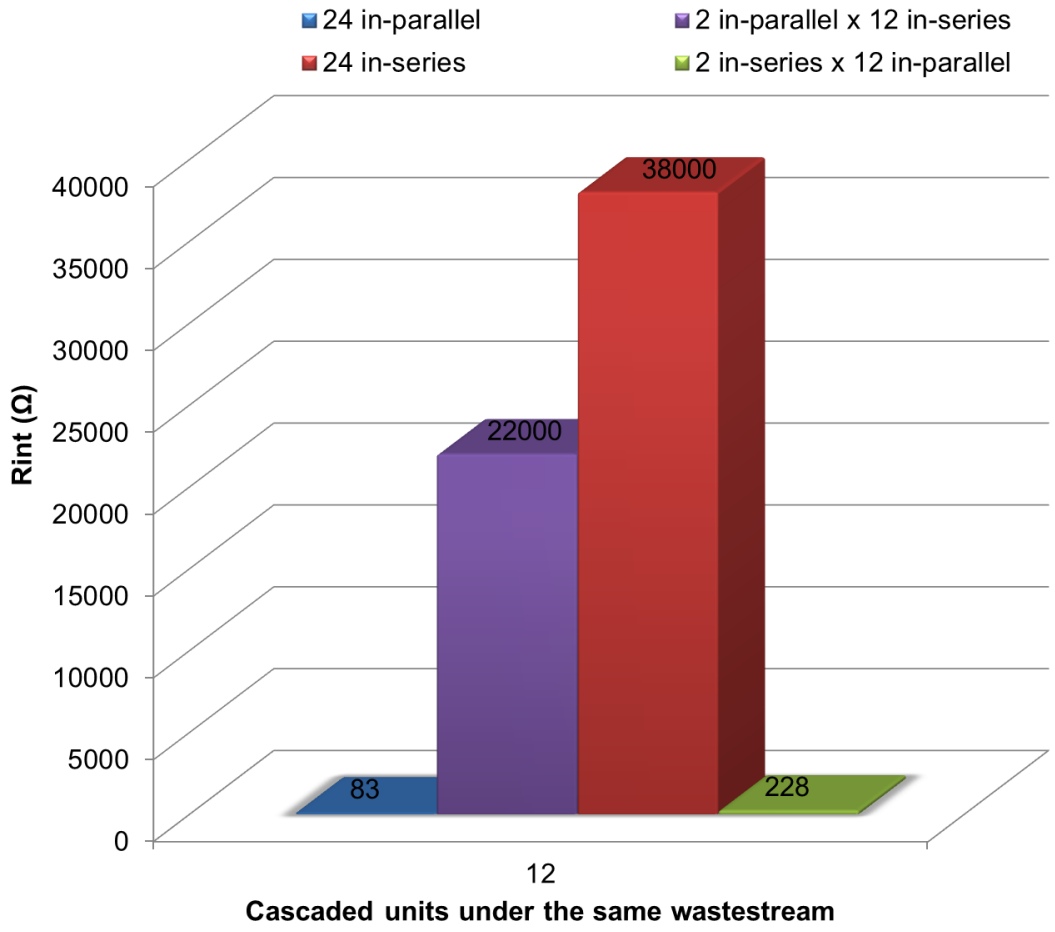

Fig. 4.33 R_{int} values based on MPP measurements from 12 MFCs x2 groups sequentially cascaded and connected in different electrical configurations

4.3.2.7. Cascades of 24 sequentially fed MFC units (**Stage 8**)

4.3.2.7.1. Performance readings

The last stage of the experiment involved the investigation of two electrical configurations that matched the 24-cascade hydraulic configuration (Fig. 4.34). As such all MFCs were tested only in-parallel and in-series electrical manner.

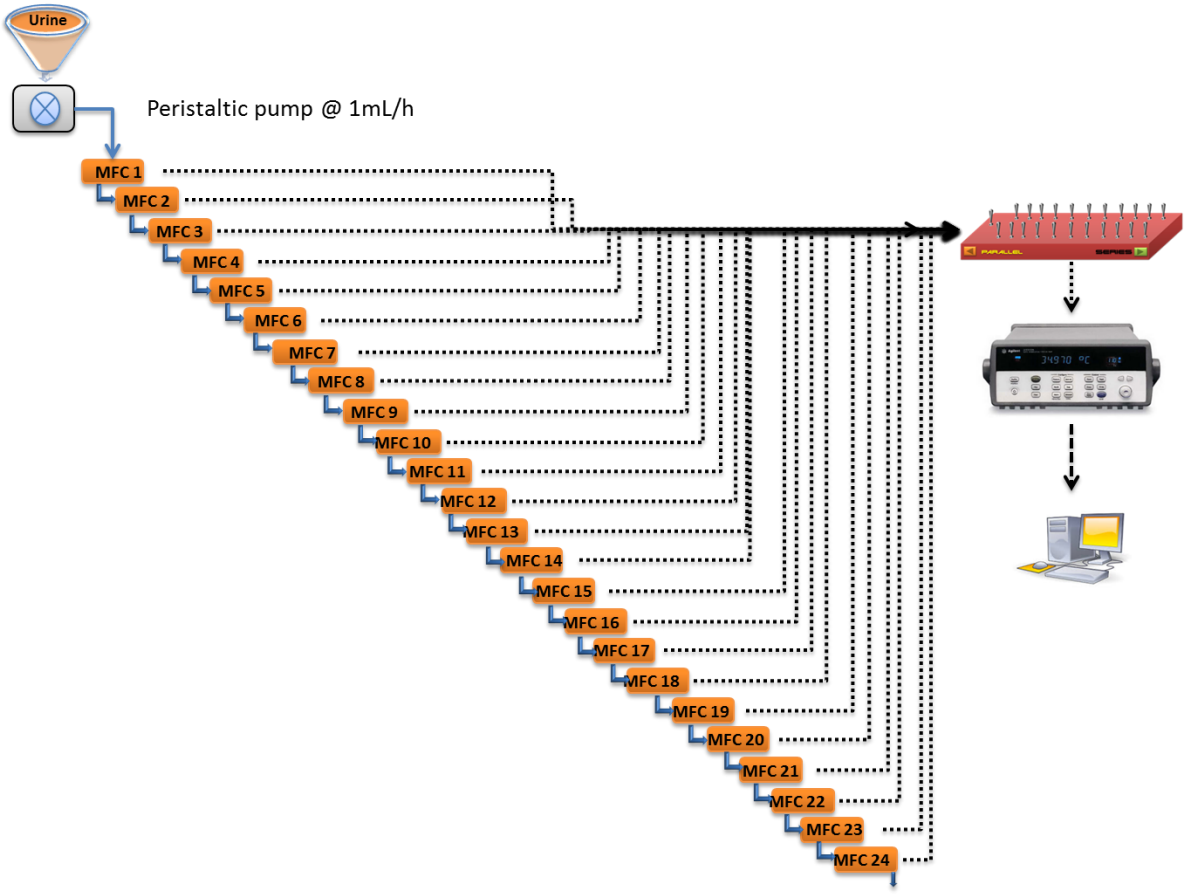

Fig. 4.34 Stage8: the MFC cascade with 24 MFCs fed from a single inlet

The parallel configuration generated a P_D of 3.4 mW/m^2 and a C_D of 14.4 mA/m^2. The in-series continued to perform at lower levels compared to the in-parallel configuration and generated a P_D of 1.3 mW/m^2 and a $C_{D\ of}$ 0.3 mA/m^2 (Fig. 4.36 and 4.35).

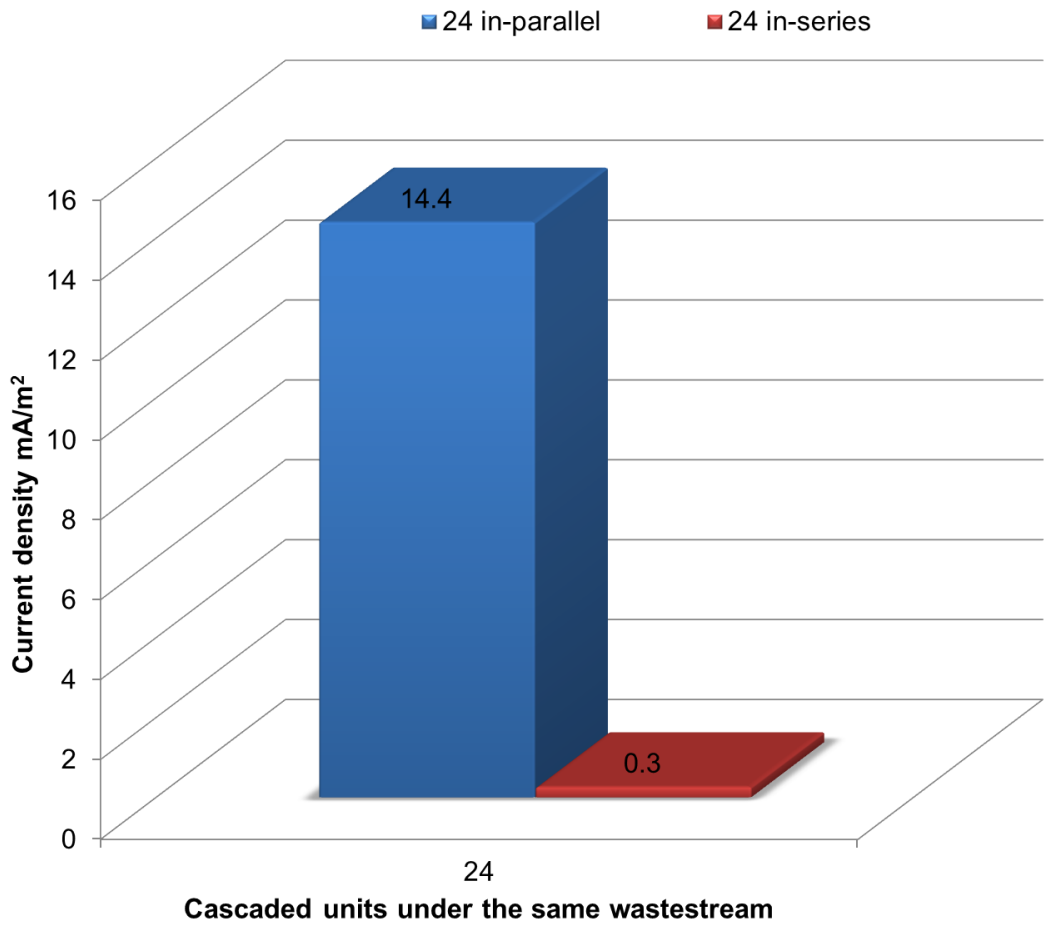

Fig. 4.35 Current density from the 24 MFC cascade in 2 different electrical configurations

The integration of all MFC units into one cascade system resulted in an improved performance from the in-parallel configuration and a decreased output from the in-series formation. This suggested that the MFC system is highly dependent on the R_{int} status within the stack and the in-parallel electrical connections allowed the system to slowly increase its performance back to levels that matched stage 3 in the experiment.

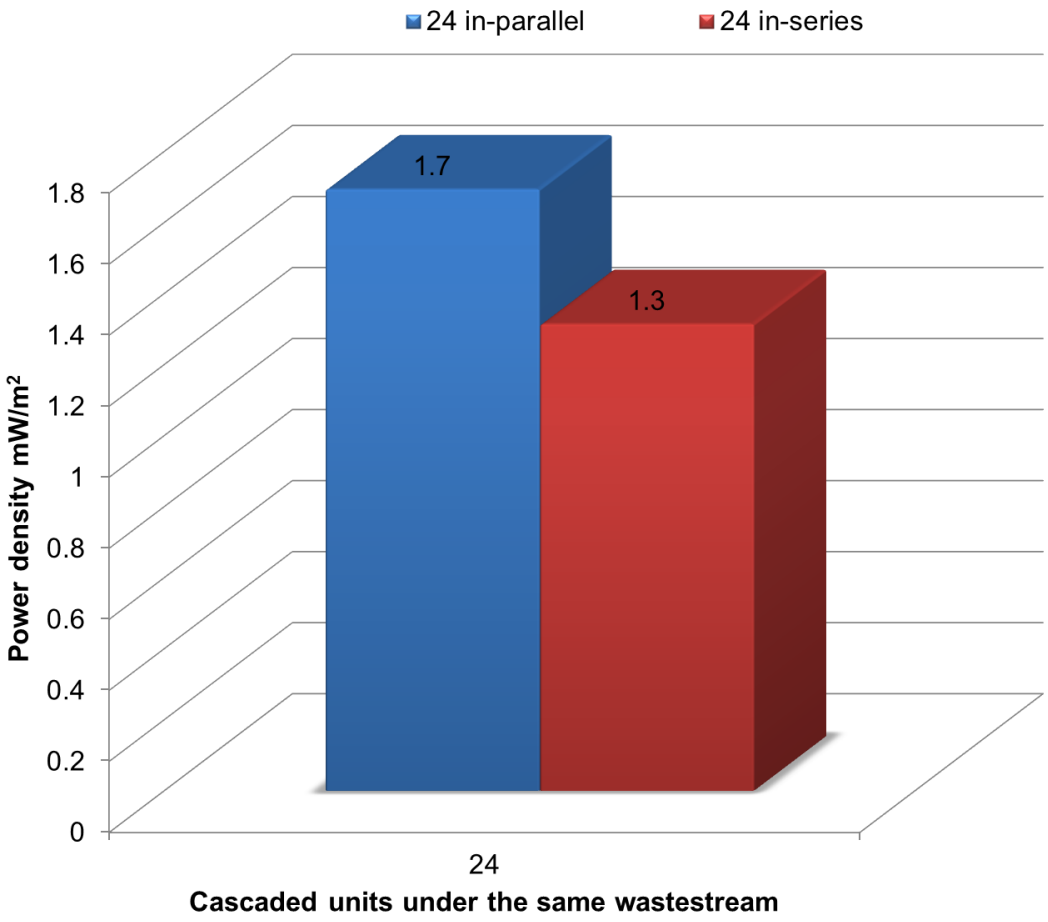

Fig. 4.36 Power density from the 24 MFCs hydraulically connected in two different electrical configurations

4.3.2.7.2. COD treatment and R_{int}: 24-unit cascade regime with electrical reconfigurations

Finally, COD measurements managed a COD degradation of 22% and 8% when configured in-parallel and in-series mode respectively (Fig. 4.37). The R_{int} where MPP occurred for the in-parallel connection was 40 Ω and 40 kΩ for the serially connected MFCs (Fig. 4.38). The drop in COD removal with the concomitant increase in C_D suggested that there was efficient substrate conversion to electricity [159] supported also by the large number of MFCs in the cascade.

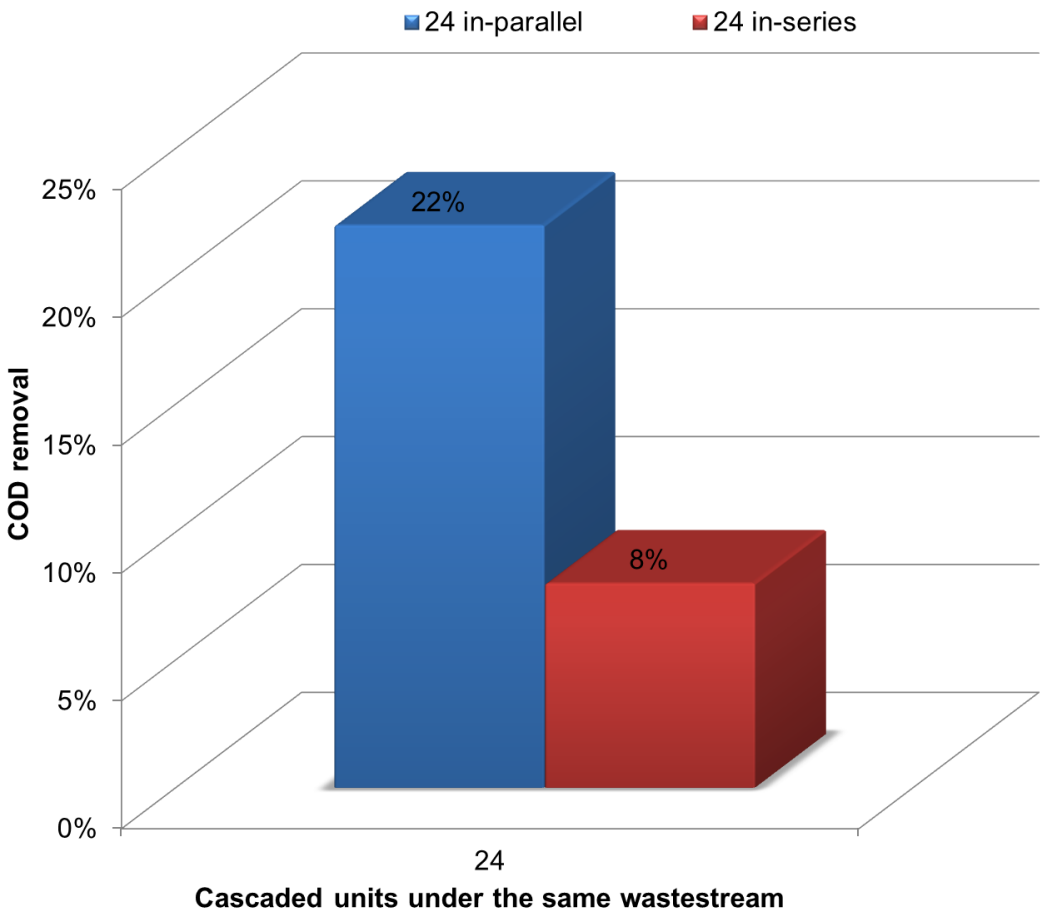

Fig. 4.37 COD treatment from 24 hydraulically connected MFCs from two electrical configurations

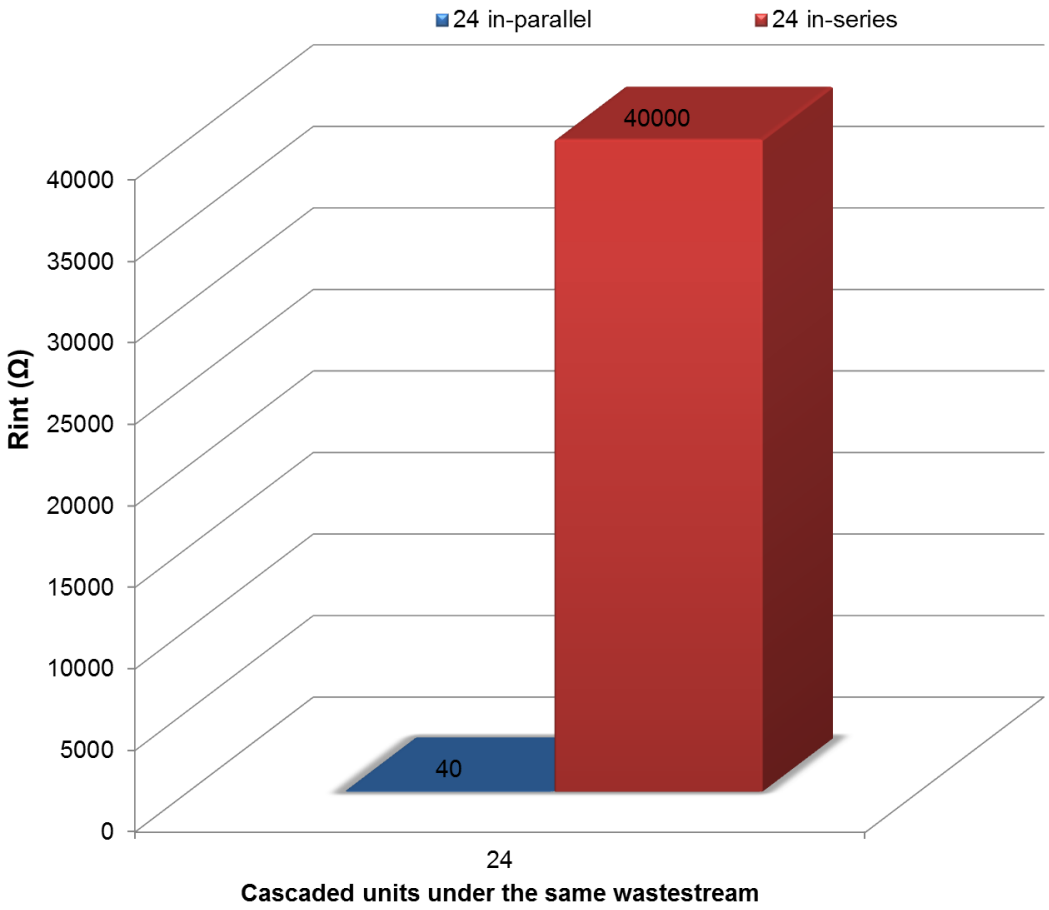

Fig. 4.38 R_{int} values based on MPP measurements from 24 MFCs hydraulically connected in two different electrical configurations

4.3.3. Overview of performance characteristics

This study examined the possible effects that the gradual addition of MFCs in a cascade mode under different electrical configurations had on the power, current, R_{int} and COD removal. A 2-MFC cascade improved the overall power density output compared to individual units. The addition of a third cascade element reduced the overall performance and later introduction of extra units in the same waste stream seemed to further decrease the power with the exception of the latest stage where the system configured in-parallel electrically, recovered to similar levels as the early

stages of the experiment. Nevertheless, as it would be expected, the MFC stack seemed to maintain the same decreasing pattern in all electrical configurations and under the different cascade scenarios, with the in-parallel electrically connected configurations showing the highest average power density generation (Fig. 4.39).

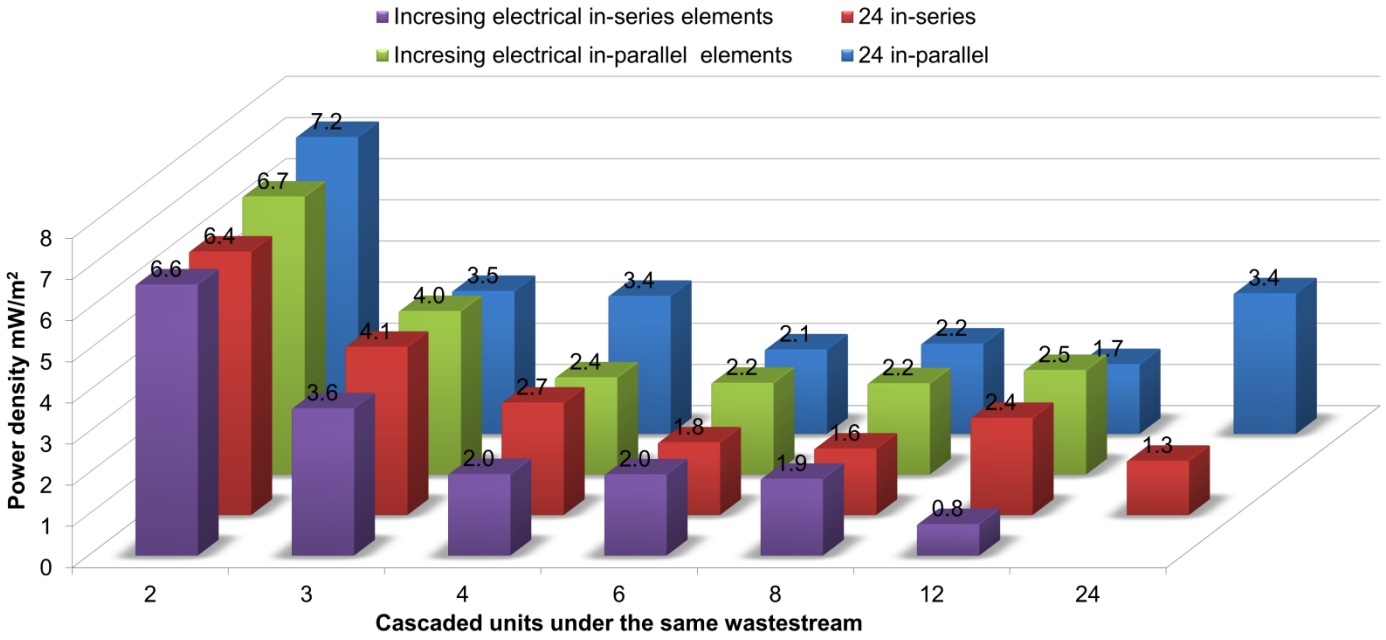

Fig. 4.39 Comparison of power densities from 24 MFCs connected in different cascade configurations and electrical combinations

Similarly, the increase of additional cascaded units in the stack affected the current generation. This was due to the substrate being utilised in the initial units within the cascade thus reducing the available organic content down the waste stream which limited the overall electron extraction. However, the in-parallel connection seemed to improve all the other electrical combinations when comparing the different cascade scenarios. As such the second best overall performance in current generation is achieved by introducing in-parallel elements into the in-series

electrically configured stack. This is also highlighted in Figure 4.40 where there is an increasing trend in current densities when in-parallel electrical units are introduced gradually in-series connected MFCs and a decrease when in-series electrical elements are brought into an electrically in-parallel configuration.

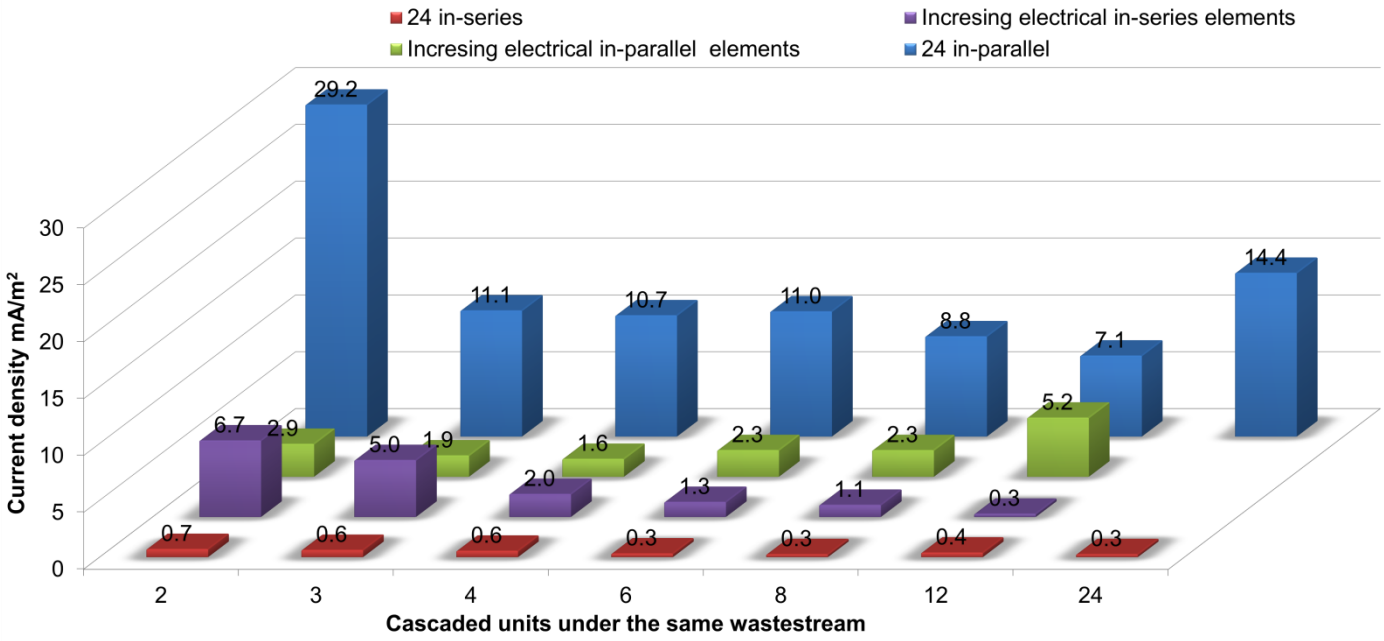

Fig. 4.40 Current density generated from the 24-MFC stack when units are repositioned into different cascade formations and electrical configurations

Overall, the main reasons for this drop in power and current generation could be attributed to (a) the low flow rate that was fixed for the duration of the experiment; (b) the cascade effect, in which the organic load is depleted in the early stages of the cascade; (c) rearranging of robust MFCs from the upper levels of the cascade to the lower levels in order to increase the MFCs in cascade has possibly resulted in an overall drop in power output.

4.3.4. Adaptation traits of MFC stacks

The experimental data suggested that shuffling of ‘’healthier’’ MFCs to lower quality substrate positions in the cascade has a positive impact on the COD removal when they are connected in-parallel rather than in-series (Fig. 4.41). Also, reinstating feedstock deprived MFCs closer to the food source could possibly have an on-off effect on their biofilms, where the MFCs recover back to a R_{int} state without necessarily providing the same power and current densities as when they were individually fed (Fig. 4.42).

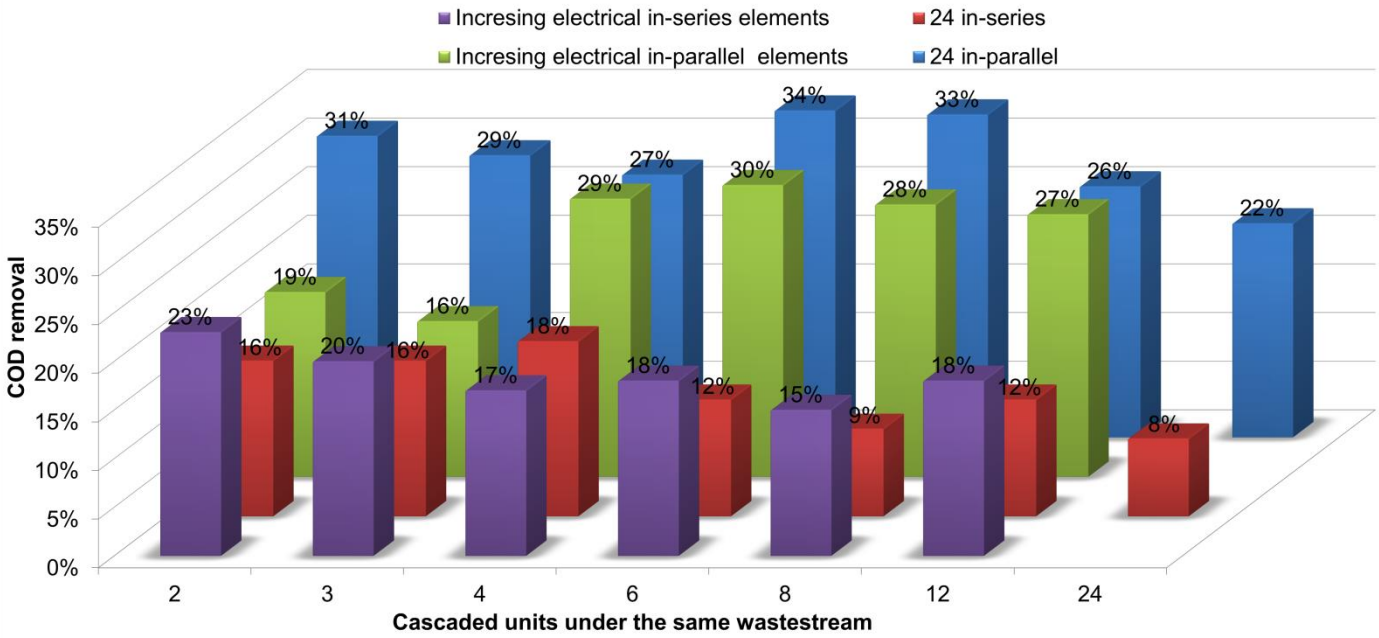

Fig. 4.41 COD remediating capability of the 24-MFC stack when units are repositioned into different cascade formations and electrical configurations

It is also hypothesised that the presence of high numbers of in-series connected MFCs led to a lower performance than in-parallel connections that possibly derived from polarity reversals. The in-parallel connection created a decreased R_{int} state within a stack which allowed for robust operation limiting the appearance of polarity

reversals that can compromise the overall performance and longevity of the system. However, in-series connections can be a positive electrical configuration when utilising MFCs for other applications as will discussed in the following chapter. The next chapters will also further investigate cell reversal and will attempt to provide insight on how to maintain low R_{int} conditions in serially connected MFC stacks.

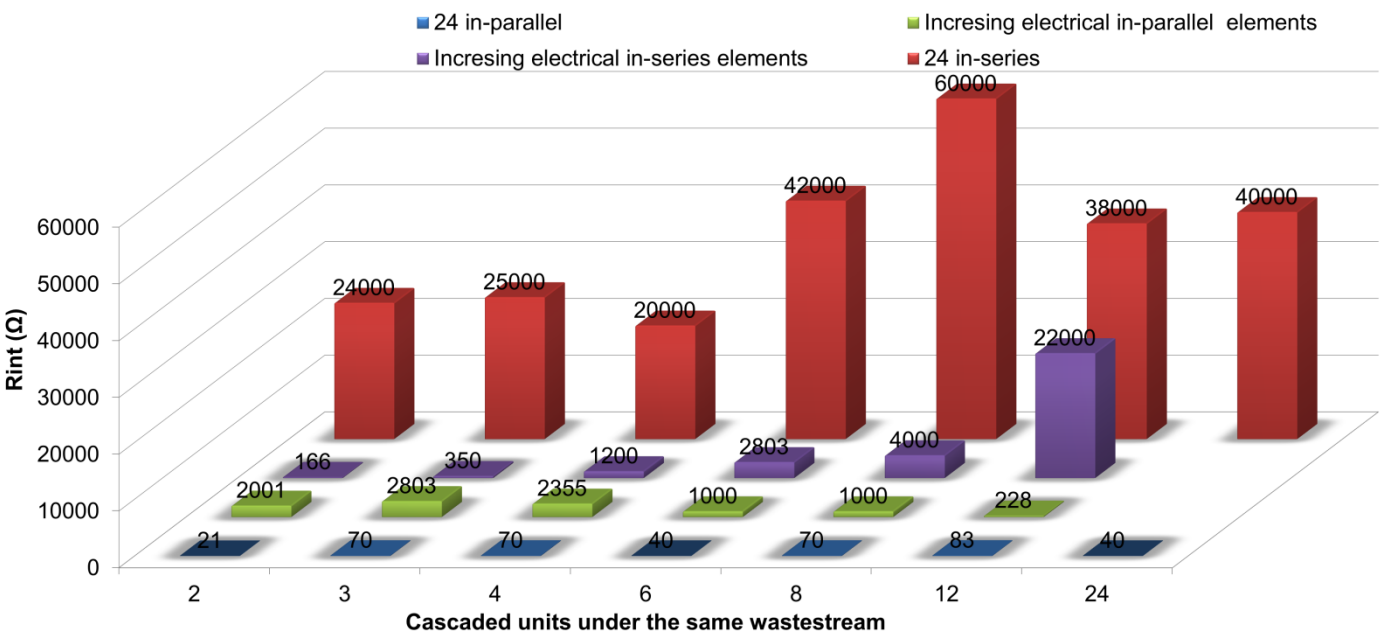

Fig. 4.42 Variance in R_{int} from all the different hydraulic and electrical scenarios

Equally important is that a variance of electrical combinations in a cascade could affect additionally the current density, the R_{int} and COD removal and it is observed that the presence of in-parallel elements numerically dominating in the MFC stack, tend to exhibit the highest overall power densities, current densities, the lowest R_{int} with the highest COD removal values.

4.4. Conclusions

When MFCs are to be employed in large scale wastewater treatment plants, then this system needs to be adaptive and capable of forming larger or smaller cascaded groups in the waste stream, depending on the flow rate and the COD reduction that is required at this stage. Additionally, MFC stacks need to be able to configure their electrical connections regime depending on the dynamic homeostatic status of the biofilms and the power output so as to ensure longevity and smooth operation of MFC units. The findings from this study suggest that the cascade configuration favours wastewater remediation at the expense of power generation that decreases due to the limited availability of organic content that reaches the MFCs lower in the waste stream. On the contrary, low number of cascaded units can maintain high levels of power generation especially when configured in-parallel electrical manner.

Finally this study hints that the urine factor should always be considered when designing a large scale-up scenario. Urine holds high chemical variability and many factors can alter its content, which could possibly lead to differences in MFC performance and biofilm dominant species. However in a theoretical scaled-up system with urinals facilitating a large number of donors, it is likely that a MFC stack can also provide useful information in terms of high energy content during a day based on power and COD- treatment performances.

Chapter 5

Parts of the following results presented in this chapter have been published in:
Papaharalabos, G., Greenman, J., Stinchcombe, A., Horsfield, I., Melhuish, C., & Ieropoulos, I. (2014). **Dynamic electrical reconfiguration for improved capacitor charging in microbial fuel cell stacks**. Journal of Power Sources, **272**, 34–38.

5. Improved energy harvesting in MFC stacks

This chapter deals with the power extraction from a MFC stack and presents **passive** and **active** energy harvesting techniques used in MFCs and their inherent characteristics. It also introduces a novel theory in bio-electronics and elaborates a revolutionary way of maximising energy output and decreasing charging times without complex electronics.

5.1. Energy extraction from MFCs

Even though MFCs have been shown to run continuously high [77,156] energy-demanding devices, the power density of a single MFC is still insufficient to start up or power most electronic devices on the fly without the assistance of commercially available energy harvesters [76]. However, if this energy is stored efficiently, then it can be released to run power intensive devices for a limited period of time. Storing energy generated by MFCs in capacitors was initially introduced in the first MFC-powered applications, for energising robots [67,69,71] and later on for intermittent energy harvesting [160]. To date, due to the increase in power output from MFCs [60,76,96] and development of efficient harvesting circuitry [149,161–163], energy is stored in high capacitance storage devices, such as super-capacitors or lithium-ion batteries [77].

The need for stepping up the voltage to higher levels for powering devices is now met with boosting circuitry that allows single MFC units to provide practical levels of voltage, but at the cost of energy transfer efficiency; improvement of the energy demand and rate of charging from these systems is on-going work [75]. The state-of-the-art energy harvesting circuitry for MFCs is currently optimised for maximum power point tracking (MPPT) and at low voltages, which is something useful for a single MFC unit, but is limited since the voltage output of single MFC units cannot exceed 0.5 V under load. Similarly, the MPPT technique in stacked MFCs harvests energy close to the operational voltage, which is 50% of the open circuit voltage [88]. An approach to boost this low voltage is either with a boost converter [76], [161] or by charging super-capacitors in-parallel and then discharging them in-series [164], which results in 50% losses associated with capacitor-capacitor energy transfer.

An effective way to increase the performance of individual MFC units is through the connection of multiple MFCs in stacks [3,67–69,72,73,88,125], where all units are configured electrically and charge to the maximum open circuit voltage point. When connected in stacks, voltage, current or both can be increased depending on the stack size and configuration. Furthermore, it has been previously suggested that the total volume of a large number of small-sized MFCs is more efficient in terms of power generation when compared to a single large MFC [42]. However, electricity production in a MFC stack is a dynamic bioelectrochemical process, which is subject to external conditions [42,165] and phenomena such as single cell failure and cell reversal [73]. The latter can occur when stacked MFC units are connected in-series at a low external resistance (Rext), or whilst charging a high capacitance super-capacitor.

This study introduces a novel way of passive harvesting, which focuses on how the dynamic reconfiguration of electrical connections can affect the charging speed and current output from a MFC stack. For this reason, eight MFCs connected to a switchbox, were tested under (i) dynamic and (ii) fixed electrical configuration regimes and compared in terms of efficiency and speed of charge.

5.2. Experimental

5.2.1. MFC stack construction, operation & feeding

Eight single chamber MFC reactors with a 6.25 mL volume each were fabricated from RC25 Nanocure as previously described[69]. Each anode consisted of a 154.8 cm^2 non-modified carbon fibre veil electrode folded 5-times so as to fit in the chamber. An IEM (Membranes International, NJ) was used as a separator between the anode and the cathode. Cathode electrodes were prepared with commercially available activated carbon (AC) powder (60±2 mg cm^{-2}) mixed with PTFE (20%wt) and then applied on a 6 cm^2 30%wt PTFE treated carbon cloth (Fuel Cell Earth) followed by hot-pressing [166]. The impregnated carbon cloth with AC was then heated to 80^oC. MFC anodes were inoculated with activated sewage sludge (pH 6.9) collected from the Wessex water Scientific Laboratory (Saltford, UK) for the first 14 days of the maturing period and subsequently fed with TYE (Tryptone 1%, Yeast extract 0.5%). MFCs were operated in fed-batch mode for the whole duration of the experiments and replenished with feedstock (5 mL of TYE) every 24h. The maturity period was two weeks, during which a fixed 500 Ω load was connected to each MFC; this value was determined from polarisation experiments carried out at the end of the first week. The MFC units were uniformly matured and maintained, which helped to keep a similar R_{int}. This enabled stable operation without cell reversal. Stability in

performance was monitored and confirmed by the real time temporal readings as well as consecutive polarisations experiments conducted on a weekly basis.

5.2.2. MFC stack reconfiguration & energy storage

To control the electrical configurations between the 8 MFCs, a device for manually switching connections between MFCs from series to parallel was used (see also chapter 4.2.2). The output of the switch box was connected to a 1 Farad ultra-low leakage current super-capacitor (Murata Electronics, UK), which was employed to charge from 0-3 V (equivalent energy of E=4.5 Joules or Q=3 Coulombs).

5.2.3. Data recording and processing

Real time voltage monitoring of the MFCs, was performed using an ADC-24 Channel Data Logger (Pico Technology Ltd., Cambridgeshire, U.K.). Voltage (V) was measured in millivolts (mV) every second. Charging current (A) was recorded in microamperes (μA) with the TENMA 72-1016 bench multimeter. Data were processed using GraphPad Prism version 5.01 software package (GraphPad, San Diego).

5.2.4. Possible electrical configurations and charging regimes

The available electrical connections for the 8 MFC stack were (i) all 8 in-parallel, (ii) 4 in-parallel elements x 2 in-series groups, (iii) 2 in-parallel elements x 4 in-series groups and (iv) all 8 units in-series.

Before charging the super-capacitor with the 8 MFC stack, it was important to identify the maximum voltage limit that each configuration can charge up to. The maximum theoretical open circuit voltage that a MFC can produce is 1.14 V, whilst the operating voltage is approximately 0.5 V [145] , hence the charging ranges were

chosen based on the maximum voltage that each configuration can generate. The graph in Figure 5.1 shows the voltages produced over time from each configuration whilst charging the super-capacitor.

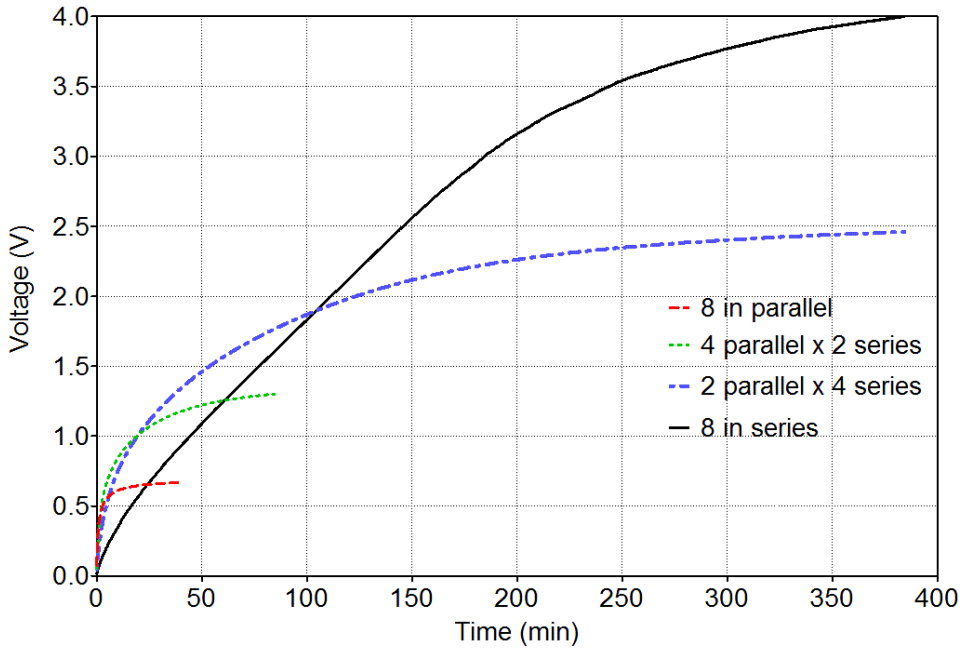

Fig. 5.1 Maximum charging voltages of a 1 F super-capacitor from each electrical configuration.

Additionally, the first derivative of the voltage curves in Figure 5.1 was examined in order to assess the voltage variance as time progressed (Fig.5.2). The voltage rate of change is expressed as charging rate ($\boldsymbol{\alpha_e}$) and is described in the equation below:

$$\alpha_e = dV/dt \quad (1)$$

Where α_e is the charging rate, dV is the change in voltage ($dV=V_2-V_1$) and dt is the change in time between two points ($dt=t_2-t_1$). The term charging rate is used in order to define the voltage at any given time for each available electrical configuration within a specific voltage range. This can be a useful technique when comparing the voltage dynamics of a given configuration and deciding on the appropriate electrical

combinations in a stack for more efficient energy harvesting. Based on this, the formation and the sequence of electrical configurations were applied for charging the 1 F super-capacitor. All experiments were repeated a minimum of five times.

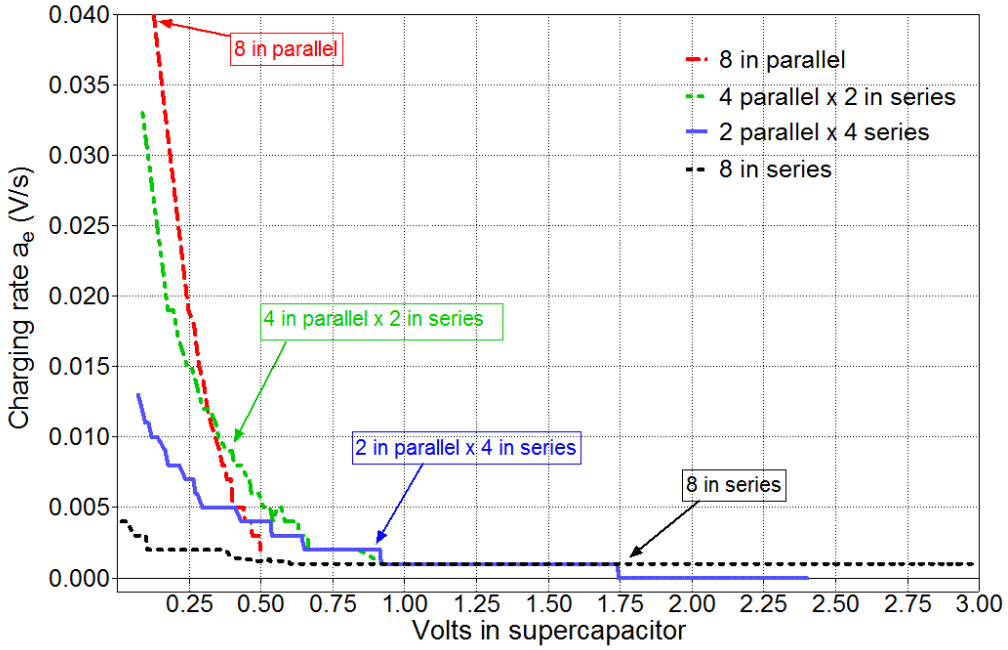

Fig. 5.2 Voltage variation from all different configurations during charging.

5.3. Results and discussion

5.3.1. Rate of charging from fixed configurations

First order derivative of the charging lines from Figure 1 was examined with respect to the charging rate (Fig. 5.2). The differentiation provides insight on each configuration's charging capability at specific voltage ranges and can suggest the optimum order for electrical configurations during charging in a reconfigurable MFC stack. Results in Figure 2, show that the lines from each electrical configuration are comparable to the results in Figure 1. For the voltage range of 0-0.45 V, the all-in-parallel connection produced the best performance; for 0.45-0.85 V the 4 units in-

parallel by 2 groups in-series gave the highest values; for the 0.9-1.8 V the 2 units in-parallel by 4 groups in-series outperformed the rest; and the in-series connection was superior for the last 1.8 – 3 V voltage range.

5.3.2. Dynamic reconfiguration and fixed configuration charging times

Based on the recorded data from the individual charging scenarios and the use of the manual switch box, the charging of the super-capacitor from 0 to 3 V is performed by applying a dynamic reconfiguration regime and a fixed electrical configuration alternatively. For the fixed electrical setup, 8 MFCs are connected in-series because this configuration is capable of charging the capacitor up to 3V. Figure 5.3 shows the charging curves when switching the configuration in real time compared to a fixed connection. The points in the graph of the dynamic switching, where the lines' rate of change varies, are the switching points based on the voltage data collected from the individual charging times. As can be seen, the overall charging rate increases every time the next configuration is switched, thus resulting in improved charge storage. On the other hand, the fixed in-series configuration, results in a fixed but lower rate of charge. The progressive addition of series electrical elements in a stack initially configured in-parallel, promotes a dynamic potential between the stack and the charging super-capacitor. This difference in potential, supplies the generated charge into the supercapacitor at a higher rate every time the switchbox reconfigures the stack with additional in-series elements.

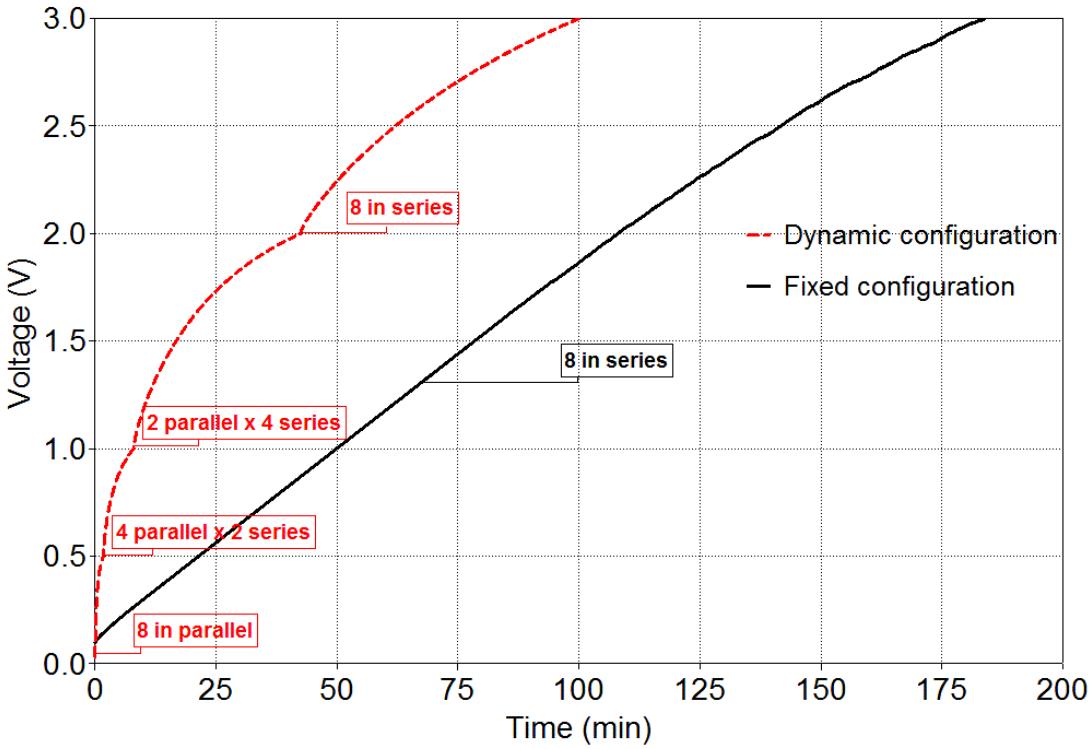

Fig. 5.3 Charging time comparison between dynamic switching and fixed configuration. Data are representative of repeated trials (n=5).

The dynamic switching results in charging the super-capacitor up to 3 V, in 93 minutes whereas the fixed regime requires twice as long (184 min) reaching the same voltage (same energy stored). The times for each voltage checkpoint are improved by 79% (max.) from 0 to 0.5 V and continue to be superior to the fixed configuration even when the variable connection is all in-series. Charging from 2 – 3 V with all MFCs in-series in the variable mode is 38% faster than the fixed in-series mode. Improved times for each step have an overall increase in rate of charging by 99%. Detailed breakdown of charging times between different voltage intervals is shown in Table 5.1.

Charging range	Dynamic switching	Fixed configuration	Difference of charging speed
0 → 0.5 V	1.7 min	8.3 min	4.9-fold
0.5 → 1 Volt	5.7 min	17.4 min	3-fold
1 → 2 V	32.2 min	55.7 min	1.7-fold
2 → 3 V	53 min	85.5 min	1.6-fold
Total	93 min	184 min	2-fold

Table 5.1 Charging times from 0-3 V using the switching converter and a fixed configuration

5.3.3. Optimising energy harvesting

During the process of charging, current transfer is recorded to examine the differences between the dynamic configuration and the fixed in-series connection (**Fig. 5.4**). When in dynamic mode, high current peaks are observed whilst switching to additional in-series elements within the stack. Every time the stack is reconfigured to more in-series elements, this increase in voltage creates a high potential difference between the stack and the existing voltage level in the super-capacitor. This increases the overall resistance in the supercapacitor which initially is unwanted, but this higher voltage state in the system, is driving momentarily higher amounts of charge (higher electromotive force) until the stack voltage equalises with that of the super-capacitor.

The generated current from the fixed in-series configuration was almost constant at 243 µA. On the contrary, the dynamic mode varies from 13.7 mA to 240 µA due to the parallel connections and the further series elements subsequently added. As a result, the dynamic mode produces an average charge output of 474 µA, which is a 2-fold higher current output than with the fixed configuration. The area under the

curve of the dynamic mode is 35% higher than the area from the fixed configuration for the same time required (93 min) to charge the super-capacitor to 3 V with the dynamic switching (Fig. 5.4).

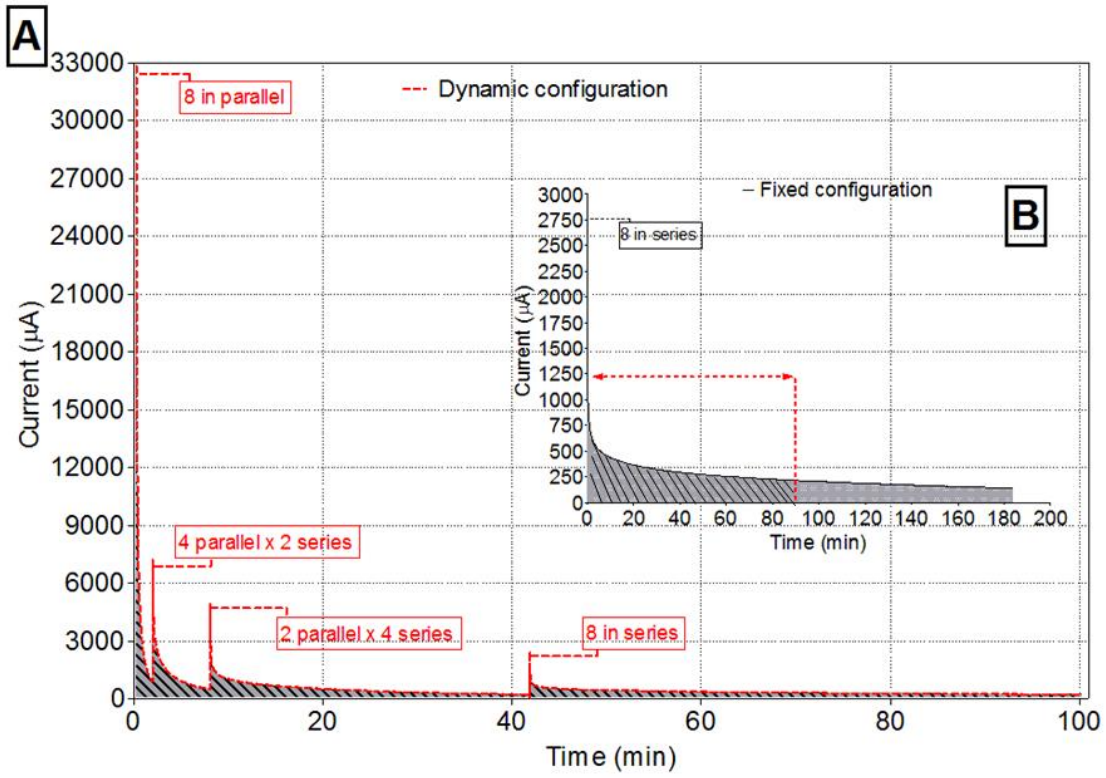

Fig. 5.4 Current transfer during charging with the equivalent area under curve from (A) dynamic reconfiguration and (B) fixed configuration. Shaded area in the inset (B) represents the same time interval required for charging the capacitor in graph (A).

5.4. Conclusions

This study presents the effects of reconfiguring in real-time the electrical connections within a stack whilst charging a super-capacitor. Dynamic reconfiguration aims at harvesting energy from MFC stacks without the use of complicated circuitry whilst maintaining a robust system for continuous operation. The findings confirm the hypothesis that the charging rate is greatly enhanced by the high number of parallel connected elements in the early stages of charging, and

dynamic configurability helps to add in-series connections gradually to step up the voltage. The dynamic reconfiguration is a method that reduces the charging times by allowing storage of the same amount of energy in a shorter period of time. The key to extract energy at higher voltage levels is to increase the number of MFC units in the stack. This will expand the number of possible connections that have different α_e for a given voltage and time frame, and provide higher charging versatility.

Dynamic reconfiguration of MFC stacks can be a useful tool when designing energy harvesting circuitry for MFC stacks. The following chapter is looking further into automating the switch box, so it is capable of computing its charging rate status at any point in time and reconfiguring the stack for optimised performance.

Chapter 6

This chapter combines findings from the previous chapter and presents a novel method for preventing cell reversal whilst optimising energy harvesting from a stack of 8 MFCs *via* an automated switch box that can modulate the stack's electrical configuration.

6. Fail-safe power management in MFC stacks

6.1. Efficiency of power management systems (PMS)

Performance tests in MFCs have shown that they can generate an operating voltage of 700−800 mV and power densities between 100−2000 mW/m^2. These power levels are not sufficient to run directly the majority of electrical circuits which require 1.5 V to 3 V and cannot be matched from the output of an MFC unit [167]. A light emitting diode (LED) needs approximately 30 mW to run [164] and most wireless sensors for environmental monitoring need at least 3 V [168–171] .

Hence, the need for increasing the output from MFCs to useful levels has been realised with the use of off-the-shelf harvesting technologies, such as capacitors, charge pumps, voltage boosting converters and MPP active harvesters [75,149,161,172–178]. Apart from the capacitor operation, the rest of the electronics have been designed for use in power sources with higher power outputs than those from MFCs, thus the need for low-consumption customised electronics is imminent. The main bottleneck is that, modified harvesters still operate at higher start-up voltage thresholds that an MFC can deliver. Therefore, an added voltage boosting is required in the initial stages of energy extraction [179] which further decreases energy losses from the embedded converters and the minimum operating voltage required for kick-start [178]. To date efficiencies from these systems reported in the literature

claim to have reached up to 100% [164,172,176,180–182] however these results use capacitor based charge pumps that have excluded the capacitor-to-capacitor 50% energy transfer losses.

An alternative strategy, to complex and energy intensive circuitries for increasing the voltage and current, is stacking of multiple MFC units so as to meet the demands of most commercial electronic devices [69,72,109,183–185]. However, MFCs respond to sudden substrate and biochemical changes which consequently can affect microbial communities and their electrical activity of the stack in general. This causes a large variation in performance within the stack and its overall efficiency is governed by the worst performing MFC [72].

A study in 2013 [76] (see chapter 3.3.4) combined both strategies so as to run a 3-Volt wristwatch continuously with the use of only two serially stacked MFCs and an energy harvesting module. However the harvester still required 20% of the generated current and 0.7 V to run smoothly. The literature reports energy harvesting efficiencies from a 40-MFC stack of up to 95.2% [156] which uses intermittent charging for storing energy into capacitors prior running energy intensive devices.

6.1.1. Cell reversal in MFCs and prevention

Because of MFCs' electrochemical subsistence, they also conform to the physical constraints that render these cells. A common phenomenon that usually occurs in serially stacked MFCs, is the change in a fuel cell's polarity when its R_{int} increases rapidly [88,109,186]. Many studies have focused on explaining and predicting this phenomenon [42,73,109,187]. To date, it has been suggested that this sudden change in R_{int} is triggered by substrate depletion [42,73]; a "heavy" external load - low Rext -

connected to the stack which draws current at levels higher than the anodophillic biofilm can deliver [72,178,188] or it is a case of slow kinetics in the anode or the cathode [187,189].

It has been thoroughly reported that fuel starvation in MFCs is likely to lead to cell reversals and that sufficient substrate supply can avoid this phenomenon. However a number of studies tend to suggest that cell reversal is clearly a matter of a high increase in R_{int} of which fuel starvation is just one part of it. Therefore, there has been a collective of studies that investigate different chargeable events that can lead to sudden increases in R_{int}.

A recent study claims that the anode is prone to a number of factors that increase overpotential. High voltage increase in the anode can affect the kinetics compared to a predictable and straight forward kinetic behaviour on the cathode[187]. This study concludes that overpotential in a MFC in a stack is likely to convert the MFC from a galvanic to an electrochemical cell which is powered by the other MFCs thus further decreasing the overall performance. Another study, debates that the ORRs on the cathode are the main reason for cell reversal in MFCs[189]. Even though cathode electrodes are quite homogenous and facilitate a single electron acceptor reaction, oxygen diffusion is frequently absent throughout the cathode's surface. This uneven distribution further creates a disparity of oxygen to proton/hydroxyl ions ratio that hinders the formation of a liquid bridge between the separator and the cathode [190,191], and could possibly lead to cell reversal. Work from the same group, also suggests that cell reversal can interchange between the anode and the cathode whenever sluggish reaction kinetics occur in either of them [187,189]. As with chemical batteries stacked in-series, in order to maintain a voltage reversal-free state, all units should exhibit same reaction kinetics on both electrodes. As mentioned before, it is

intriguing to ensure steady anodic reaction rates in the electro-active biofilm. The main factors that can alter the anode potential are substrate diffusion and concentration, pH, temperature, presence of oxygen, biofilm community structure, biofilm thickness and density [192–196].

Another probable cause for cell reversal is usually observed when running MFCs at MPP and many research groups have attempted to develop PMS for tackling it successfully[173,197,198]. In 2011, Pinto *et al*.[198] suggested that a MPP matching algorithm could possibly prevent MFCs operating at values below the R_{int} hence avoid reversal. It was not until 2014 that Boghani *et al.* [197] developed a USB powered MPP matching PMS capable of preventing cell reversal in serially stacked MFC whilst maximising energy harvesting, That was achieved by monitoring the voltage continuously whilst applying a dynamic resistance MPP matching to each cell in the stack. The tracking algorithm of this PMS would automatically adjust the Rext to the R_{int} at any given moment thus not allowing a MFC with low voltage levels to undergo into negative potential because the algorithm would increase the Rext.

A different approach was attempted by Kim *et al*.[173] whereby a capacitor-based system was used to increase the overall voltage from a MFC stack (in-parallel configured) by charging a group of capacitors in-parallel and then discharging then in a series manner. This was one of the first attempts to boost the voltage without the use of DC-DC converters but it didn't take into account the efficiency losses from the capacitor-to-capacitor charge transfer.

Based on previous findings (see Chapter 5.3), dynamic reconfiguration of electrical connections in a MFC stack allowed for decreased charging times of a super-capacitor by gradually switching from parallel to serial connections[199].

However the improvement in performance also highlights another advantage whereby the stack can avoid polarity reversals. So, the present study illustrates the feasibility of an automated switching circuitry for simultaneous energy optimisation and cell reversal prevention, by dynamically combining a range of all physical electrical connections within a stack.

6.2. Experimental

6.2.1. MFC stack construction and operation

Eight single chamber MFCs with an anodic volume of 6.25mL each, were 3D printed using light-curing RC25 Nanocure[69]. Each anode consisted of a 155cm^2 catalyst-free carbon fibre veil electrode, folded 5-times to form a cuboid and had an IEM (CMI, Membranes International, USA) as a separator. Open-to-air cathode electrodes consisted of a catalyst-free carbon cloth with a s.a of 6cm^2 coated with a mixture of activated carbon (AC) particles (60±2 mg/cm^2) PTFE (20% wt) as previously described [200]. For this study, the AC and PTFE were coated on the carbon cloth surface at 200^{o}C and 300psi. Activated sewage sludge (Wessex Water Scientific Laboratory, Saltford, UK) was used as the inoculum and feedstock (pH 6.9) for a period of two weeks. During this period, each MFC was connected to a fixed 1 kΩ resistive load. This value was chosen based on impedance matching experiments from the same type of MFC, as used in a previous study[76]. Following this period, the feedstock was replaced with neat human urine and MFCs were fed 5 mL every 24 hours for the duration of the experiments; all MFCs were operated in fed-batch mode under controlled ambient temperature conditions (22±1 ^{o}C).

6.2.2. Data logging and processing

Voltage in milliV was recorded every 1 second interval using the switch converter's (see Section 2.3) and logged via the LabVIEW interface used for switching control and automation. Current was measured every 1 second with a TENMA 72-1016 bench multimeter. Triplicates of polarisation runs were performed on a weekly basis after the maturity period to monitor changes in performance, by applying a range of 40 resistor values starting at 1 MΩ and progressively decreasing to 4Ω in 3-minute intervals. This process was done either with the use of a Resistorstat [105] or with the use of a manual variable resistor for OCV values exceeding 2.5 V, using the same range of resistance values and time intervals. Data processing was performed with GraphPad Prism version 5.01 (GraphPad, San Diego). Power and current density were normalised using the cathode s.a ($6cm^2$) and volumetric P_D was calculated based on the overall reactor volume (6.25mL). The cathode was used as a means of normalisation based on a previous study where the performance of this type of MFC was greatly affected by the cathodic half-cell [76].

6.2.3. MFC stack digital switch converter

For configuring the electrical connections within the MFC stack, a digital 8–channel switchbox without any boosting or harvesting circuitry was developed. The hardware comprises a main data distribution controller (PIC32, Microchip. Inc, USA) connected to eight microcontrollers (PIC24) each assigned to a MFC. Each microcontroller operates four latching relays (double pole/double throw), which facilitates series/parallel reconfiguration with adjacent MFCs and also individual external load connection *via* differential channels. The time required for switching the position of a relay is estimated to be 10ms. A built-in 24-bit 8-channel differential chip monitors

individual MFC voltage levels and sends the data to the main controller, which interfaces *via* USB to a desktop computer, which also powers the switchbox (Fig. 6.1). Customised software enables the control of each microcontroller and relay separately based on the user's data input. The energy extracted from the stack is stored in a super-capacitor (1 Farad), which is charged up to 3 V, resulting in a corresponding energy transfer of 4.5 Joules (or electric charge of 3 Coulombs).

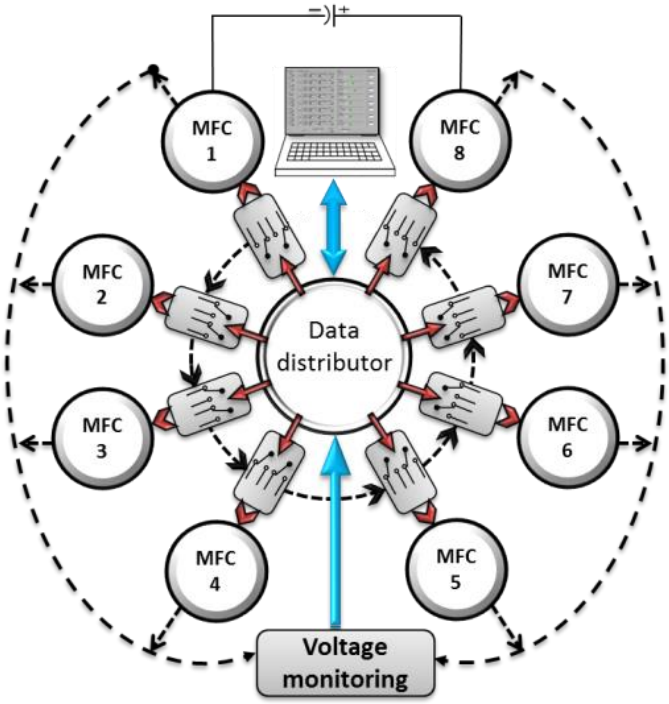

Fig. 6.1 Schematic of the digital switch converter operation

6.2.4. Selection of electrical configurations and switching intervals

Based on the number of MFCs, four different electrical configurations were investigated; i) 8 MFCs in-parallel (*8P*), ii) 4 MFCs connected in-parallel - the 2 resulting groups in-series (*4P2S*), iii) 2 MFCs in-parallel - the 4 resulting pairs in-series (*2P4S*) and iv) all 8 MFCs in-series (*8S*). Each electrical configuration was used to charge the 1F super-capacitor to the level where a charging plateau occurs

and the super-capacitor's voltage equalises with the OCV of the configuration. These steady-state points defined the voltage range where each configuration reaches its maximum charging level. The charging process was repeatedly tested for consistency and accuracy (n=5). The current measured from each configuration, allowed for calculation of the average power within each voltage range. This indicated the order of switching to the configuration with the next highest value that the stack needs to be reconfigured to in order to increase the voltage (Table 6.1). Thus, the software of the switch converter, was set to change the configuration based on the order defined by the power outputs at specific voltage thresholds; 8P→4P2S→2P4S→8S.

Average power	Voltage range			
Configuration	0-0.5 Volts	0.5-1 Volts	1-2 Volts	2-3 Volts
8P	888 µW	-	-	-
4P2S	646 µW	895 µW	-	-
2P4S	166 µW	562 µW	574 µW	-
8S	75 µW	394 µW	526 µW	624 µW

Table 6.1 Average power produced from all available configurations within specific voltage ranges

6.3. Results and discussion

6.3.1. Performance of individual units (n=8)

Polarisation experiments were performed every seven days over a three week period post inoculation, so as to verify that the MPP had been reached and ensure stable operation. Results demonstrated differences between MFCs even though all units were maintained in a uniform manner [201]. It is common in the literature to find discrepancies in similarly treated MFCs, whereby the feedstock, the concentration is similar but the biofilm formation is different due to dissimilar anode potentials [24,202,203]. An additional possible explanation could be the use of wastewater (activated sewage sludge) as an inoculum and the later use of human urine which could possibly apply selective pressure on the biofilm's ecology [187] that may reflect in power generation.

Power and current outputs from the 8 MFCs ranged between 72-147 μW and 226-370 μA, respectively; these were equivalent to P_D and C_D ranges of 120-245 mW/m^2 and 426-616 mA/m^2, respectively (Table 6.2). MFCs 3, 5 and 7 generated similar power and exhibited the same internal resistance (R_{int} = 1003 Ω), as reflected in the polarisation curves. MFCs 1 and 8 reached similar power levels with the previous group of 3 MFCs but at a higher R_{int} of 1200 Ω and seemed to suffer more from ohmic losses, and power overshoots (type D) [204] in the area of 0.3 V (data not shown). In the case of MFCs 2 and 6, the power output was limited to ~73 μW, which was 51% lower than the majority of MFCs and had the highest R_{int} of 1500 Ω, which could similarly be attributed to biofilm immaturity. The best performing MFC4 produced 147 μW, at a R_{int} of 1102 Ω, which was higher than the second best performing MFCs. The scope of this study is investigating cell reversal in stacked

MFCs whilst charging a super-capacitor and discrepancies in R_{int} - albeit operated under identical conditions - are necessary for examining the effect of the consequent resistance imbalance within the stack and demonstrating how that affects energy harvesting.

	MFC 1	MFC 2	MFC 3	MFC 4	MFC 5	MFC 6	MFC 7	MFC 8	**Avg**
Power µW (mW/m^2) (W/m^3)	110 (183) (18)	72 (120) (12)	99 (165) (16)	147 (245) (24)	107 (178) (17)	74 (123) (12)	112 (186) (18)	109 (182) (17)	**103** **(173)** **(17)**
Current µA (mA/m^2) (A/m^3)	271 (451) (43)	256 (426) (41)	297 (495) (48)	370 (616) (59)	314 (523) (50)	226 (376) (36)	313 (521) (50)	265 (441) (42)	**289** **(481)** **(46)**
Resistance (Ω)	1200	1500	1003	1102	1003	1500	1003	1200	**1188**

Table 6.2 Performance of individual MFC units

6.3.2. Performance of electrical configurations

The 8 MFCs were configured in four different electrical configurations as described above (section 6.2.4) and their performance was examined under polarisation runs (Fig. 6.2). All polarisations (single or stacked MFCs) were performed at appropriate times so that changes in the anodophilic biofilm remained minimal and the output remained representative of the collective from single units. In principle, the normalised performance from stacked MFCs was expected to be relatively identical to the power density of a single MFC [72]. However, studies using different experimental MFC setups have shown that stacking with various electrical configurations, exhibited dissimilar power and current densities, where some configurations produced higher values than those from single MFCs [88,186]. MFCs connected in an 8P electrical formation reached a maximum of 1243 µW (258

mW/m^2) at a CCV of 0.36V and a corresponding current of 3427μA (714mA/m^2), which was 49% and 48% higher than the P_D and the C_D of a single unit (Table 6.3). When the MFCs were connected in a 4P2S configuration, the maximum power was 1146 μW (238 mW/m^2), which was marginally lower by 8% from the 8P configuration but still 37% higher compared to a single MFC unit. The current at MPP was 2361 μA (492 mA/m^2), which was 45% lower than the 8P connection and 2% higher than that of a single unit. The R_{int} in the 8P was 105 Ω, which equates to approximately 840 Ω per MFC and which was 41% lower than the average R_{int} from the 8 MFCs. Similarly the 4P2S recorded a 205 Ω R_{int}, which again was 65% lower than the equivalent R_{int} of 8 MFCs (~594 Ω). According to conventional circuit theory, the overall resistance in a parallel connection always tends to the lowest value of the individual resistances. Based on the higher number of parallel elements in both the 8P and 4P2S configurations, it can be suggested that the improvement in performance was related with the consequent decrease of the collective R_{int}. This suggests that the individual power characteristics and the resultant theoretical projection from a group of MFCs may not always be representative of their real power capability [88].

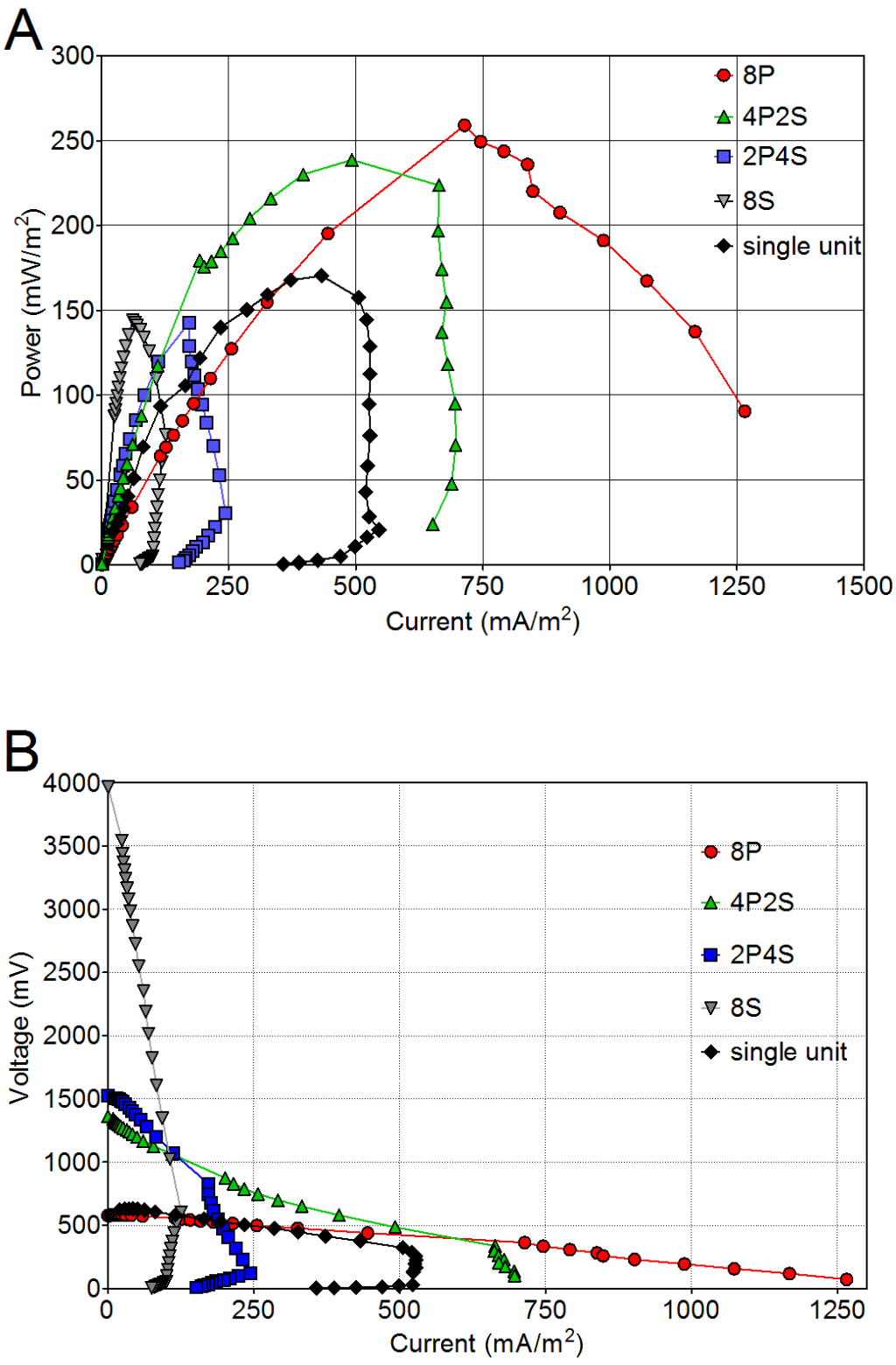

Fig. 6.2 (A) Power and (B) voltage curves from the four different configurations, compared with the average (n=8) from a single unit (closed diamonds). Lines that show a reversed trajectory at the last stages of the power and polarisation curves are due to fuel starvation that occurred in the batch-fed MFCs after the increased demand for electrons at low external resistance values.

The introduction of additional in-series element in the 2P4S configuration resulted in a peak power of 692 μW (144 mW/m^2), which was 20% lower than the average P_D from a single MFC (173 mW/m^2) and 80% lower than the 8P configuration. Current was limited to 826 μA (172 mA/m^2), which was 180% lower than the C_D of a single MFC, however the absolute current produced from this configuration was 42% higher than the theoretical sum from two individual MFCs in-parallel (578 μA). The R_{int} was found to be 1003 Ω, which is the equivalent of 501 Ω/MFC. The 8S configuration reached a similar power point of 686 μW (143 mW/m^2) and a current of 294 μA (62 mA/m^2). The power and the current remained at lower levels than the densities of a single unit even though the R_{int} was 8000 Ω, a value 19% lower than the theoretical one (9504 Ω) for 8 units connected in-series. The high number of series elements along with the decrease in performance in both the 2P4S and 8S seemed to be related with the resistance values at certain points in the polarisation process that limited the stack from reaching at least the densities of a single unit.

MFC status	Power μW (mW/m^2) (W/m^3)	Current μA (mA/m^2) (A/m^3)	R_{int} Ω	OCV (V)	Voltage in MPPT (V)
MFC unit*	103 (173) (17)	289 (481) (46)	1188	0.62	0.32
8P	1243 (258) (25)	3427 (714) (68)	105	0.57	0.36
4P2S	1146 (238) (23)	2361 (492) (47)	205	1.36	0.48
2P4S	692 (144) (14)	826 (172) (16)	1003	1.52	0.82
8S	686 (143) (13.7)	294 (62) (6)	8000	3.92	2.35

Table 6.3 Performance characteristics from 4 electrical configurations compared to a single unit. *Mean power derived from 8 units.

6.3.3. Polarity reversal during charging in a series configuration

Based on a series configuration of batteries, a weaker cell causes an imbalance when the stack is required to perform at increased energy demand levels [205]. The weak cells may not reverse immediately but will decrease in voltage and current more quickly than the strongest ones under a “heavy” load. Therefore both forward and backward polarisations [72] with individual voltage monitoring of each MFC were performed for the 8S configuration. The 8S configuration was chosen to be investigated due to the direct comparison with a dynamic reconfiguration whilst charging from 0 to 3 V. Figures 6.3A and 6.3B show the differences in voltage from each MFC and where the voltage is becoming negative, when a sequence of resistances is applied in an increasing or decreasing manner. In the forward polarisation the individual monitoring showed that five MFCs reversed in polarity across the 6 kΩ – 3 Ω range. Similarly, the backward polarisation recorded four MFCs with a negative potential within the range of 3 Ω – 6 kΩ. After this point, all MFCs returned to positive values as the external resistance was increasing. In both cases the 6 kΩ was the resistance value just before or after the MPP -8 kΩ- with the highest current from both the 8S and 2P4S. MFCs 5, 6 and 7 reversed their polarity in both polarisations with MFC 6 having the highest R_{int} (1500 Ω). However, the rest of the MFCs that underwent reversal were different in each polarisation with a R_{int} either 1003 Ω or 1200 Ω. This internal condition discrepancy from different units when performing the forward and backward polarisations, suggests that voltage reversal led to a ‘cascading effect’ in the stack and affected even well-performing MFCs with low R_{int} and overall high power [206]. MFCs 1 and 4 were not affected by this voltage stress during these processes. Hence, when high voltages are required,

stacked MFCs in-series require accurate R_{int} matching, especially under heavy loads for robust electrical performance.

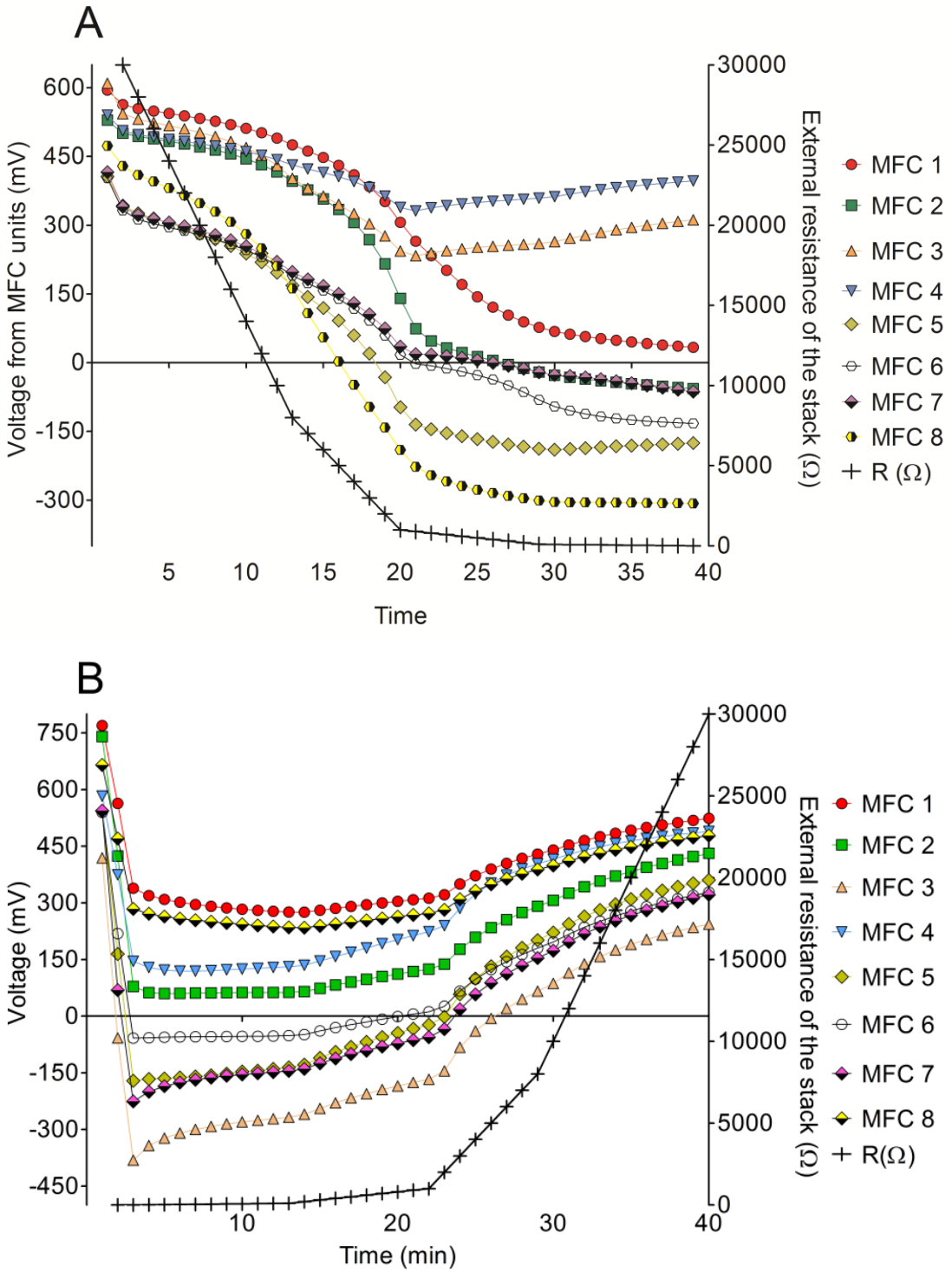

Fig 6.3 Voltage monitoring on each unit from forward (A) and reverse (B) polarisations when all 8 MFCs are in-series.

6.3.4. Energy extraction from both dynamic and fixed configurations

6.3.4.1. Fixed configuration

The OCV from the 8 MFCs in-series was 4.2 V and it took approximately 3 hours (184±3 min) to charge the super-capacitor from 0-3 V (repeated charge cycles). Detailed voltage monitoring of the MFCs charging the super-capacitor revealed that during the first 60 minutes 3 MFCs went into reversal, two of which recovered to positive values after 40 minutes, with the third MFC recovering 20 minutes later as the overall voltage in the super-capacitor was rising (Fig.6.4A). Subsequently the reversed MFCs recovered to positive values and continued to increase their operating voltage. Cell reversals that occurred in the stack whilst charging compared to the ones during the polarisations from the 8S stack showed that the reversed MFCs were different to the units that changed polarity in the backward polarisation. Moreover, the impedance of a super-capacitor is determined by the difference in potential between the stack and the super-capacitor, which acts as a dynamic current mechanism with a negligible equivalent series resistance (ESR). It was also observed that the same MFCs that reversed during the charging process reversed also in the forward polarisation. Therefore, it can be suggested that cell reversal propagation in a series connected stack could be predicted based on the OCV and the R_{int} of individual MFCs [188]. During this process, the average current value was 240 μA (Fig.6.4B).

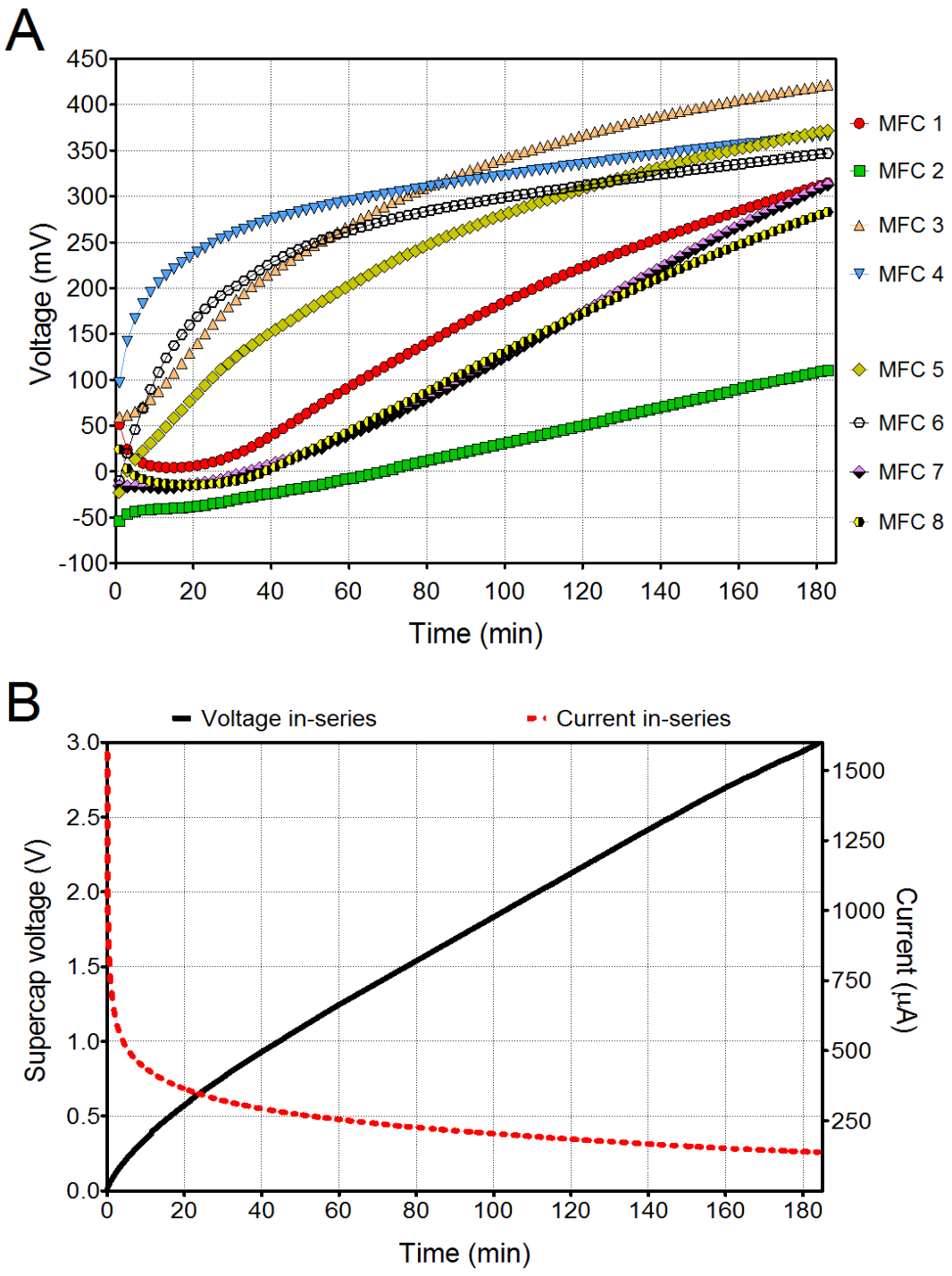

Fig. 6 4 (A) Monitoring of individual MFC voltages configured in-series whilst charging a 1F super-capacitor to 3 V and (B) overall charging voltage and current.

6.3.4.2. Dynamic re-configuration

Charging from 0 - 0.5 V started with the 8P so as to maximise the current flow from the stack into the empty super-capacitor. The configuration was automatically switched to 4P2S and continued charging until 1 V. Following this, the system was switched to 2P4S, which resulted in the voltage reaching 2 V. From that point all MFCs were connected in-series and left charging until 3 V. Voltage readings (Fig.6.5) showed that none of the MFCs reversed as was the case for the fixed series configuration. The gradual switching from parallel to series elements established a lower overall R_{int} in the stack and seemed to prevent cell reversal within the critical range of 0 to 1.4V. In addition, the MFC that showed the lowest voltage value during charging was MFC 4, previously identified as the best performing MFC, which strengthens the hypothesis that a stack with previously reversing MFCs, could affect ‘’healthy’’ units (as with standard batteries). This suggested that the stack was prone to reversal but the presence of parallel elements prevented this by maintaining balance.

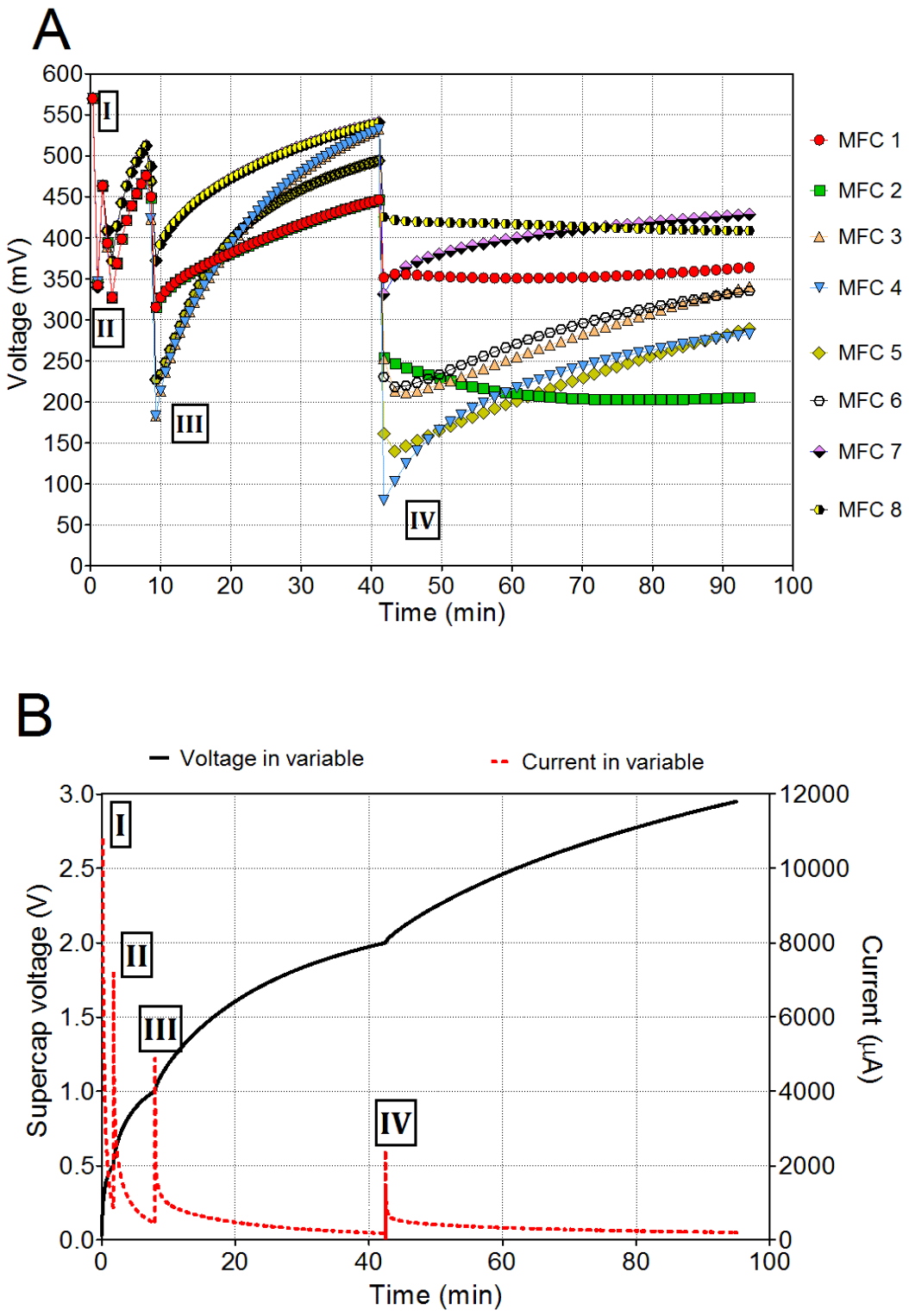

Fig. 6.5 Voltage lines from individual units during charging with the variable reconfiguration mode. Latin numerals indicate configuration switch points (I) 8P, (II) 4P2S, (III) 2P4S and (IV) 8S. (B) Overall voltage and current curves whilst charging.

6.3.5. Optimising power transfer

It has previously been reported that the manual variable reconfiguration in stacked MFCs, achieved higher energy transfer and halved the charging times from a fixed configuration [199]. Similarly, the automated variable switching improved power transfer from the stack during the charging process. When all MFCs were under the dynamic switching mode, the charging lasted 93±2 min, which is twice as fast as the fixed in-series formation (184 min) (Fig. 6.6). The improvement in charging times could be correlated with the 2-times higher average power produced from the dynamic switching mode (770 μW) compared to the fixed mode (374 μW), in the same period of time, confirmed by the highlighted area-under-curve in Figure 6.7.

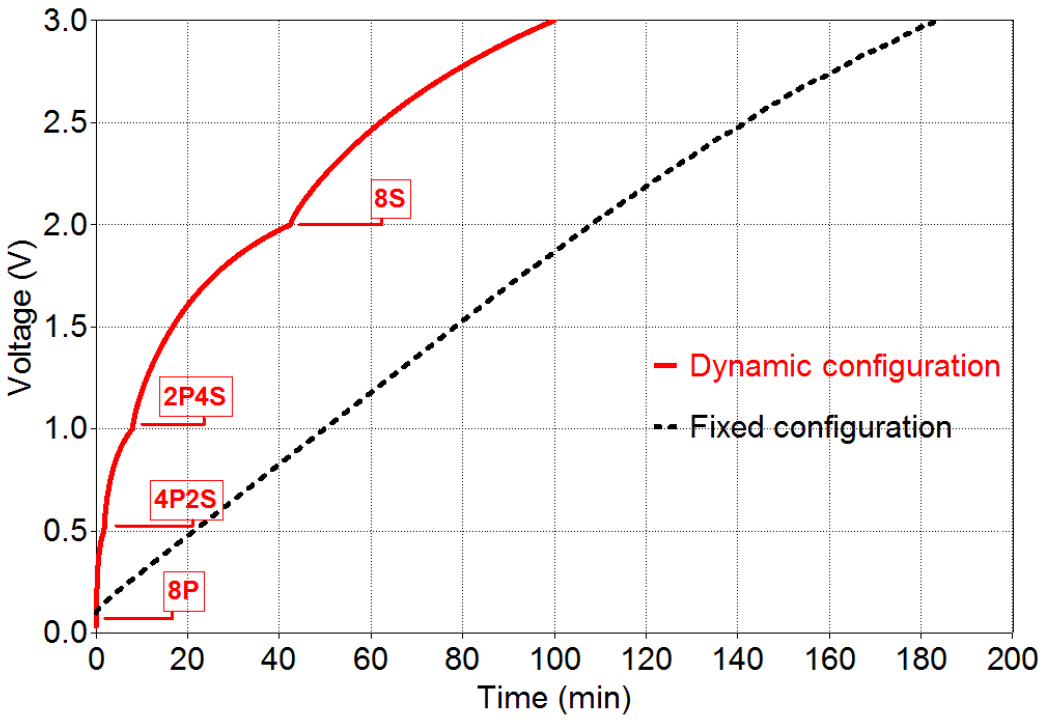

Fig. 6.6 Voltage curves against time from the dynamic and the fixed configuration.

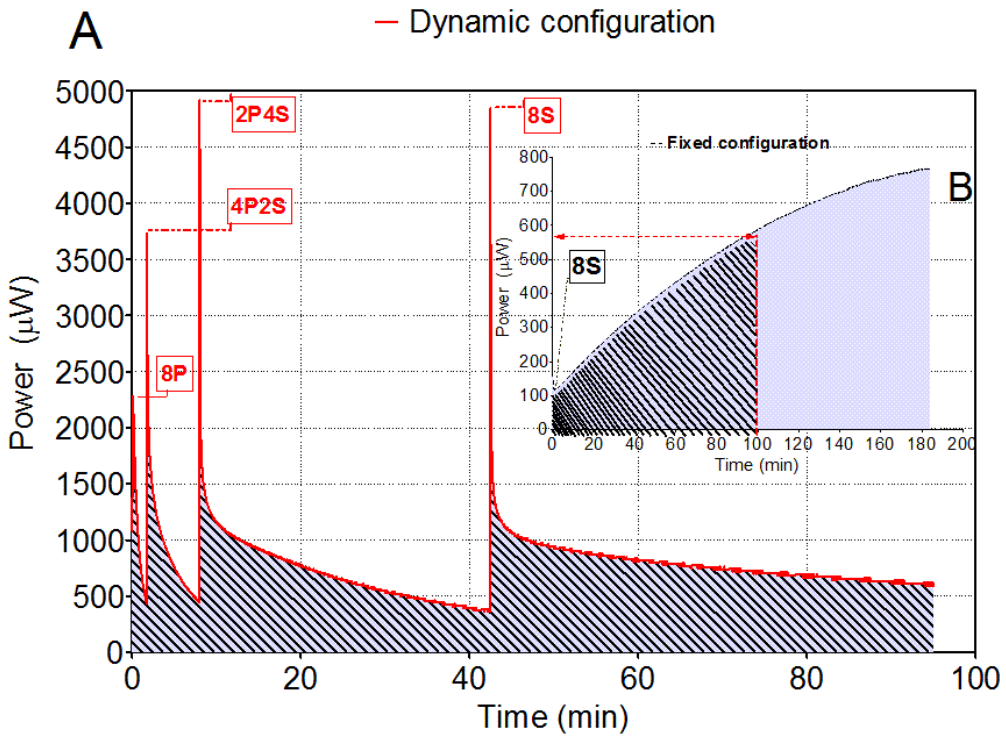

Fig. 6.7 Power levels during charging from (A) dynamic mode and (B) (inset) fixed mode. Filled areas indicate the same charging time.

6.3.6. Energy autonomous electronics for energy harvesting in MFC stacks

6.3.6.1. Challenges for energy autonomous PMS

One of the key elements for sustainable energy harvesting is minimising energy losses from the PMSs. As mentioned before, PMS in MFCs are bespoke off-the-shelf electronics designed originally for operating under $P_{Ds'}$ that a single MFC can only run intermittently [178]. Hence, it is often the fact that an external voltage supply is required for either kick-starting or continuous operation of the energy harvester. Even though the auxiliary power supply ensures robust operation and longevity of the PMS, it is far from being energy sufficient.

To date, many studies have put effort into eliminating the provision of external energy with either minimising the initial jump-start voltage[179] or completely removing the need for one, resulting to pure energy autonomous harvesters [167,172,207–209].

6.3.6.2. Efficiency of automated dynamic switching

The proof-of-concept along of the automated switch box was the springboard to showcase whether the switch box could possibly operate without the need of external power supply. The challenge in doing this was to substitute the external voltage supply with the power generated from the 8 MFC stack and still maintain the same power transfer and charging times as with the USB voltage supply; let alone protection against cell reversal.

The automated switch box consists of seven latching relays and is powered *via* a USB port. A latching relay is an electromechanical switch whereby a low voltage pulse can move the switch and remain in its position without the consumption of extra energy. According to the relay's specifications, the power required to operate continuously is 35 mW at 3 V. However, the time for switching from one position to the other is approximately 10ms which equates to 350 µJ. In order for the system to provide the energy for the initial switching, the stack could be configured in-series, charging a 3 V, 6.8 mF capacitor. The size of the 6.8 mF capacitor has been determined to be sufficient to provide enough switching energy for one full cycle of the system. This process requires approximately 15 minutes and delivers 30.6 mJ which is sufficient for switching seven latching relays (7 x 350 µJ) to parallel position for the start-up, and will consume 2.45 mJ. The maximum losses from switching all the relays at once would vary between 1.2% and 8.4% of the total energy stored in the start-up super-capacitor; an efficiency of over 90%. Hence the harvested energy

from the 8 MFC stack can deliver enough power to perform the switching during the reconfiguration of electrical connections and store the excess of energy.

6.3.6.3. Feasibility of a self-powered PMS circuit with automated switching

Based on these theoretical projections, a novel PMS for automated switching was built and tested on the 8-MFC stack. As described in the aforementioned paragraph, the external power supply was substituted with a small 6.7 mF capacitor that harvested sufficient energy to run continuously the microcontroller for switching and voltage monitoring. However based on previous studies describing the development of MPPT active harvesters, it was deemed best to substitute all latching relays with transistors [161,210]; metal-oxide-semiconductor-field-effect-transistors (MOSFET) that act as a switch and consume 1000-times less energy compared to a latching relay (~30 μJ each).

Preliminary results showed that after running continuously for a period of 18 hours, the PMS managed to perform fourteen complete charging/discharging cycles within this period (Fig. 6.8A). This suggested that every cycle required an average of 80 (± 2) minutes, which is 18% faster than the automated switching technique previously reported in this chapter (see section 6.3.5). The voltage on the start-up capacitor confirmed further the smooth operation of the auxiliary capacitor (Fig. 6.8B). On top of that, logging of voltage in individual MFCs showed that the system prevented cell reversal even though at the beginning of each cycle the stack was configured in-series charging the auxiliary capacitor (Fig. 6.8C).

A

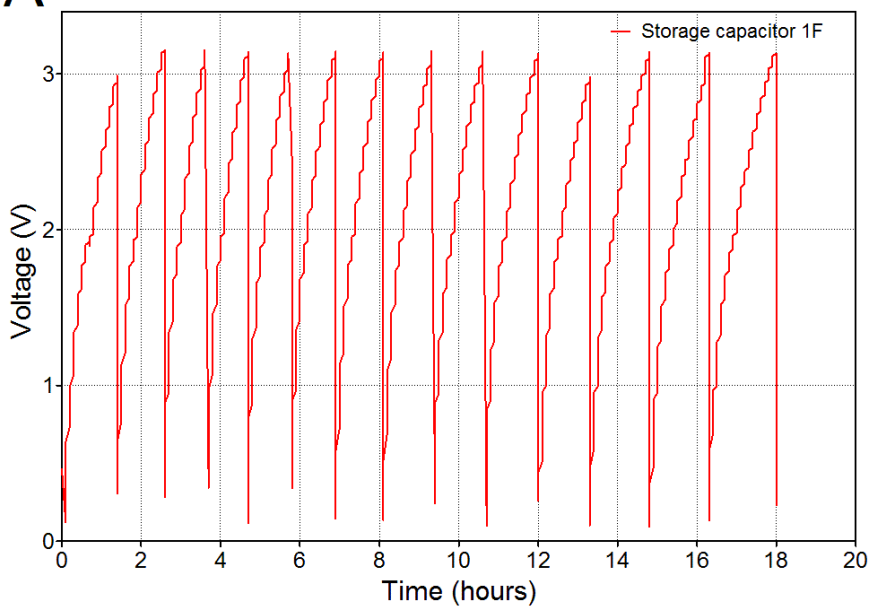
Storage capacitor 1F
Voltage (V)
Time (hours)
0
1
2
3
0
2
4
6
8
10
12
14
16
18
20

B

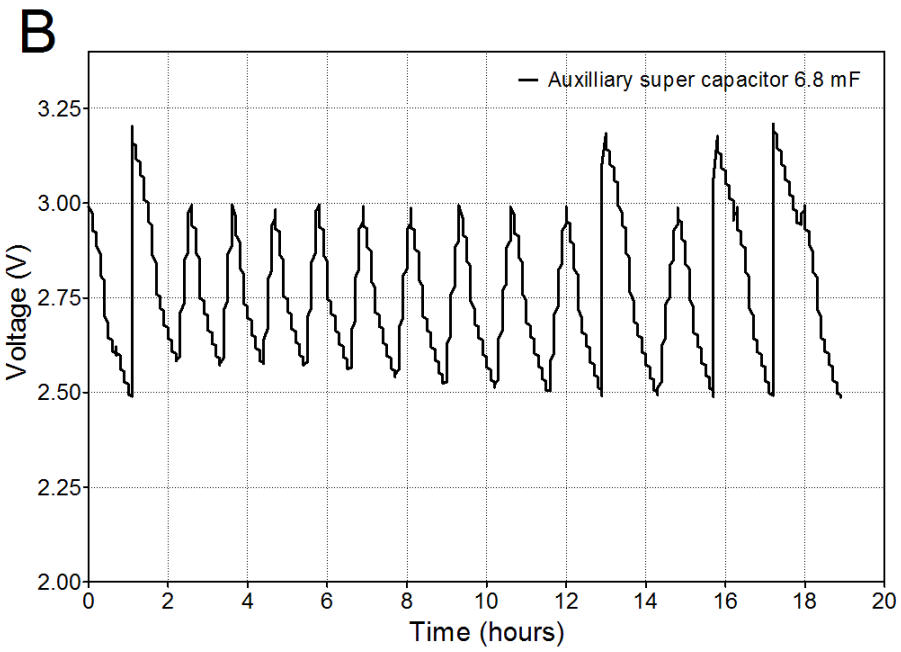
Auxilliary super capacitor 6.8 mF
Voltage (V)
Time (hours)
2.00
2.25
2.50
2.75
3.00
3.25
0
2
4
6
8
10
12
14
16
18
20

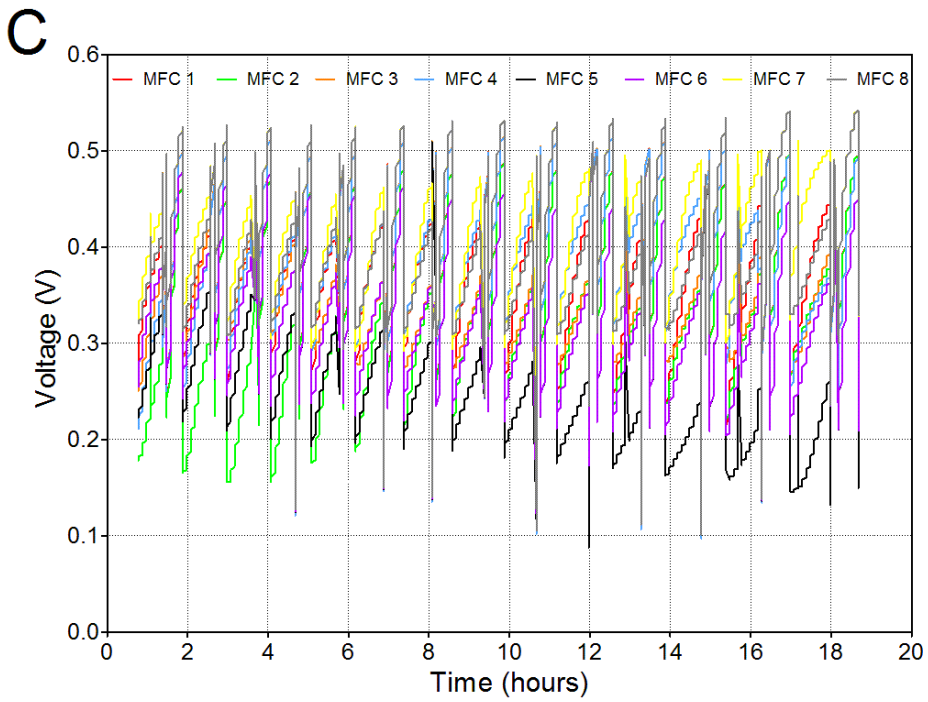

Fig. 6.8 (A) Charging/discharging of a 1 F supercap from 0 to 3 V, (B) charging and gradual discharging of the auxiliary capacitor whilst running the PMS and (C) voltage monitoring of all 8 MFC units in the stack during the 14 cycles of operation.

6.4. Conclusions

Differences in R_{int} can lead to cell reversal in stacked MFCs when a low external resistance is applied. MFCs with the highest R_{int} are expected to go into reversal; however results show that reversed MFCs are likely to affect the better performing units. This propagation effect cannot yet be easily predicted, but it is considered to be a function of R_{int} combined with position in the stack that hinder rates of reaction in an anode, which is connected to the cathode of a reversed MFC.

The theory behind the variable switching is to maximise the transfer of the generated charge from the MFC stack into the storage device – in this instance a super-capacitor – by gradually substituting parallel elements for series within the

stack. This has an additional positive effect on the R_{int} which is reduced thus allowing for faster current flow by maintaining a potential disparity between the stack and the super-capacitor. As a consequence dynamic switching enhances the stack's robustness by minimising cell reversal and improving performance without the use of complicated electronics.

Over and above that, the theory of dynamic switching allowed for the development of a prototype MFC-powered PMS that uses commercially available electronics without any voltage boosting components that can reduce the overall efficiency. Thus, dynamic switching PMS is capable of achieving efficiencies higher than 90%, avoid any capacitor-to-capacitor losses and provide a fail-safe performance for long-term operation. Future direction of this experimental PMS is the transferability to other energy storage technologies.

Chapter 7

Parts of the following results presented in this chapter have been published in:

- Papaharalabos, G., Greenman, J., Stinchcombe, A., Melhuish, C., & Ieropoulos, I. A. (2014). **Artificial control of microbial life: Towards urine fuelled robot**. ALIFE 14. http://evobliss.eu/uploads/publications/alife/4-papaharalabos.pdf
- Boghani, H. C., Papaharalabos, G., Michie, I., Fradler, K. R., Dinsdale, R. M., Guwy, A. J., Premier, G. C. (2014). **Controlling for peak power extraction from microbial fuel cells can increase stack voltage and avoid cell reversal.** Journal of Power Sources, **269,** 363–369.

7. Developing an intelligent microbial electrical system

7.1. Knowledge transferability on a MFC testing platform: EcoBot-IV

In 2010 the 3rd generation of the self-sustainable EcoBot series [69] was presented, which was a robot capable of simulating biological functions, such as food ingestion, digestion and waste egestion. EcoBot-III, a 6kg robot, utilised a stack of 48 Microbial Fuel Cells (MFCs) for energising a complex robotic platform, which performed energy intensive tasks. This symbiotic relationship between living microorganisms and robotic devices was the first example of Symbots [97].

Since then, extensive experiments have taken place with MFC stacks to increase their performance and efficiency. The idea behind this preliminary work is to expand the knowledge from the self-sustainability perspective. For this reason, a novel monitoring system was developed which, along with dynamic reconfiguration of the electrical connections in a stack of 24 MFCs, seemed to decrease the charging times of the super-capacitor that powers the processing and controlling units of the testing platform.

7.1.1.1. Specifications of the testing platform

EcoBot-IV[77] (Fig. 7.1) was initially designed to operate with a stack of 48 fluidically isolated MFCs, however the increase in power using new electrode materials resulted in improved performance from the MFCs (see chapter 3), thus reducing the number of MFCs required to run the robot, to only 24. Similar to EcoBot-III, EcoBot-IV holds the ability to monitor its fluid levels, move towards the nearest food source and get rid of its own waste. After ‘’foraging’’, the robot would process the food and water, and distribute it equally to all MFCs, providing a uniform amount of carbon energy to all units, in order to sustain its operation.

EcoBot-IV retains the same principle of a self-sustainable robot but differs from its predecessor in terms of both mechanical and electrical approaches. It is capable of transmitting telemetry data via a two-way wireless communication link, thus sending feedback to the user about the ‘health’ status of the MFCs. Furthermore, it allows the user to manually reconfigure the electrical connections within the MFC stack, so as to better match the current or voltage requirements, depending on the level of energy under different conditions.

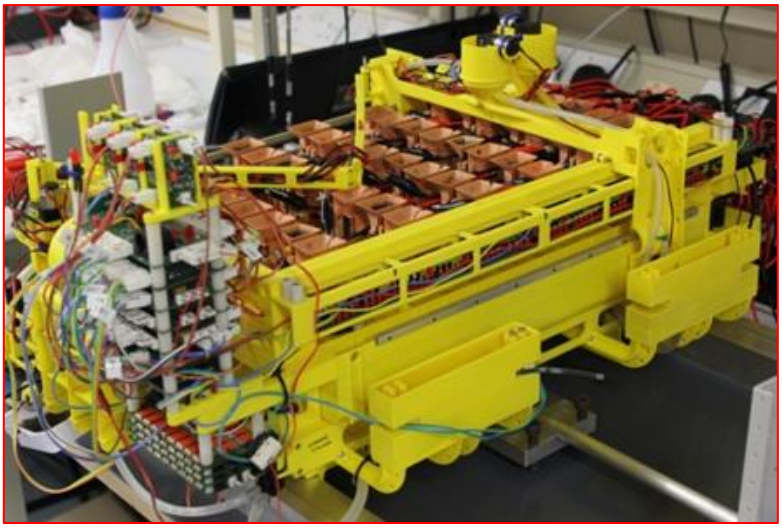

Fig. 7.1 The testing platform of EcoBot-IV

The electronics of the platform require a voltage range between 2.0 and 2.97 V to operate, depending on the actuation (i.e. a voltage differential between 0.8 – 1 V). The time between charging the capacitors from the lower threshold of 2.0 V to the upper limit of 2.97 V, varies on parameters such as biofilm, internal resistance, ambient temperature, pH, concentration of organic matter in the anolyte, hydration of the cathode, oxygen diffusion on the cathode electrode and most importantly the electrical configuration of the stack.

7.1.1.2. Monitoring the 'health status' of the robot's MFC stack

When operating in a stack, the performance of MFCs varies due to the collective R_{int}. It is therefore critical to monitor in real time the performance of each unit within the stack and understand the reaction of individual units when in stress, reversed or when fed and hydrated. Hence, a switch box was developed to connect the MFCs with the provision of dynamic reconfiguration and also to monitor the voltage (or 'health') of each unit. This process is monitored in real-time with an Agilent 34970A

(Hewlett Packard, USA). A special interface for monitoring and analysis was developed, which enables the user to wirelessly receive these data (Fig. 7.2).

Fig. 7.2. Software interface for monitoring MFC status

7.1.1.3. Dynamic switching

Originally, the electrical configuration of the stack was 3 MFCs in-parallel, and the resulting 8 groups of these MFCs, in-series. This produced a OCV of 4.8 V and 600μA (under load), enough to charge the robot's supercapacitors (1.5 F) in approximately 40 minutes and produce an actuation of 20 seconds. However, after the discovery of the variable electrical reconfiguration (see chapter 5) then the system operated in a dynamic charging mode.

Figure 7.3 shows that dynamic switching improved charge transfer by 35% at a 90% efficiency of the energy stored in the super-capacitor. It also suggested that the time to charge from 2 to 3 V was decreased by 25% (20 minutes faster) compared to

a fixed electrical configuration that was applied previously on this platform and EcoBot-III stack in order to charge the super-capacitor to 3 V. The configuration was changed every 0.5 V and during the process, additional in-series elements were introduced in the stack to step-up the voltage. The gradual addition of series elements increased the slope of the charging curve. As previously explained, this can be attributed to the instantaneous increase of voltage in the system that results in a higher potential difference between the stack and the super-capacitor.

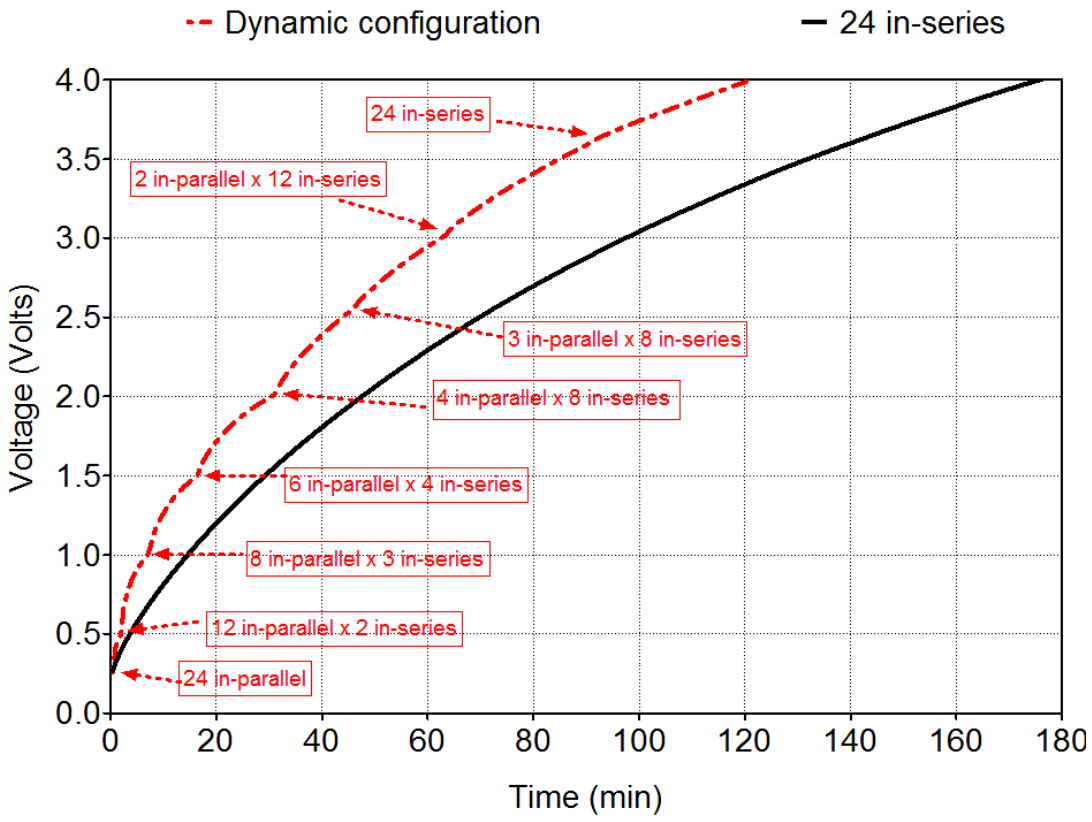

Fig. 7.3 Charging times in dynamic reconfiguration compared to a fixed configuration.

7.1.1.4. MFC adaptation in substrate adverse conditions

As in chemical batteries, MFCs are dictated by an internal resistance (R_{int}) that affects the voltage output and the overall performance. The increasing number of MFCs in a cascade mode, showed that the electro-active biofilm responded

differently in all 8 cascade cases and that the bacteria managed to bounce back to lower levels of R_{int} every time the system was rearranged to more hydraulic connections in cascade. This can suggest that the bacteria in the fuel cells and in the stack collectively, demonstrated a pattern of maintaining a physical balance whilst returning to a previous state that would serve their electrical equilibrium even though the feeding quality was continuously becoming unfavourable.

EcoBot-IV operated for 3 days before a mechanical failure (pumping component). The behaviour results suggest that the charging rate gradually improved during this period, whilst demonstrating self-sustainability (Fig. 7.4). The smaller number of MFCs on the EcoBot-IV platform not only maintained the robot's energetic requirements, but continued to improve their performance through time, which depended on the frequency of feeding and amount of substrate they were supplied with, throughout the operation period.

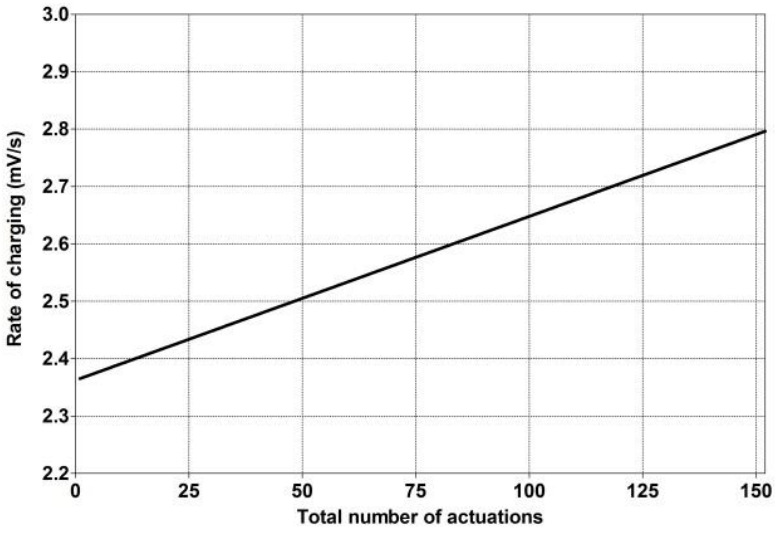

Fig. 7.4 Increase in the rate of charging rate within a period of 3 days. The system managed to perform a total of 153 actuations, which meant an actuation every 30 minutes.

7.1.1.5. Artificial control of microbial life: Towards a urine fuelled robot

Since the appearance of the first food powered mobile robot some fourteen years ago [125], the concept of building self-sustainable Symbots with bioinspired features has led research in MFCs to the next level.

Self-maintenance in EcoBot-IV can be seen in two levels that cross over so as to achieve a common goal. In this context the MFC stack is an autonomous system (biological system) that collaborates with the automated system (mechatronics) of EcoBot-IV so both can preserve their longevity. Ecobot-IV can be described as an agent that has self-interest in seeking for resources that will ensure its own existence. Consequently, the bacterial 'engine' is the living 'user' that will profit from the functions that the mechatronic side will perform in order to maintain the whole EcoBot-IV robot through behavioural stability and 'user satisfaction' [125,211]. The basic cycle that EcoBot-IV follows for maintaining viability can be correlated with one of the basic cycles of activities; the ''unproductive energy loss''[212] where energy is lost when the robot is seeking for a food source. As such, the automated dynamic switching on EcoBot-IV allows for rapid agent adaptation to the energy demanding tasks [125] by accelerating the bioelectrical activities of the 'user'. Similarly, the hydraulic reconfiguration of the urine supply system in the stack, can affect power production from the 'engine' and affect consequently the control and energy management systems.

Although the technology cannot operate a robot like common chemical batteries, bench research on MFC stacks is proof that energy autonomy is both plausible and feasible. To date, stacks of MFCs have powered small electronic devices such as LEDs, small DC motors, wristwatches, mobile phones and it is envisaged that laptop computers could be next. The EcoBot Project is a constantly evolving research area

that is using novel technologies to provide insight towards MFC stack performance and efficiency with regards to robotic autonomy and sustainability. Results show that MFC stacks can become a smart power source that could energise their electrical and hydraulic configuration circuitry based on their metabolic status so as to efficiently drive robotic platforms capable of maintaining their homeostasis whilst performing various tasks.

7.2. Alternative PMS strategy

7.2.1. MPPT without the occurrence of cell reversal

As previously mentioned, a few studies have focused in developing PMS capable of preventing cell reversal and harvesting energy at the same time. Nevertheless, the R_{int} of a MFC varies with changes in substrate concentration, operating temperature, buffer concentration, pH, biofilm ecology and structure, during its operation, all of which might be expected when treating wastewater. The state of the system is therefore seldom likely to be static. An MFC could be operated to match its real-time impedance [213,214], which could be coupled to the charging and discharging of capacitors by suitable control of current sourcing. Therefore, this parallel line of work seeks to determine if controlling the current sourced from individual MFCs while simultaneously connected in-series can avoid cell reversal and maximise the power they generate.

The application of the MPPT controller and the connection strategy presented here can increase stack potentials and avoid the reversal of cell potential, whilst also applying a control mechanism that facilitates peak power extraction from MFCs in

real-time. The strategy is transferable between different designs of MFC and with different substrates.

7.2.1.1. In-series small-MFCs (sMFCs) under MPPT scenarios

For running the MPPT controller, three small 6.25 mL MFCs[69] were configured electrically in-series. S-MFCs were operated at ambient temperature (22 ± 3 ^{o}C) and supplied with fresh urine. S-MFC1 and s-MFC3 were given undiluted urine (as organic substrate) and s-MFC2 was provided with 1:1 diluted urine with distilled water. S-MFCs were operated under three different Rext scenarios (Fig. 7.5).

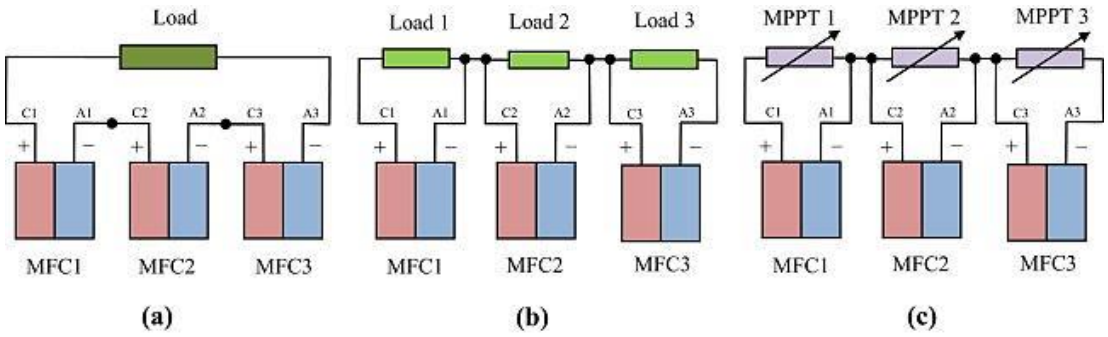

Fig. 7.5 (a) MFCs connected in series across an overall load of 8 kΩ to match the collective internal resistance, CASE-1. (b) MFCs connected to the loads individually, matching their individual internal resistances, CASE-2; and (c) connected to MPPTs individually which are then connected in series, CASE-3.

CASE-1: The MFCs were connected in-series, connecting anodes to cathodes and a static load of 8 kΩ was used to match the overall internal resistance of the s-MFCs (Fig. 7.5a);

CASE-2: Each MFC was connected to the maximum power point load of 2 kΩ (static) determined a *priori* using power curves (power vs. current). The MFCs and associated loads were then connected in-series as shown in Fig. 7.5b. Static loads

of were used for s-MFC1 and s-MFC3, and 4 kΩ static load for s-MFC2 and; During CASE-1 and CASE-2 experiments, the potential drop across the individual MFC loads and the stack potential were sampled at 30 second intervals using a PC equipped with LabVIEW™ and NI USB-6218 (National Instruments, Newbury, UK).

CASE-3: As shown in Fig. 7.5c, each MFC was connected to a maximum power point tracking (MPPT) device which controlled the current sourced from each MFC. Boolean logic based hill climbing control[215] was implemented by varying the load in response to the gradient of the power curve and of its rate of change. Additionally, logic increased the load in steps if MFC potential < 0.1 V. A digital potentiometer (Intersil® X9C102, Farnell UK Ltd., Leeds) was used as the load to control the current *via* a PC equipped with LabVIEW™ and NI USB-6218. The current sourced from the MFCs was regulated using digital potentiometers and thus actuated the MPPT. The potential drops across these potentiometric loads and across the entire stack were digitally sampled at intervals of 150 seconds. All s-MFCs were operated in batch until the substrate was depleted.

7.2.1.2. Cell reversal avoidance

Fig. 7.6 shows that after the addition of substrate, the s-MFCs responded to the addition of substrate very rapidly and developed voltages as per their normal performance (Fig. 7.6). However, the potential of s-MFC1 reversed after 1 day of operation in-series, recovering on day 3 and at the same time s-MFC3 reversed indicating a cell potential of -0.3 V by day 5.5 approx.

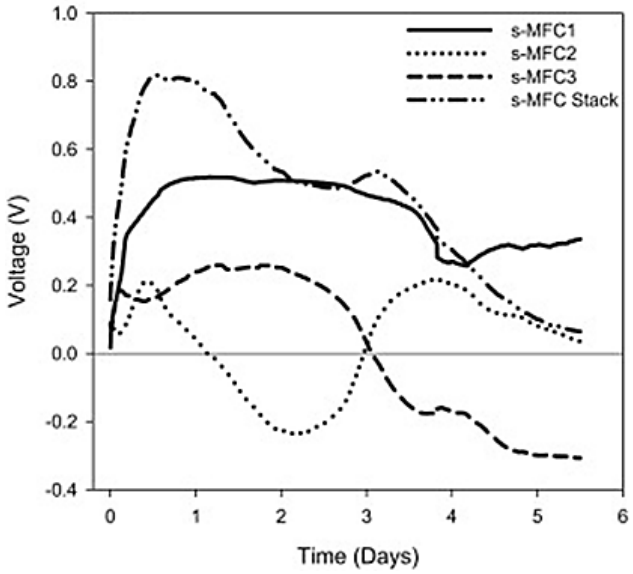

Fig. 7.6 s-MFCs with stack load of 8 kΩ

Notably, in CASE-2 (Fig. 7.7), when s-MFCs were connected to their respective loads, the potential drop across the load was 0.4 V immediately, but it dropped to approx. 0.2 V by hour 12, continuing to gradually decrease until day 7 as the substrate depleted (Fig. 7.7).

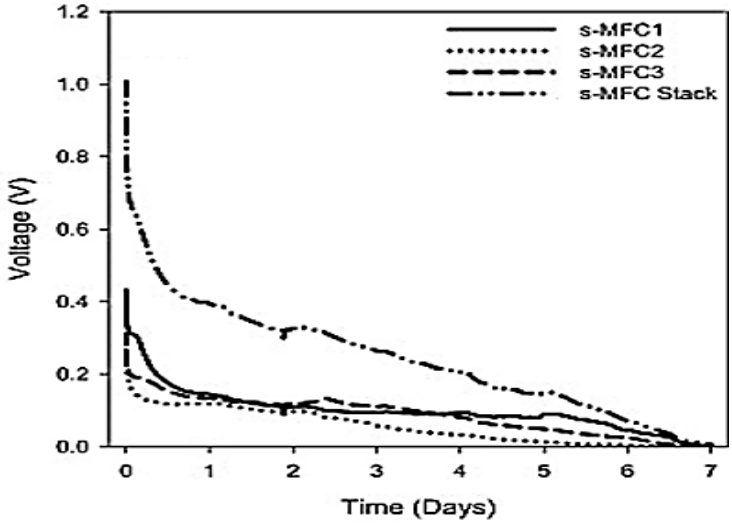

Fig. 7.7 Voltage across static loads on individual MFCs and overall stack voltage as in CASE-2 for s-MFCs

In CASE-3, the initial electrical MPPT load for the s-MFCs was selected to be 4.7 kΩ. The MPPT system was able to track the maximum power point from measures of the MFCs' individual potentials. In the case of s-MFCs (Fig. 7.8), the MPPT loads tracked the maximum power and the individual voltages were approximately 0.1 V before substrate depletion became a dominant factor. Lack of substrate is evidenced through the dropping cell potential and increasing external load where s-MFC2 load started increasing first out of the other ones, confirming comparative less substrate available in s-MFC2. The data shown in Fig. 7.7 and 7.8 have been reduced by resampling at 15 min intervals in order to reduce the quantity of data. However, the procedure does not alter the information content of the data in respect of the observations and conclusions drawn.

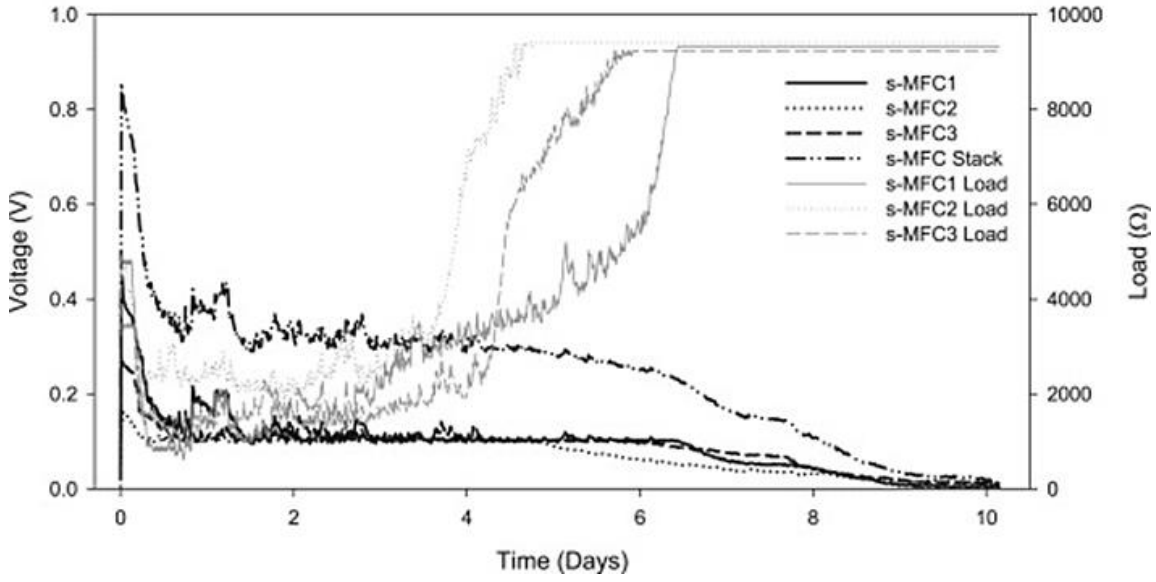

Fig. 7.8 Voltage across MPPT loads on individual MFCs and overall stack voltage as in CASE-3 for s-MFCs.

7.2.2. Results and discussion

In order to consider the mechanism by which cell potential becomes reversed the anode and cathode connections to the three MFCs may be identified as A1, A2 and

A3 (anodes) and C1, C2, C3 (cathodes) respectively (Fig. 7.5). In CASE-1, when insufficient substrate is available to generate electronic current from A2, its potential will assume that of C3, to which it is connected. Cationic current in MFC2 will also be minimal compared to other MFCs in the stack. The cathodic reaction in MFC2 will then also largely cease. And hence C2, unable to sink electronic current from A1, will assume the potential of A1. So, the reversal in potentials of MFC2 (A2 and C2) will result. MFC2 thus becomes a parasitic internal load, through which electronic current must pass to reach from A1 to C3. The stack potential will be lowered as a consequence and this is clearly seen in Fig. 7.5. This indicates that s-MFC2, unable to provide electrons and protons for the current flow, becomes a very high parasitic load in the circuit.

In CASE-2 and CASE-3, the individual MFCs with their individual loads are subsequently connected in-series, which appears as bridging throughout the whole stack (Fig. 7.5b). When A2 stops producing an electronic current, the electrons used in the reduction of C3 can come through the external load of MFC3 (and/or MFC2) and similarly when the cathodic reaction in MFC2 is seriously restricted by lack of cations, the electrons generated at A1 can reach C1 and C3 via external loads. So, in this way, the underperforming MFC can be by-passed with minimal diminution of the performance of the whole stack. This can be seen in Fig. 7.7 and Fig. 7.8 from the fact that none of the s-MFCs exhibited potential reversal. Furthermore, the power generation from s-MFC2 was also producing somewhat lower power than the other s-MFCs in the stack but did not affect their performances (Fig. 7.7 and after day 5 in Fig. 7.8).

When the s-MFCs were connected to MPPT, the current sourced from the anode's electrogens, was controlled to ensure peak power output, which would correlate to maximum COD removal by the electrogens. In practice, stacking of MFCs is likely to be required and it is desirable that each MFC operates at its instantaneous peak capacity. Also, obstructions in the flow pathways could cause MFCs to receive reduced or unbalanced (cell to cell in a stack) organic loading, which if unchecked could cause temporary or permanent inactivation and cell reversal. CASE-3 demonstrates that individual MFCs could be operated at their maximum power point (Fig. 7.8) and the potential could be boosted despite MFCs, electrically connected in-series, not having identical substrate concentrations; so avoiding cell reversal. However, appropriate energy harvesting mechanisms are required. The strategy presented here, along with the MPPT, was effective in preventing cell reversal while extracting available maximum power.

Using power from MFCs deployed in practical systems will require potentials to be increased above cell potentials, which can be achieved by stacking in-series, but this approach risks the occurrence of cell potential reversals, which affects the whole stack. When serially wired MFCs are operating at similar and sufficient substrate concentration, with fully enriched electrogenic biofilms on their anodes and with active cathode, they may be expected to produce comparable electrical and ionic currents to each other and voltage reversal should not occur during the stack operation [216]. An imbalance in the organic strength of substrate supplied to stacked MFC cells is likely to occur in practice and in circumstances where volumetric throughput is important, such as in wastewater treatment applications; it is even more likely as MFCs will tend to be hydraulically connected in-series (i.e in cascade

arrangement) and substrate will be progressively consumed as it passes through the system [217].

When stack operation is considered, given that MFCs running at different levels of substrate concentration are susceptible to voltage reversal, it may be difficult in practice to distribute substrate equally amongst cells. Therefore it is necessary to adopt a strategy or device to avoid voltage reversal in MFCs when operated in stacks. The strategy presented has been shown to be transferable between substantively different MFC designs and substrates used and may be suitable for application to energy harvesting from MFCs and may be implemented using low power digital electronics.

7.3. Concluding remarks

7.3.1. Future scopes for MFC stacks

The scope of this thesis has been primarily structured around the development of small-sized and large number MFCs that could power the latest generation of a self-sustainable robot, the EcoBot-IV. During this project, the challenges that needed to be addressed were miniaturisation, power increase, and the efficient stacking of MFCs with the added bottlenecks that arise when numbers increase. Findings from this series of experiments have led to the construction of a new design MFC with enhanced properties, the improvement in power with the introduction of a new cathode electrode, the optimisation of urine utilisation in a changeable stack and a revolutionary energy harvesting technique. Additionally, the development of a MFC powered device capable of modulating energy extraction at a high efficiency has opened new directions in PMS and robustness for MFC stacks operation. Each

finding from this study forms a unique part of the overall spectrum that a MFC system comprises. Regardless of their substantiality, there is still the need for transferability of this theoretical knowledge in a collective manner whereby the synergy of these findings could result in a highly integrated MFC stack system.

Based on the generated knowledge, it is suggested that these results are conclusive and have set the foundations towards further MFC stack evolution. This work has been widely disseminated and has received acknowledgement by other scientific groups in the area of MFCs, thus fulfilling its scientific objectives.

8. References

1. Piccolino, M. Luigi Galvani and animal electricity: two centuries after the foundation of electrophysiology. *Trends Neurosci.* **20,** 443–448 (1997).
2. M C Potter. Electrical Effects Accompanying the Decomposition of Organic Compounds Published by : The Royal Society Electrical Effects accompanying the Decormposition of Organic. **84,** 260–276 (2010).
3. Cohen, B. The Bacteria Culture as an Electrical Half-Cell. **21,** (1931).
4. Rohrback GH, Scott, WR, Canfield, J. Biochemical fuel cells. in *Proc. 16th Annu. Power Sources Conf.* p. 18. (1962).
5. Williams, K. R. & Koslow, R. An Introduction to Fuel Cells. *J. Electrochem. Soc.* **113,** 139C (1966).
6. YAO, S. J., APPLEBY, A. J., GEISEL, A., CASH, H. R. & WOLFSON, S. K. Anodic Oxidation of Carbohydrates and their Derivatives in Neutral Saline Solution. *Nature* **224,** 921–922 (1969).
7. Karube, I., Ikemoto, H., Kajiwara, K., Tamiya, E. & Matsuoka, H. Photochemical energy conversion using immobilized blue-green algae. *J. Biotechnol.* **4,** 73–80 (1986).
8. Bennetto, H. P., Stirling, J. L., Tanaka, K. & Vega, C. A. Anodic reactions in microbial fuel cells. *Biotechnol. Bioeng.* **25,** 559–68 (1983).
9. Thurston, C. F. *et al.* Glucose Metabolism in a Microbial Fuel Cell. Stoichiometry of Product Formation in a Thionine-mediated Proteus vulgaris Fuel Cell and its Relation to Coulombic Yields. *Microbiology* **131,** 1393–1401 (1985).
10. Allen, R. M. & Bennetto, H. P. Microbial fuel-cells. *Appl. Biochem. Biotechnol.* **39-40,** 27–40 (1993).
11. Davis, J. B. & Yarbrough, H. F. Preliminary Experiments on a Microbial Fuel Cell. *Science* **137,** 615–6 (1962).
12. Bennetto, H. P. Electricity generation by microorganisms. *Biotechnol. Educ.* **1,** 163–168 (1990).
13. Rabaey, K., Boon, N., Siciliano, S. D., Verhaege, M. & Verstraete, W. Biofuel cells select for microbial consortia that self-mediate electron transfer. *Appl. Environ. Microbiol.* **70,** 5373–82 (2004).
14. Gorby, Y. A. *et al.* Electrically conductive bacterial nanowires produced by Shewanella oneidensis strain MR-1 and other microorganisms. *Proc. Natl. Acad. Sci. U. S. A.* **103,** 11358–63 (2006).
15. Reguera, G. *et al.* Extracellular electron transfer via microbial nanowires. *Nature* **435,** 1098–101 (2005).
16. Reguera, G. *et al.* Biofilm and nanowire production leads to increased current in Geobacter sulfurreducens fuel cells. *Appl. Environ. Microbiol.* **72,** 7345–8 (2006).

17. Chaudhuri, S. K. & Lovley, D. R. Electricity generation by direct oxidation of glucose in mediatorless microbial fuel cells. *Nat. Biotechnol.* **21,** 1229–1232 (2003).

18. Kim, B. H. *et al.* Electrochemical activity of an Fe(III)-reducing bacterium, Shewanella putrefaciens IR-1, in the presence of alternative electron acceptors. *Biotechnol. Tech.* **13,** 475–478

19. Scholz, F. & Schröder, U. Bacterial batteries. *Nat. Biotechnol.* **21,** 1151–2 (2003).

20. Ieropoulos, I. a., Greenman, J., Melhuish, C. & Hart, J. Comparative study of three types of microbial fuel cell. *Enzyme Microb. Technol.* **37,** 238–245 (2005).

21. Kim, H. J. *et al.* A mediator-less microbial fuel cell using a metal reducing bacterium, Shewanella putrefaciens. *Enzyme Microb. Technol.* **30,** 145–152 (2002).

22. Bond, D. R. & Lovley, D. R. Electricity production by Geobacter sulfurreducens attached to electrodes. *Appl. Environ. Microbiol.* **69,** 1548–55 (2003).

23. Gregory, K. B., Bond, D. R. & Lovley, D. R. Graphite electrodes as electron donors for anaerobic respiration. *Environ. Microbiol.* **6,** 596–604 (2004).

24. Torres, C. I. *et al.* Selecting anode-respiring bacteria based on anode potential: phylogenetic, electrochemical, and microscopic characterization. *Environ. Sci. Technol.* **43,** 9519–24 (2009).

25. Aelterman, P., Versichele, M., Marzorati, M., Boon, N. & Verstraete, W. Bioresource Technology Loading rate and external resistance control the electricity generation of microbial fuel cells with different three-dimensional anodes. **99,** 8895–8902 (2008).

26. Phung, N. T. *et al.* Analysis of microbial diversity in oligotrophic microbial fuel cells using 16S rDNA sequences. *FEMS Microbiol. Lett.* **233,** 77–82 (2004).

27. Logan, B. E. & Regan, J. M. Electricity-producing bacterial communities in microbial fuel cells. *Trends Microbiol.* **14,** 512–8 (2006).

28. Kim, G. T. *et al.* Bacterial community structure, compartmentalization and activity in a microbial fuel cell. *J. Appl. Microbiol.* **101,** 698–710 (2006).

29. Jung, S. & Regan, J. M. Comparison of anode bacterial communities and performance in microbial fuel cells with different electron donors. *Appl. Microbiol. Biotechnol.* **77,** 393–402 (2007).

30. KIM, J., JUNG, S., REGAN, J. & LOGAN, B. Electricity generation and microbial community analysis of alcohol powered microbial fuel cells. *Bioresour. Technol.* **98,** 2568–2577 (2007).

31. Kim, B. H. *et al.* Enrichment of microbial community generating electricity using a fuel-cell-type electrochemical cell. *Appl. Microbiol. Biotechnol.* **63,** 672–81 (2004).

32. Logan, B. E., Murano, C., Scott, K., Gray, N. D. & Head, I. M. Electricity generation from cysteine in a microbial fuel cell. *Water Res.* **39,** 942–52 (2005).

33. Costerton, J. W., Lewandowski, Z., Caldwell, D. E., Korber, D. R. & Lappin-Scott, H. M. Microbial biofilms. *Annu. Rev. Microbiol.* **49,** 711–45 (1995).

34. Reimers, C. E., Tender, L. M., Fertig, S. & Wang, W. Harvesting energy from the

marine sediment--water interface. *Environ. Sci. Technol.* **35,** 192–5 (2001).

35. Ieropoulos, I., Melhuish, C. & Greenman, J. Artificial gills for robots: MFC behaviour in water. *Bioinspir. Biomim.* **2,** S83–93 (2007).

36. Gil, G.-C. *et al.* Operational parameters affecting the performannce of a mediator-less microbial fuel cell. *Biosens. Bioelectron.* **18,** 327–334 (2003).

37. Logan, B. E. *et al.* Microbial Fuel Cells: Methodology and Technology †. *Environ. Sci. Technol.* **40,** 5181–5192 (2006).

38. Pant, D. *et al.* An introduction to the life cycle assessment (LCA) of bioelectrochemical systems (BES) for sustainable energy and product generation: Relevance and key aspects. *Renew. Sustain. Energy Rev.* **15,** 1305–1313 (2011).

39. Foley, J. M., Rozendal, R. A., Hertle, C. K., Lant, P. A. & Rabaey, K. Life cycle assessment of high-rate anaerobic treatment, microbial fuel cells, and microbial electrolysis cells. *Environ. Sci. Technol.* **44,** 3629–37 (2010).

40. Oh, S., Min, B. & Logan, B. E. Cathode performance as a factor in electricity generation in microbial fuel cells. *Environ. Sci. Technol.* **38,** 4900–4904 (2004).

41. Freguia, S., Rabaey, K., Yuan, Z. & Keller, J. Non-catalyzed cathodic oxygen reduction at graphite granules in microbial fuel cells. *Electrochim. Acta* **53,** 598–603 (2007).

42. Ieropoulos, I., Greenman, J. & Melhuish, C. Improved energy output levels from small-scale Microbial Fuel Cells. *Bioelectrochemistry* **78,** 44–50 (2010).

43. NOVICK, A. Growth of bacteria. *Annu. Rev. Microbiol.* **9,** 97–110 (1955).

44. Tchobanoglous, G., Burton, F. L., Stensel, H. D. & Eddy, M. &. *Wastewater Engineering: Treatment and Reuse*. (2003). at <https://books.google.gr/books/about/Wastewater_Engineering_Treatment_and_Reu.html?id=L1MAXTAkL-QC&pgis=1>

45. Suzuki, S., Karube, I. & Matsunaga, T. Application of a biochemical fuel cell to wastewaters. *Biotechnol. Bioeng. Symp.; (United States)* **8,** (1978).

46. Pant, D., Van Bogaert, G., Diels, L. & Vanbroekhoven, K. A review of the substrates used in microbial fuel cells (MFCs) for sustainable energy production. *Bioresour. Technol.* **101,** 1533–43 (2010).

47. Kim, N., Choi, Y., Jung, S. & Kim, S. Effect of initial carbon sources on the performance of microbial fuel cells containing Proteus vulgaris. *Biotechnol. Bioeng.* **70,** 109–14 (2000).

48. Lu, N., Zhou, S., Zhuang, L., Zhang, J. & Ni, J. Electricity generation from starch processing wastewater using microbial fuel cell technology. *Biochem. Eng. J.* **43,** 246–251 (2009).

49. Ren, Z., Steinberg, L. M. & Regan, J. M. Electricity production and microbial biofilm characterization in cellulose-fed microbial fuel cells. *Water Sci. Technol.* **58,** 617–22 (2008).

50. Zhang, Y., Min, B., Huang, L. & Angelidaki, I. Generation of electricity and analysis of

microbial communities in wheat straw biomass-powered microbial fuel cells. *Appl. Environ. Microbiol.* **75,** 3389–95 (2009).

51. Zhang, C., Li, M., Liu, G., Luo, H. & Zhang, R. Pyridine degradation in the microbial fuel cells. *J. Hazard. Mater.* **172,** 465–71 (2009).

52. Luo, H., Liu, G., Zhang, R. & Jin, S. Phenol degradation in microbial fuel cells. *Chem. Eng. J.* **147,** 259–264 (2009).

53. Zhu, X. & Ni, J. Simultaneous processes of electricity generation and p-nitrophenol degradation in a microbial fuel cell. *Electrochem. commun.* **11,** 274–277 (2009).

54. You, S., Zhao, Q. & Jiang, J. [Biological wastewater treatment and simultaneous generating electricity from organic wastewater by microbial fuel cell]. *Huan Jing Ke Xue* **27,** 1786–90 (2006).

55. Feng, Y., Wang, X., Logan, B. E. & Lee, H. Brewery wastewater treatment using air-cathode microbial fuel cells. *Appl. Microbiol. Biotechnol.* **78,** 873–80 (2008).

56. Gálvez, A., Greenman, J. & Ieropoulos, I. Landfill leachate treatment with microbial fuel cells; scale-up through plurality. *Bioresour. Technol.* **100,** 5085–91 (2009).

57. Patil, S. A. *et al.* Electricity generation using chocolate industry wastewater and its treatment in activated sludge based microbial fuel cell and analysis of developed microbial community in the anode chamber. *Bioresour. Technol.* **100,** 5132–9 (2009).

58. Freguia, S. *et al.* Microbial fuel cells operating on mixed fatty acids. *Bioresour. Technol.* **101,** 1233–8 (2010).

59. Morris, J. M. & Jin, S. Feasibility of using microbial fuel cell technology for bioremediation of hydrocarbons in groundwater. *J. Environ. Sci. Health. A. Tox. Hazard. Subst. Environ. Eng.* **43,** 18–23 (2008).

60. Min, B., Cheng, S. & Logan, B. E. Electricity generation using membrane and salt bridge microbial fuel cells. *Water Res.* **39,** 1675–86 (2005).

61. Lovley, D. R. Bug juice: harvesting electricity with microorganisms. *Nat. Rev. Microbiol.* **4,** 497–508 (2006).

62. Du, Z., Li, H. & Gu, T. A state of the art review on microbial fuel cells: A promising technology for wastewater treatment and bioenergy. *Biotechnol. Adv.* **25,** 464–82 (2007).

63. Rabaey, K., Boon, N., Höfte, M. & Verstraete, W. Microbial Phenazine Production Enhances Electron Transfer in Biofuel Cells. *Environ. Sci. Technol.* **39,** 3401–3408 (2005).

64. Park, D. H. & Zeikus, J. G. Improved fuel cell and electrode designs for producing electricity from microbial degradation. *Biotechnol. Bioeng.* **81,** 348–55 (2003).

65. Madigan MT, M. J. in *Brock Biol. Microorg.* 64–66 (Pearson Prentice Hall, Upper Saddle River, 2006).

66. Moon, H., Chang, I. S., Jang, J. K. & Kim, B. H. Residence time distribution in microbial fuel cell and its influence on COD removal with electricity generation. *Biochem. Eng. J.*

27, 59–65 (2005).

67. Ieropoulos, I., Melhuish, C., Greenman, J. & Horsfiel, I. EcoBot-II: An artificial agent with a natural metabolism. *Int. J. Adv. Robot. Syst.* 1 (2005). doi:10.5772/5777

68. Ieropoulos, I. Imitating Metabolism : Energy Autonomy in Biologically Inspired Robots. 1–4 (2003).

69. Ieropoulos, I., Greenman, J., Melhuish, C. & Horsfield, I. EcoBot-III-A Robot with Guts. *Proc. Alife XII Conf.* 733–740 (2010). at <https://mitp-web2.mit.edu/sites/default/files/titles/alife/0262290758chap131.pdf>

70. Wilkinson, S. Gastronome" - A pioneering food powered mobile robot. in *Proc. 8th IASTED Int. Conf. Robot. Appl. 2000 Aug 14-16; Honolulu, Hawaii* 314–337 (2004).

71. Ieropoulos, I., Melhuish, C. & Greenman, J. Artificial metabolism: towards true energetic autonomy in artificial life. in *Adv. Artif. Life* (W. Banzhaf et al) 792–799 (Springer Berlin Heidelberg, 2003). at <http://link.springer.com/chapter/10.1007/978-3-540-39432-7_85>

72. Aelterman, P., Rabaey, K., Pham, H. T., Boon, N. & Verstraete, W. Continuous electricity generation at high voltages and currents using stacked microbial fuel cells. *Environ. Sci. Technol.* **40,** 3388–3394 (2006).

73. Oh, S.-E. & Logan, B. E. Voltage reversal during microbial fuel cell stack operation. *J. Power Sources* **167,** 11–17 (2007).

74. Larminie, J. & Dicks, A. *Fuel Cell Systems Explained*. (John Wiley & Sons, Ltd,., 2003). doi:10.1002/9781118878330

75. Wu, P. K., Biffinger, J. C., Fitzgerald, L. a. & Ringeisen, B. R. A low power DC/DC booster circuit designed for microbial fuel cells. *Process Biochem.* **47,** 1620–1626 (2012).

76. Papaharalabos, G. *et al.* Increased power output from micro porous layer (MPL) cathode microbial fuel cells (MFC). *Int. J. Hydrogen Energy* **38,** 11552–11558 (2013).

77. Ieropoulos, I. a *et al.* Waste to real energy: the first MFC powered mobile phone. *Phys. Chem. Chem. Phys.* **15,** 15312–6 (2013).

78. Choi, S. & Chae, J. An array of microliter-sized microbial fuel cells generating 100μW of power. *Sensors Actuators A Phys.* **177,** 10–15 (2012).

79. Ibrahim, H., Ilinca, A. & Perron, J. Energy storage systems—Characteristics and comparisons. *Renew. Sustain. Energy Rev.* **12,** 1221–1250 (2008).

80. Debabov, V. G. Electricity from microorganisms. *Microbiology* **77,** 123–131 (2008).

81. Madou, M. J. *Fundamentals of Microfabrication: The Science of Miniaturization, Second Edition*. (CRC Press, 2002). at <http://books.google.com/books?hl=en&lr=&id=9bk3gJeQKBYC&pgis=1>

82. Lee, H.-S., Torres, C. I. & Rittmann, B. E. Effects of Substrate Diffusion and Anode Potential on Kinetic Parameters for Anode-Respiring Bacteria. *Environ. Sci. Technol.* **43,** 7571–7577 (2009).

83. Torres, C. I., Kato Marcus, A. & Rittmann, B. E. Proton transport inside the biofilm limits electrical current generation by anode-respiring bacteria. *Biotechnol. Bioeng.* **100,** 872–81 (2008).

84. Lee, J. W. & Kjeang, E. A perspective on microfluidic biofuel cells. *Biomicrofluidics* **4,** 41301 (2010).

85. Rabaey, K. & Verstraete, W. Microbial fuel cells: novel biotechnology for energy generation. *Trends Biotechnol.* **23,** 291–8 (2005).

86. Kjeang, E., Djilali, N. & Sinton, D. Microfluidic fuel cells: A review. *J. Power Sources* **186,** 353–369 (2009).

87. Clauwaert, P. *et al.* Minimizing losses in bio-electrochemical systems: the road to applications. *Appl. Microbiol. Biotechnol.* **79,** 901–13 (2008).

88. Ieropoulos, I., Greenman, J. & Melhuish, C. Microbial fuel cells based on carbon veil electrodes: Stack configuration and scalability. *Int. J. Energy Res.* **32,** 1228–1240 (2008).

89. Stein, N. E., Hamelers, H. V. M. & Buisman, C. N. J. Stabilizing the baseline current of a microbial fuel cell-based biosensor through overpotential control under non-toxic conditions. *Bioelectrochemistry* **78,** 87–91 (2010).

90. Liu, H., Cheng, S., Huang, L. & Logan, B. E. Scale-up of membrane-free single-chamber microbial fuel cells. *J. Power Sources* **179,** 274–279 (2008).

91. Rinaldi, A. *et al.* Engineering materials and biology to boost performance of microbial fuel cells: a critical review. *Energy Environ. Sci.* **1,** 417 (2008).

92. Li, W.-W., Sheng, G.-P., Liu, X.-W. & Yu, H.-Q. Recent advances in the separators for microbial fuel cells. *Bioresour. Technol.* **102,** 244–52 (2011).

93. Wei, J., Liang, P. & Huang, X. Recent progress in electrodes for microbial fuel cells. *Bioresour. Technol.* **102,** 9335–44 (2011).

94. Osman, M. H., Shah, A. A. & Walsh, F. C. Recent progress and continuing challenges in bio-fuel cells. Part II: Microbial. *Biosens. Bioelectron.* **26,** 953–63 (2010).

95. Dewan, A., Beyenal, H. & Lewandowski, Z. Scaling up Microbial Fuel Cells. *Environ. Sci. Technol.* **42,** 7643–7648 (2008).

96. Logan, B. E. Scaling up microbial fuel cells and other bioelectrochemical systems. 1665–1671 (2010). at <http://link.springer.com/article/10.1007/s00253-009-2378-9/fulltext.html>

97. Melhuish, C., Ieropoulos, I., Greenman, J. & Horsfield, I. Energetically autonomous robots: Food for thought. *Auton. Robots* **21,** 187–198 (2006).

98. Ledezma, P., Ieropoulos, I. & Greenman, J. Comparative analysis of different polymer materials for the construction of microbial fuel cell stacks. *J. Biotechnol.* **150,** 143–143 (2010).

99. Kim, J. R. *et al.* Increasing power recovery and organic removal efficiency using extended longitudinal tubular microbial fuel cell (MFC) reactors. *Energy Environ. Sci.*

4, 459 (2011).

100. Kim, J. R., Premier, G. C., Hawkes, F. R., Dinsdale, R. M. & Guwy, A. J. Development of a tubular microbial fuel cell (MFC) employing a membrane electrode assembly cathode. *J. Power Sources* **187,** 393–399 (2009).

101. Winfield, J., Chambers, L. D., Stinchcombe, A., Rossiter, J. & Ieropoulos, I. *The power of glove: Soft microbial fuel cell for low-power electronics*. *J. Power Sources* **249,** (2014).

102. Ieropoulos, I. A., Greenman, J. & Melhuish, C. Miniature microbial fuel cells and stacks for urine utilisation. *Int. J. Hydrogen Energy* **38,** 492–496 (2013).

103. Ieropoulos, Ioannis A., Greenman, J., Lewis, D. & Knoop, O. Energy production and sanitation improvement using microbial fuel cells. *J. Water, Sanit. Hyg. Dev.* 1–9 (2013).

104. You, J., Greenman, J., Melhuish, C. & Ieropoulos, I. Small-scale microbial fuel cells utilising uric salts. *Sustain. Energy Technol. Assessments* **6,** 60–63 (2014).

105. Ledezma, P. *et al.* Dynamic polarisation reveals differential steady-state stabilisation and capacitive-like behaviour in microbial fuel cells. *Sustain. Energy Technol. Assessments* **5,** 1–6 (2014).

106. Winfield, J., Ieropoulos, I., Greenman, J. & Dennis, J. The overshoot phenomenon as a function of internal resistance in microbial fuel cells. *Bioelectrochemistry* **81,** 22–7 (2011).

107. Gaymans, R. J., Hamberg, M. J. J. & Inberg, J. P. F. The BrittIe - DuctiIe Transition Temperature of Polycarbonate as a Function of Test Speed. *Polym. Eng. Sci. Soc. Plast. Eng.* **40,** 256–62 (2000).

108. Senden, D. J. A., Engels, T. A. P., Söntjens, S. H. M. & Govaert, L. E. The effect of physical aging on the embrittlement of steam-sterilized polycarbonate. *J. Mater. Sci.* **47,** 6043–6046 (2012).

109. Ledezma, P., Greenman, J. & Ieropoulos, I. MFC-cascade stacks maximise COD reduction and avoid voltage reversal under adverse conditions. *Bioresour. Technol.* **134,** 158–65 (2013).

110. Zhuang, L. & Zhou, S. Substrate cross-conduction effect on the performance of serially connected microbial fuel cell stack. *Electrochem. commun.* **11,** 937–940 (2009).

111. Ledezma, P. Development and Integration of Microbial Fuel Cell Stacks for powering Low Energy Applications. (2012).

112. O'Hayre, R., Fabian, T., Lee, S.-J. & Prinz, F. B. Lateral Ionic Conduction in Planar Array Fuel Cells. *J. Electrochem. Soc.* **150,** A430 (2003).

113. Zuo, Y., Cheng, S., Call, D. & Logan, B. E. Tubular Membrane Cathodes for Scalable Power Generation in Microbial Fuel Cells. *Environ. Sci. Technol.* **41,** 3347–3353 (2007).

114. Santoro, C., Agrios, A., Pasaogullari, U. & Li, B. Effects of gas diffusion layer (GDL) and micro porous layer (MPL) on cathode performance in microbial fuel cells (MFCs). *Int. J. Hydrogen Energy* **36,** 13096–13104 (2011).

115. Mathias, M. F., Roth, J., Fleming, J. and Lehnert, W. in *Handb. Fuel Cells* (2010).

116. Li, H. *et al.* A review of water flooding issues in the proton exchange membrane fuel cell. *J. Power Sources* **178,** 103–117 (2008).

117. Passalacqua, E., Lufrano, F., Squadrito, G., Patti, a & Giorgi, L. Influence of the structure in low-Pt loading electrodes for polymer electrolyte fuel cells. *Electrochim. Acta* **43,** 3665–3673 (1998).

118. Minoru Inaba. in *Polym. Electrolyte Fuel Cell Durab.* ((1), F. N. B., (2), M. I. & (3), T. J. S.) 57–69 (Springer New York, 2009).

119. Klinedinst, K. A., Vogel, W. M. & Stonehart, P. The interaction between PTFE and porous metals and metal blacks ? rheological characterization and thermal degradation of the polymer. *J. Mater. Sci.* **11,** 209–214 (1976).

120. Klinedinst, K. A., Vogel, W. M. & Stonehart, P. Rheological characterization and thermal degradation of PTFE. *J. Mater. Sci.* **11,** 794–800 (1976).

121. Klinedinst, K. A. in *Adhes. Asp. Polym. Coatings* (K. L. Mittal) 253–261 (Springer US, 1983).

122. Klinedinst, K. A. & Vogel, W. M. Electrochemical Aspects of Adhesive Joint Failure. *J. Adhes.* **9,** 123–133 (1978).

123. Klinedinst, K. A., Vogel, W. M. & Stonehart, P. An electrochemical tool for studying composite formation from PTFE and contacting porous materials. *J. Mater. Sci.* **12,** 693–698 (1977).

124. Santoro, C., Lei, Y., Li, B. & Cristiani, P. Power generation from wastewater using single chamber microbial fuel cells (MFCs) with platinum-free cathodes and pre-colonized anodes. *Biochem. Eng. J.* **62,** 8–16 (2012).

125. Wilkinson, S. ‘ Gastrobots ’— Benefits and Challenges of Microbial Fuel Cells in Food Powered Robot Applications. 99–111 (2000).

126. (4), I. K. & (5), C. M. Advances in Artificial Life. SlugBot: A Robot Predator. in *6th Eur. Conf. ECAL 2001 Prague, Czech Republic, Sept. 10–14, 2001 Proc.* ((1), J. K. jozef. kelemen@fpf. slu. c. & (1), P. S. petr. sosik@fpf. slu. c.) (2001).

127. Union, E., Waste, U. & Treatment, W. Waste water treatment in the United Kingdom – 2012. (2012).

128. Liu, H., Ramnarayanan, R. & Logan, B. E. Production of electricity during wastewater treatment using a single chamber microbial fuel cell. *Environ. Sci. Technol.* **38,** 2281–5 (2004).

129. Rose, C., Parker, A., Jefferson, B. & Cartmell, E. The Characterization of Feces and Urine: A Review of the Literature to Inform Advanced Treatment Technology. *Crit. Rev. Environ. Sci. Technol.* **45,** 1827–1879 (2015).

130. LARSEN, T. & GUJER, W. Separate management of anthropogenic nutrient solutions (human urine). *Water Sci. Technol.* **34,** 87–94 (1996).

131. Larsen, T. A., Maurer, M., Udert, K. M. & Lienert, J. Nutrient cycles and resource

management: implications for the choice of wastewater treatment technology. *Water Sci. Technol.* **56,** 229–37 (2007).

132. Heinonen-Tanski, H. & van Wijk-Sijbesma, C. Human excreta for plant production. *Bioresour. Technol.* **96,** 403–11 (2005).

133. Maurer, M., Pronk, W. & Larsen, T. a. Treatment processes for source-separated urine. *Water Res.* **40,** 3151–66 (2006).

134. Liu, Z. *et al.* Urea hydrolysis and recovery of nitrogen and phosphorous as MAP from stale human urine. *J. Environ. Sci. (China)* **20,** 1018–24 (2008).

135. Lienert, J. & Larsen, T. a. Soft paths in wastewater management - The pros and cons of urine source separation. *Gaia* **16,** 280–288 (2007).

136. Udert, K. M., Larsen, T. a., Biebow, M. & Gujer, W. Urea hydrolysis and precipitation dynamics in a urine-collecting system. *Water Res.* **37,** 2571–2582 (2003).

137. Udert, K. M., Larsen, T. a. & Gujer, W. Biologically induced precipitation in urine-collecting systems. *Water Sci. Technol. Water Supply* **3,** 71–78 (2003).

138. Udert, K. M., Larsen, T. A. & Gujer, W. Estimating the precipitation potential in urine-collecting systems. *Water Res.* **37,** 2667–77 (2003).

139. Maurer, M., Schwegler, P. & Larsen, T. A. Nutrients in urine: energetic aspects of removal and recovery. *Water Sci. Technol.* **48,** 37–46 (2003).

140. El Diwani, G., El Rafie, S., El Ibiari, N. N. & El-Aila, H. I. Recovery of ammonia nitrogen from industrial wastewater treatment as struvite slow releasing fertilizer. *Desalination* **214,** 200–214 (2007).

141. Etter, B., Tilley, E., Khadka, R. & Udert, K. M. Low-cost struvite production using source-separated urine in Nepal. *Water Res.* **45,** 852–862 (2011).

142. Ryu, H. D., Lim, C. S., Kang, M. K. & Lee, S. I. Evaluation of struvite obtained from semiconductor wastewater as a fertilizer in cultivating Chinese cabbage. *J. Hazard. Mater.* **221-222,** 248–255 (2012).

143. Habermann, W. & Pommer, E. H. Biological fuel cells with sulphide storage capacity. *Appl. Microbiol. Biotechnol.* **35,** (1991).

144. Rabaey, K. & Lissens, G. Microbial fuel cells : performances and perspectives. (2005).

145. Kim, B. H., Chang, I. S. & Gadd, G. M. Challenges in microbial fuel cell development and operation. *Appl. Microbiol. Biotechnol.* **76,** 485–94 (2007).

146. Chung, K. & Okabe, S. Continuous power generation and microbial community structure of the anode biofilms in a three-stage microbial fuel cell system. *Appl. Microbiol. Biotechnol.* **83,** 965–77 (2009).

147. Fangzhou, D., Zhenglong, L., Shaoqiang, Y., Beizhen, X. & Hong, L. Electricity generation directly using human feces wastewater for life support system. *Acta Astronaut.* **68,** 1537–1547 (2011).

148. Winfield, J., Ieropoulos, I. & Greenman, J. Investigating a cascade of seven hydraulically connected microbial fuel cells. *Bioresour. Technol.* **110,** 245–50 (2012).

149. Ren, S., Xia, X., Yuan, L., Liang, P. & Huang, X. Enhancing charge harvest from microbial fuel cells by controlling the charging and discharging frequency of capacitors. *Bioresour. Technol.* **146,** 812–5 (2013).

150. Ieropoulos, I., Greenman, J. & Melhuish, C. Urine utilisation by microbial fuel cells; energy fuel for the future. *Phys. Chem. Chem. Phys.* **14,** 94–8 (2012).

151. Kuntke, P. *et al.* Ammonium recovery and energy production from urine by a microbial fuel cell. *Water Res.* **46,** 2627–36 (2012).

152. Boggs, B. K., King, R. L. & Botte, G. G. Urea electrolysis: direct hydrogen production from urine. *Chem. Commun. (Camb).* 4859–61 (2009). doi:10.1039/b905974a

153. Zang, G.-L. *et al.* Nutrient removal and energy production in a urine treatment process using magnesium ammonium phosphate precipitation and a microbial fuel cell technique. *Phys. Chem. Chem. Phys.* **14,** 1978 (2012).

154. Santoro, C. *et al.* Current generation in membraneless single chamber microbial fuel cells (MFCs) treating urine. *J. Power Sources* **238,** 190–196 (2013).

155. Logan, B. E. Simultaneous wastewater treatment and biological electricity generation. *Water Sci. Technol.* **52,** 31–7 (2005).

156. Ledezma, P., Stinchcombe, A., Greenman, J. & Ieropoulos, I. The first self-sustainable microbial fuel cell stack. *Phys. Chem. Chem. Phys.* **15,** 2278–81 (2013).

157. Winfield, J., Ieropoulos, I., Greenman, J. & Dennis, J. Investigating the effects of fluidic connection between microbial fuel cells. *Bioprocess Biosyst. Eng.* **34,** 477–84 (2011).

158. Greenman, J., Gálvez, A., Giusti, L. & Ieropoulos, I. Electricity from landfill leachate using microbial fuel cells: Comparison with a biological aerated filter. *Enzyme Microb. Technol.* **44,** 112–119 (2009).

159. Santoro, C. *et al.* Power generation and contaminant removal in single chamber microbial fuel cells (SCMFCs) treating human urine. *Int. J. Hydrogen Energy* **38,** 11543–11551 (2013).

160. Dewan, A., Beyenal, H. & Lewandowski, Z. Intermittent energy harvesting improves the performance of microbial fuel cells. *Environ. Sci. Technol.* **43,** 4600–5 (2009).

161. Alaraj, M., Ren, Z. J. & Park, J.-D. Microbial fuel cell energy harvesting using synchronous flyback converter. *J. Power Sources* **247,** 636–642 (2014).

162. Wang, H., Park, J.-D. & Ren, Z. Active energy harvesting from microbial fuel cells at the maximum power point without using resistors. *Environ. Sci. Technol.* **46,** 5247–52 (2012).

163. Park, J.-D. & Ren, Z. Hysteresis controller based maximum power point tracking energy harvesting system for microbial fuel cells. *J. Power Sources* **205,** 151–156 (2012).

164. Kim, Y., Hatzell, M. C., Hutchinson, A. J. & Logan, B. E. Capturing power at higher voltages from arrays of microbial fuel cells without voltage reversal. *Energy Environ. Sci.* **4,** 4662 (2011).

165. Ha, P. T., Moon, H., Kim, B. H., Ng, H. Y. & Chang, I. S. Determination of charge transfer resistance and capacitance of microbial fuel cell through a transient response analysis of cell voltage. *Biosens. Bioelectron.* **25,** 1629–34 (2010).

166. Santoro, C. *et al.* Parameters Characterization and Optimization of Activated Carbon (AC) Cathodes for Microbial Fuel Cell Application. *Bioresour. Technol.* (2014). doi:10.1016/j.biortech.2014.03.091

167. Erbay, C., Carreon-Bautista, S., Sanchez-Sinencio, E. & Han, A. High performance monolithic power management system with dynamic maximum power point tracking for microbial fuel cells. *Environ. Sci. Technol.* **48,** 13992–9 (2014).

168. Shantaram, A., Beyenal, H., Veluchamy, R. R. A. & Lewandowski, Z. Wireless Sensors Powered by Microbial Fuel Cells. *Environ. Sci. Technol.* **39,** 5037–5042 (2005).

169. Yang, F., Zhang, D., Shimotori, T., Wang, K.-C. & Huang, Y. Study of transformer-based power management system and its performance optimization for microbial fuel cells. *J. Power Sources* **205,** 86–92 (2012).

170. Zhang, D., Yang, F., Shimotori, T., Wang, K. C. & Huang, Y. Performance evaluation of power management systems in microbial fuel cell-based energy harvesting applications for driving small electronic devices. *J. Power Sources* **217,** 65–71 (2012).

171. Donovan, C., Dewan, A., Peng, H., Heo, D. & Beyenal, H. Power management system for a 2.5 W remote sensor powered by a sediment microbial fuel cell. *J. Power Sources* **196,** 1171–1177 (2011).

172. Degrenne, N. *et al.* Self-Starting DC : DC Boost Converter for Low-Power and Low-Voltage Microbial Electric Generators. 889–896 (2011).

173. Kim, Y., Hatzell, M. C., Hutchinson, A. J. & Logan, B. E. Capturing power at higher voltages from arrays of microbial fuel cells without voltage reversal. *Energy Environ. Sci.* **4,** 4662 (2011).

174. Park, J.-D. & Ren, Z. Efficient energy harvester for microbial fuel cells using DC/DC converters. in *2011 IEEE Energy Convers. Congr. Expo.* 3852–3858 (IEEE, 2011). doi:10.1109/ECCE.2011.6064292

175. Gong, Y. *et al.* Benthic microbial fuel cell as direct power source for an acoustic modem and seawater oxygen/temperature sensor system. *Environ. Sci. Technol.* **45,** 5047–53 (2011).

176. Donovan, C., Dewan, A., Heo, D., Lewandowski, Z. & Beyenal, H. Sediment microbial fuel cell powering a submersible ultrasonic receiver: New approach to remote monitoring. *J. Power Sources* **233,** 79–85 (2013).

177. Zhang, F., Tian, L. & He, Z. Powering a wireless temperature sensor using sediment microbial fuel cells with vertical arrangement of electrodes. *J. Power Sources* **196,** 9568–9573 (2011).

178. Wang, H., Park, J. & Ren, Z. J. Practical Energy Harvesting for Microbial Fuel Cells: A Review. *Environ. Sci. Technol.* 150211042126005 (2015). doi:10.1021/es5047765

179. Wu, P. K., Biffinger, J. C., Fitzgerald, L. A. & Ringeisen, B. R. A low power DC/DC

booster circuit designed for microbial fuel cells. *Process Biochem.* **47,** 1620–1626 (2012).

180. Hatzell, M. C., Kim, Y. & Logan, B. E. Powering microbial electrolysis cells by capacitor circuits charged using microbial fuel cell. *J. Power Sources* **229,** 198–202 (2013).

181. Zhang, B. & He, Z. Energy production, use and saving in a bioelectrochemical desalination system. *RSC Adv.* **2,** 10673 (2012).

182. Gao, H., Meehan, A. & Lewandowski, Z. New microbial fuel cell power system for efficiency improvement. *2011 Int. Conf. Electr. Mach. Syst.* 1–5 (2011). doi:10.1109/ICEMS.2011.6073381

183. Rahimnejad, M., Ghoreyshi, A. A., Najafpour, G. D., Younesi, H. & Shakeri, M. A novel microbial fuel cell stack for continuous production of clean energy. *Int. J. Hydrogen Energy* **37,** 5992–6000 (2012).

184. Li, Z., Yao, L., Kong, L. & Liu, H. Electricity generation using a baffled microbial fuel cell convenient for stacking. *Bioresour. Technol.* **99,** 1650–5 (2008).

185. Choi, J. & Ahn, Y. Continuous electricity generation in stacked air cathode microbial fuel cell treating domestic wastewater. *J. Environ. Manage.* **130,** 146–52 (2013).

186. Zhuang, L. *et al.* Scalable microbial fuel cell (MFC) stack for continuous real wastewater treatment. *Bioresour. Technol.* **106,** 82–8 (2012).

187. An, J. & Lee, H.-S. Occurrence and implications of voltage reversal in stacked microbial fuel cells. *ChemSusChem* **7,** 1689–95 (2014).

188. Zhang, Y. & Angelidaki, I. Self-stacked submersible microbial fuel cell (SSMFC) for improved remote power generation from lake sediments. *Biosens. Bioelectron.* **35,** 265–70 (2012).

189. An, J., Kim, B., Chang, I. S. & Lee, H.-S. Shift of voltage reversal in stacked microbial fuel cells. *J. Power Sources* **278,** 534–539 (2015).

190. Popat, S. C., Ki, D., Rittmann, B. E. & Torres, C. I. Importance of OH(-) transport from cathodes in microbial fuel cells. *ChemSusChem* **5,** 1071–9 (2012).

191. Arends, J. B. A. & Verstraete, W. 100 years of microbial electricity production: three concepts for the future. *Microb. Biotechnol.* **5,** 333–346 (2012).

192. Lee, H.-S., Vermaas, W. F. J. & Rittmann, B. E. Biological hydrogen production: prospects and challenges. *Trends Biotechnol.* **28,** 262–71 (2010).

193. Jiang, D. *et al.* A pilot-scale study on utilizing multi-anode/cathode microbial fuel cells (MAC MFCs) to enhance the power production in wastewater treatment. *Int. J. Hydrogen Energy* **36,** 876–884 (2011).

194. An, J. & Lee, H.-S. Implication of endogenous decay current and quantification of soluble microbial products (SMP) in microbial electrolysis cells. *RSC Adv.* **3,** 14021 (2013).

195. Lee, H.-S. & Rittmann, B. E. Characterization of energy losses in an upflow single-chamber microbial electrolysis cell. *Int. J. Hydrogen Energy* **35,** 920–927 (2010).

196. Lee, H.-S. & Rittmann, B. E. Significance of biological hydrogen oxidation in a continuous single-chamber microbial electrolysis cell. *Environ. Sci. Technol.* **44,** 948–54 (2010).

197. Boghani, H. C. *et al.* Controlling for peak power extraction from microbial fuel cells can increase stack voltage and avoid cell reversal. *J. Power Sources* **269,** 363–369 (2014).

198. Pinto, R. P., Srinivasan, B., Guiot, S. R. & Tartakovsky, B. The effect of real-time external resistance optimization on microbial fuel cell performance. *Water Res.* **45,** 1571–8 (2011).

199. Papaharalabos, G. *et al.* Dynamic electrical reconfiguration for improved capacitor charging in microbial fuel cell stacks. *J. Power Sources* **272,** 34–38 (2014).

200. Santoro, C. *et al.* Parameters characterization and optimization of activated carbon (AC) cathodes for microbial fuel cell application. *Bioresour. Technol.* **163C,** 54–63 (2014).

201. Dekker, A., Ter Heijne, A., Saakes, M., Hamelers, H. V. M. & Buisman, C. J. N. Analysis and improvement of a scaled-up and stacked microbial fuel cell. *Environ. Sci. Technol.* **43,** 9038–42 (2009).

202. Aelterman, P., Freguia, S., Keller, J., Verstraete, W. & Rabaey, K. The anode potential regulates bacterial activity in microbial fuel cells. *Appl. Microbiol. Biotechnol.* **78,** 409–18 (2008).

203. Wei, J., Liang, P., Cao, X. & Huang, X. A new insight into potential regulation on growth and power generation of Geobacter sulfurreducens in microbial fuel cells based on energy viewpoint. *Environ. Sci. Technol.* **44,** 3187–91 (2010).

204. Hong, Y., Call, D. F., Werner, C. M. & Logan, B. E. Adaptation to high current using low external resistances eliminates power overshoot in microbial fuel cells. *Biosens. Bioelectron.* **28,** 71–6 (2011).

205. McKissock, B. Loyselle, Vogel, P. & Elisa. *Guidelines on Lithium ion Battery Use in Space*. (2009). at <http://ntrs.nasa.gov/archive/nasa/casi.ntrs.nasa.gov/20090023862.pdf>

206. Kiran, V. & Gaur, B. Microbial fuel cell: technology for harvesting energy from biomass. *Rev. Chem. Eng.* **29,** 189–203 (2013).

207. Adami, S. *et al.* Autonomous Ultra-Low Power DC / DC Converter for Microbial Fuel Cells. *Int. Conf. Electron. Circuits, Syst.* 398–401 (2011). doi:10.1109/ICECS.2011.6122297

208. Zhang, X. *et al.* A High-Efficiency DC-DC Boost Converter for a Miniaturized Microbial Fuel Cell. *IEEE Trans. Power Electron.* **30,** 2041–2049 (2015).

209. Degrenne, N. *et al.* Comparison of 3 self-starting step-up DC:DC converter topologies for harvesting energy from low-voltage and low-power microbial fuel cells. *Proc. 2011 14th Eur. Conf. Power Electron. Appl.* 1–10 (2011).

210. Park, J.-D. & Ren, Z. High efficiency energy harvesting from microbial fuel cells using a

synchronous boost converter. *J. Power Sources* **208,** 322–327 (2012).

211. Steels, L. When are robots intelligent autonomous agents? *Rob. Auton. Syst.* **15,** 3–9 (1995).

212. McFarland, D. & Spier, E. Basic cycles, utility and opportunism in self-sufficient robots. *Rob. Auton. Syst.* **20,** 179–190 (1997).

213. Premier, G. C., Kim, J. R., Michie, I., Dinsdale, R. M. & Guwy, A. J. Automatic control of load increases power and efficiency in a microbial fuel cell. *J. Power Sources* **196,** 2013–2019 (2011).

214. Woodward, L., Perrier, M., Srinivasan, B., Hc, C. & Tartakovsky, B. Maximizing Power Production in a Stack of Microbial Fuel Cells Using Multiunit Optimization Method. (2009). doi:10.1021/bp.115

215. Boghani, H. C., Kim, J. R., Dinsdale, R. M., Guwy, A. J. & Premier, G. C. Control of power sourced from a microbial fuel cell reduces its start-up time and increases bioelectrochemical activity. *Bioresour. Technol.* **140,** 277–85 (2013).

216. Zhuang, L. *et al.* Scalable microbial fuel cell (MFC) stack for continuous real wastewater treatment. *Bioresour. Technol.* **106,** 82–8 (2012).

217. Kim, J. R. *et al.* Modular tubular microbial fuel cells for energy recovery during sucrose wastewater treatment at low organic loading rate. *Bioresour. Technol.* **101,** 1190–8 (2010).